ATF5 is Required For the Normal Stress Response During Skeletal Muscle Denervation

Jared Kuthe

A THESIS SUBMITTED TO THE FACULTY OF GRADUATE STUDIES IN PARTIAL FULFILLMENT OF THE REQUIREMENTS FOR THE DEGREE OF

Master of Science

Graduate Program in Kinesiology and Health Science

York University
Toronto, Ontario
October 2025

ABSTRACT

Muscle inactivity is associated with the development of various negative health outcomes and is often accompanied by the decline in mitochondrial health. Mitochondria reside within skeletal muscle cells and are responsible for creating energy by metabolizing dietary substrates. During muscle inactivity, these mitochondria become damaged, which leads to a reduction in energy production and whole cell metabolism. To help prevent this outcome, various stress-responsive proteins within muscle cells help repair and minimize mitochondrial damage. Specifically, the stress-responsive protein ATF5 is known to help alleviate mitochondrial damage. To help understand more about these proteins in skeletal muscle, our study employed a mouse model of muscle inactivity. Our results suggest that ATF5 plays an important role in the maintenance of mitochondria and skeletal muscle health in response to muscle inactivity. This information could help us identify potential treatments for individuals experiencing severe muscle-loss related symptoms.

ACKNOWLEDGEMENTS

I would like to acknowledge my parents for their constant support during my academic endeavours and my fellow lab members for their guidance and continuous encouragement.

LIST OF FIGURES

CHAPTER 1: REVIEW OF LITERATURE

Fig. 1 - Graphical illustration of the mitochondria and its components. 6

Fig 2 - Graphical illustration of the steps of mitophagy/autophagy within the cell 9

Fig 3 - The Role of ATF5 during the ISR/UPR^{mt} 14

CHAPTER 2: MANUSCRIPT

Fig 1 - Seven days of denervation leads to a reduction in muscle mass in ATF5 KO and WT. ... 67

Fig 2 - Mitochondrial content after seven days of denervation in WT and ATF5 KO mice..... 68

Fig 3 - High resolution respirometry and ROS emissions of WT and ATF5 KO mice 69

Fig 4 - Mitophagy/autophagy related protein expression in response to denervation in WT and ATF5 KO mice 70

Fig 5- ISR protein content in response to denervation in response to 7 days of denervation in WT and ATF5 KO mice 71

Fig 6 - UPR^{mt} protein content in response to denervation in WT and ATF5 KO mice 72

Fig 7 - Antioxidant protein content in response to denervation in WT and ATF5 KO mice 73

Fig 8 - Lysosomal protein content in response to denervation in WT and ATF5 mice 74

Fig 9 - Signaling pathways involved in regulating mitochondrial function during the ISR and UPR^{mt} 75

Fig 10 – Conclusion schematic of results section..... 76

APPENDIX B: ADDITIONAL DATA

Fig. S1 - Additional hindlimb muscle weight and bodyweight measurements of WT and ATF5 KO mice post denervation 110

Fig. S2 - Raw hindlimb muscle weight measurements of male and female WT and ATF5 KO mice.....111

Fig. S3 - Comparisons between right and left hindlimb muscle groups in non-denervated WT mice.....112
Fig. S4 - Total protein content of sestrin2 in WT and ATF5 KO mice 113

LIST OF TABLES

CHAPTER 2: MANUSCRIPT

Table 1 - List of primary/secondary antibodies and concentrations 66

APPENDIX A: DATA AND STATISTICAL ANALYSIS

Table 1 - LC3 I Protein Expression in sham-operated and denervated samples 79

Table 2 - LC3 II Protein Expression in sham-operated and denervated samples 80

Table 3 - LC3 II/I Protein Expression in sham-operated and denervated samples 81

Table 4 - Beclin1 Protein Expression in sham-operated and denervated samples 82

Table 5 - P62 Protein Expression in sham-operated and denervated samples 83

Table 6 - ATF4 Protein Expression in sham-operated and denervated samples 84

Table 7 - CHOP Protein Expression in sham-operated and denervated samples 85

Table 8 - Total-eIF2α Protein Expression in sham-operated and denervated samples 86

Table 9 - Phosphorylated-eIF2α Protein Expression in sham-operated and denervated samples 87

Table 10 - Phosphorylated/Total-eIF2α Protein Expression in sham-operated and denervated samples 88

Table 11 - LONP1 Protein Expression in sham-operated and denervated samples 89

Table 12 - mtHSP70 Protein Expression in sham-operated and denervated samples 90

Table 13 - HSP60 Protein Expression in sham-operated and denervated samples 91

Table 14 - ClpP Protein Expression in sham-operated and denervated samples 92

Table 15 - CPN10 Protein Expression in sham-operated and denervated samples 93

Table 16 - Nrf-2 Protein Expression in sham-operated and denervated samples 94

Table 17 - NQO1 Protein Expression in sham-operated and denervated samples 95

Table 18 - HO-1 Protein Expression in sham-operated and denervated samples 96

Table 19 - Catalase Protein Expression in sham-operated and denervated samples 97

Table 20 - Glutathione Reductase Protein Expression in sham-operated and denervated samples 98

Table 21 - Cathepsin B (Immature) Protein Expression in sham-operated and denervated samples 99

Table 22 - Cathepsin B (mature) Protein Expression in sham-operated and denervated samples 100

Table 23 - Cathepsin B (Mature/Immature) Protein Expression in sham-operated and denervated samples..... 101

Table 24 - LAMP1 Protein Expression in sham-operated and denervated samples 102

Table 25 - Cytochrome c Oxidase enzyme activity in sham-operated and denervated samples 103

Table 26 - Respiration levels in sham-operated and denervated samples 104

Table 27 - Reactive oxygen species production in sham-operated and denervated samples 105

Table 28 - Gastrocnemius muscle weight normalized to bodyweight in sham-operated and denervated samples 106

Table 29 - Soleus muscle weight normalized to bodyweight in sham-operated and denervated samples..... 107

Table 30 - Total bodyweight of WT/KO male/female mice..... 108

Table 31 - Male epididymal fat normalized to bodyweight in WT/KO male mice..... 109

LIST OF ABBREVIATIONS

ATP – Adenosine triphosphate
OMM – Outer mitochondrial membrane
IMM – Inner mitochondrial membrane
IMS – Intermembrane space
ETC – Electron transport chain
mtDNA – Mitochondrial DNA
TCA – Tricarboxylic acid cycle
NADH – Nicotinamide adenine dinucleotide
$FADH_2$ - Flavine adenine dinucleotides
GTP - Guanosine triphosphate
GDP – Guanosine diphosphate
PINK1 - PTEN-induced kinase 1
PARKIN - Parkin RBR E3 ubiquitin Protein Ligase
LC3 I/II – Microtubule-associated protein 1 light chain 3
Ub – Ubiquitin
UPR^{mt} – Mitochondrial unfolded protein response
UPR^{er} – Endoplasmic reticulum unfolded protein response
ISR – Integrated stress response
ROS – Reactive oxygen species
eIF2*α* - eukaryotic translation initiation factor subunit alpha
PKR - Protein kinase RNA-dependent
HRI - heme regulated inhibitor kinase
GCN2 - general control nonderepressible 2
PERK - PKR-like ER kinase
TC – Ternary complex
PIC – preinitiation complex
5'UTR – five prime untranslated region
ATF4 – Activating transcription factor 4
ATF5 - Activating transcription factor 5
CHOP – C/EBP homologous Protein
CEBPA – CCAAT/enhancer-binding protein alpha
CEBPA - CCAAT/enhancer-binding protein beta
DR4, DR5 - death receptor 4/5
BIM – Bcl-2 interacting mediator of cell death
PUMA – p53 Up-regulated modulator of apoptosis
BCL-XL – B-cell lymphoma-extra large
BCL2 – B-cell leukemia/lymphoma 2
PPP1R15A – Protein phosphatase 1 regulatory subunit 15A
OMA1 – Metalloendopeptidase OMA1
DELE1 – DAP3-dinbind cell death enhancer 1
S-DELE1 - DAP3-dinbind cell death enhancer 1 short form
TIM – Translocase of the inner membrane
TOM – Translocase of the outer membrane
O^{-}_2 – Superoxide

H_2O_2 – Hydrogen Peroxide
FOS – Finkel-biskis-jinkins murine osteosarcoma virus oncogene
CREB – cAMP response element-binding protein
Nrf-2 – Nuclear factor erythroid 2-realted factor 2
MTS – Mitochondrial targeting sequence
NES – Nuclear export sequence
NLS – Nuclear localization sequence
uORF – upstream open reading frame
Cdc34 – ubiquitin-conjugating enzyme E2 R1
bZIP – Basic-leucine zipper protein
LONP1 – Lon peptidase 1
ClpP – Caseinolytic mitochondrial matrix peptidase proteolytic subunit
HSP60 – Heat shock protein family D 60
mtHSP70 – Mitochondrial heat shock protein 70
CPN10 – Chaperonin 10
NQO1 – NAD(P)H quinone dehydrogenase 1
HO1 – Heme oxyenase-1
MnSOD – Manganese superoxide dismutase
SIRT3 – NAD-dependent deacetylase sirtuin-3
KEAP1 - Kelch-like ECH-associated protein 1
Cul3 - cullin 3
AREs – antioxidant responsive element
COX - cytochrome c oxidase
PI3K – Phosphatidylinositol 30kinase
AKT – Protein Kinase B
SP-1 – Specificity Protein 1
c-JUN – Jun protooncogene AP-1 transcription factor subunit
PGC-1α – Peroxisome proliferator-activated receptor gamma coactivator-1 alpha
GR – Glutathione Reductase
LAMP1 – Lysosome-associated membrane protein 1
MNRR1 – Mitochondrial nuclear retrograde regulator 1

TABLE OF CONTENTS

Abstract ... ii

Acknowledgments ... iii

List of figures ... iv

List of tables ... vi

List of abbreviations ... viii

Table of contents ... x

Chapter 1: Review of Literature ... 1

1.0. Skeletal muscle ... 2
1.1 Structure ... 2
1.2 Fiber types ... 3
1.3 Mitochondria ... 4
1.3.1 Structure ... 4
1.3.2 Function ... 6
2.0. Muscle disuse and skeletal muscle wasting ... 7
2.1 Autophagy/mitophagy ... 7
2.2 Skeletal muscle disorders and mitochondria ... 10
2.3 Importance of exercise ... 10
3.0. Mitochondrial Stress Response Pathways ... 11
3.1 Integrated stress response ... 12
3.1.1 ATF5 and the ISR ... 15
3.2 Mitochondrial unfolded protein response ... 16
3.2.1 ATF5 and the UPR^{mt} ... 18
3.3 Antioxidant response ... 19
3.3.1 ISR and Nrf-2 Relationship ... 20
3.4 Other roles of ATF5 in various cell types ... 21
4.0. Sex Specific Adaptations of the ISR/UPR^{mt} ... 23

Research Objectives ... 25

Hypothesis ... 25

CHAPTER 2: MANUSCRIPT **26**
ATF5 is required for the normal stress response during skeletal muscle denervation 27
Abstract 28
Introduction 29
Methods 32
Results 35
Discussion 41
Conclusion 46
References 47
Figure Legends 65
Future directions & Limitations 77
APPENDIX A: DATA AND STATISTICAL ANALYSIS **78**
APPENDIX B: ADDITIONAL DATA **110**
APPENDIX C: LABORATORY METHODS AND PROTOCOLS **115**
Sciatic nerve transection 116
Isolating whole muscle protein extracts 117
Western blotting protocol 118
Gel electrophoresis-SDS page (protein BIORAD system) 119
Western blotting – transfer and immunodetection 120
Cox enzyme activity assay 122
High-resolution respirometry and ROS emission in permeabilized fibers 123
Cryosectioning and SDH staining 125
APPENDIX D: OTHER CONTRIBUTIONS TO THE LITTERATURE **126**
Published abstracts 126

CHAPTER 1:
REVIEW OF LITERATURE

1.0. Skeletal muscle

Skeletal muscle is a major organ that is found throughout the body and is predominantly known for adapting to different types of stress-induced stimuli. In humans, roughly 40% of total body mass contains skeletal muscle along with contributing to 50-75% of all body proteins[1,2]. The main functions of skeletal muscle is to produce voluntary movement, sustain posture, maintain body temperature, store nutrients, stabilize joints and contribute significantly to metabolizing energy. To efficiently carry out these roles in response to various types of stimuli, skeletal muscle can undergo significant changes in morphology and physiology[1,2]. This ability to adapt is a well-known characteristic of skeletal muscle and is one of the major reasons for its vast interest within the scientific community. Due to the complexity and importance of this organ, researchers aim to better understand the biochemical and physiological pathways involved in this adaptive response to various forms of stimuli. Although there is a significant amount of research highlighting the importance of skeletal muscle for overall health, longevity and quality of life, the information behind the exact molecular mechanisms that are responsible for this adaptive 'plasticity' remains incomplete.

1.1. Structure

Skeletal muscle is largely composed of water (75%), protein (20%) and other substrates including fats and carbohydrates (5%). However, when water is removed, single muscle fibers contain roughly 80% protein. The architecture of skeletal muscle is comprised of an arrangement of multi-nucleated muscle cells that form long cylindrical striated myofibers. Within these myofibers resides thousands of myofibrils that contain billions of myofilaments. Sarcomeres form when myofilaments are assembled together and are responsible for the basic contractile properties of skeletal muscle . The two most important proteins that comprise roughly 70-80% of the sarcomere are actin and myosin, along with other proteins such as troponin and tropomyosin, which are involved in the activation and force generation of the myofilament[3]. Other important cellular components that exist within the structure of skeletal muscle include the transverse tubular system (T tubule) and the sarcoplasmic reticulum (SR)[1]. The T tubule is

responsible for guiding the action potential evenly throughout the interior of the muscle cell, while the SR is responsible for the release, reuptake and storage of calcium. When activated via electrical stimulation, the SR will trigger the release of calcium into the cytosol where it will bind to troponin C, causing a conformational change that shifts tropomyosin. This will allow the myosin filament to bind to actin, creating a cross-bridge cycle in the presence of ATP, thus creating a muscle contraction[4]. The speed, recovery and duration of these physiological events will determine the contractile properties of the muscle fiber, highlighting the importance of structurally different phenotypes within skeletal muscle.

1.2. Fiber Types

Depending on the contractile/metabolic properties, speed of shortening, degree of fatigability and calcium handling, skeletal muscle can be further classified into different fiber types. The most widely used classification system for human skeletal muscle includes fiber types: type I (slow, oxidative, fatigue-resistant), IIA (fast, oxidative, intermediate metabolic properties), and IIx/IIb (fastest, glycolytic, most fatigable), with type IIb only being present in rodent tissue[5]. However, this classification system can become even more complex when you measure the percentage of different myosin heavy chain isoforms that reside in each fiber. For instance, a single fiber can have an assortment of type I, type IIa and type IIx isoforms, but the overall percentage of these isoforms will determine if the muscle is classified as fast, slow or intermediate[6]. Likewise, when needle biopsies were taken from young untrained male vastus lateralis muscle, which is considered a predominantly intermediate-twitch fiber, and were further analyzed to observe the different percentages of hybrid fibers, researchers observed that the muscle expressed 26.9% type I fibers, 32.2% type IIa fibers, and 0% type IIx fibers. The remaining fibers consisted of hybrid type fibers such as I/IIa (14.1%), IIa/IIx (24.3%) and I/IIa/IIx (2.4%)[7]. Much like non-hybrid fibers, these hybrid fibers exist in every muscle group and have been shown to respond differently to varying stimuli. Researchers have since expanded their knowledge on the myosin heavy chain gene family in mammals by further characterizing specific genes of different tissues such as the heart, jaw and developing/extraocular muscles[6]. Further analyzing these specific fibers can help us determine what

specific roles each protein has during varying levels of acute or chronic stress. This will allow us to identify the level of susceptibility or adaptability each fiber is predisposed to.

1.3. Mitochondria

Mitochondria are organelles that are present in almost all mammalian eukaryotic cells and are responsible for producing most of the energy that is needed for cell function. Mitochondria have been theorized to have evolved from free-living bacteria that combined with eukaryotic cells via endosymbiosis to create a favorable interaction. This relationship allowed the cell to produce its own energy in the form of adenosine triphosphate (ATP), which dramatically improved its survivability and efficiency[8]. Along with energy production, mitochondria are responsible for contributing to calcium homeostasis, cell growth/differentiation, cell cycle control and cell death[9,10,11]. Maintaining a constant supply of functional mitochondria is important for sustaining these metabolic processes, and dysfunctions in mitochondrial shape, quantity or function have been associated with deleterious effects such as age related disorders, neurodegenerative diseases, cancer and other respiratory illnesses[9,12]. Much like skeletal muscle, mitochondria have been shown to share this 'plasticity' in the presence of various stimuli. Thus, understanding these multifactorial roles can help highlight the importance of maintaining mitochondrial health and the positive outcomes it brings.

1.3.1 Mitochondrial Structure

The structure of mitochondria consists of two phospholipid membranes, the outer mitochondrial membrane (OMM) and the inner mitochondrial membrane (IMM). These two membranes separate the mitochondrial matrix and the intermembrane space (IMS). To ensure maximal surface area for oxidative phosphorylation, these membranes are organized into folds that form the cristae and cristae junctions[8]. Under normal conditions, these folds are required for optimal energy production and protein import/export, whereas irregular cristae formation is associated with mitochondrial dysfunction. Within the cristae resides the electron transport chain (ETC), which is a series of five complexes that are responsible for oxidizing substrates into energy in the form of ATP. For these structures to function

optimally, various proteins are needed for the assembly and maintenance of these processes. Mitochondria are comprised of roughly 1200 proteins, with 99% being nuclear-encoded and 1% of these gene products being encoded by mitochondrial DNA (mtDNA). The structure that is responsible for encoding these mitochondrial proteins is the circular DNA within the mitochondrial matrix. The 37 genes within this structure are responsible for encoding 13 proteins that required for the assembly of complexes I, III, IV and V of the ETC, with the remaining proteins being imported from the nucleus[8,13,14]. Although the quantity of mtDNA is small in comparison to nuclear-encoded DNA, mutations or alterations in mtDNA are associated with pathological consequences[15].

1.3.2 Mitochondrial Function

The main function of the mitochondria is to supply the cell with ATP to sustain basic survival functions and/or to meet elevated energy demands in response to stressful stimuli. As shown in figure 1, the first step in optimizing energy production involves the tricarboxylic acid cycle (TCA). The TCA operates within the mitochondrial matrix and involves nine different enzymatic reactions with each round generating three nicotinamide adenine dinucleotide (NADH) molecules, one flavine adenine dinucleotides ($FADH_2$) and one guanosine triphosphate (GTP) from a single acetyl-CoA molecule. NADH and $FADH_2$ can also be produced through a process known as fatty acid beta-oxidation, which also occurs within the mitochondrial matrix. However, the structure that is primarily responsible for energy production within the mitochondria is the electron transport chain (ETC), which consists of five complexes that reside within the inner mitochondrial membrane. The complexes known as NADH dehydrogenase (complex I) and succinate dehydrogenase (complex II) receive electrons via NADH and FADH2, respectively. These electrons travel down the ETC and eventually get transferred to oxygen, forming water. Meanwhile, this transport of electrons creates the potential energy required for protons to get pumped into the phospholipidic bilayer through complexes I, III, and IV via proton transporters. The energy created by this

flow of protons is used by the ATP synthase (complex V) to generate ATP in the presence of ADP and phosphate[8].

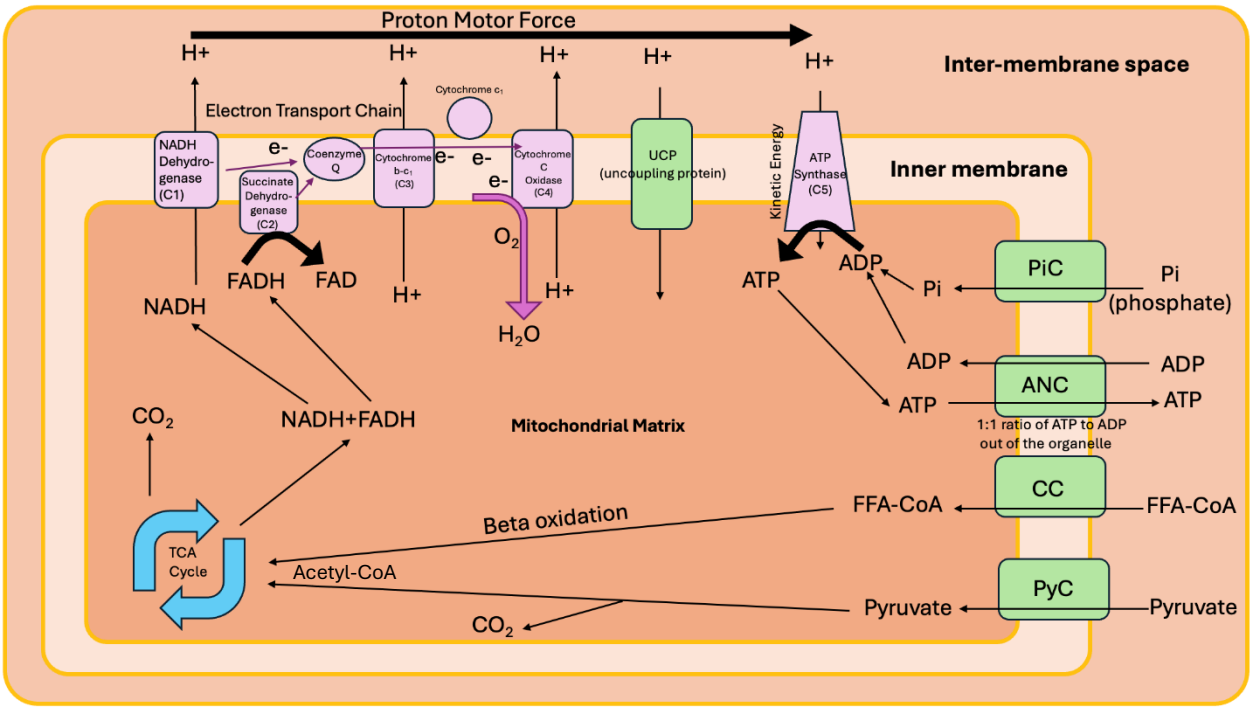

Figure 1. Graphical illustration of the mitochondria and its components. Metabolism of substrates such as carbohydrates and fatty acids leads to the production of pyruvate and free fatty acid-coenzyme A (FFA-CoA). These molecules are transported into the mitochondria via their respective channels. FFA-CoA and pyruvate are further metabolized into acetyl-CoA within the mitochondrial matrix. Acetyl-CoA will enter the tricarboxylic acid cycle (TCA) and be metabolised into NADH and FADH molecules. These molecules will donate electrons to the electron transport chain (ETC) at the appropriate complexes. Complex I (NADH dehydrogenase) will accept electrons from NADH and complex II (succinate dehydrogenase) will accept electrons from FADH. These protons will be pumped into the inter-membrane space, creating an electrochemical potential gradient. Protons will then re-enter the mitochondrial matrix via the ATP synthase. This proton motor force will create enough kinetic energy to allow ADP to bind with free phosphate, creating energy in the form of ATP. Phosphate and ADP are continuously imported into the mitochondrial matrix via the phosphate import channel (PiC) and the adenine nucleotide channel (ANC), respectively. The electrons will be transferred down the ETC by ubiquinone (Coenzyme Q) and complex 3 (cytochrome b-c_1). From complex III, the electrons are picked up by cytochrome c and transported to complex IV (Cytochrome c oxidase or COX). As COX accept electrons from cytochrome c, it transports them to oxygen (O_2), where it will bind to create water (H_2O). The free energy that is released when electrons flow through complex I, III and IV is used to pump the protons into the IMS.

2.0. Muscle Disuse and Skeletal Muscle Wasting

A significant amount of research has been dedicated to understanding the consequences of muscle disuse and its effect on skeletal muscle health and mitochondria. Skeletal muscle disuse can be characterized as prolonged periods of inactivity which results in the significant loss of muscle mass, aerobic capacity and power output. Examples include denervation, hindlimb unloading, microgravity or bed rest due to illness, injury or immobilization[16,17]. Due to the quantity of skeletal muscle and the wide array of biological processes it is responsible for maintaining, the significant loss of this vital organ is associated with a plethora of negative health outcomes such as a reduction in glucose tolerance, an increase in insulin resistance and a greater susceptibility to falls and fractures[18,19]. These consequences can be observed within just five days of bedrest in both young and aged populations, with elderly patients experiencing the greatest losses in muscle mass and power[20]. Skeletal muscle wasting is the major consequence of muscle disuse, likewise, minimizing its onset is crucial for the maintenance of muscle functionality and overall quality of life.

Another important contributor to skeletal muscle wasting involves the age-related decline in muscle mass in the middle aged and elderly population, commonly described as sarcopenia. Due to the multifactorial issues that arise within the aging population, it is difficult to pinpoint the main culprit that is responsible for this age-related decline in muscle mass. After the fifth decade, muscle mass beings to decline at a rate of 1-2% per year along with a corresponding 1.5% decrease in strength. This decline in muscle mass further increases to 3% after the sixth decade and has been shown reach up to 11-50% after the eighth decade and onward[21]. Therefore, understanding the physiological mechanisms involved can help provide insight on future treatments or strategies to help mitigate the detrimental effects that accompany the significant loss of skeletal muscle mass.

2.1 Autophagy/Mitophagy

To understand skeletal muscle disuse and its consequences, it is important to first understand the various survival pathways involved in the maintenance of these cells and organelles. Autophagy is a

process that cells undergo to remove any damaged or dysfunctional components via a lysosome-dependent regulated mechanism. This stress response is necessary for mitigating damage during harsh conditions and the proteins involved act to balance the beneficial/harmful effects in the presence of stressful stimuli[22–24]. During autophagy, a section of the cytoplasm is engulfed by a phagophore, creating an autophagosome (Figure 2). This structure will fuse with a lysosome to create an autolysosome, leading to the degradation of its contents via lysosomal enzymes. Likewise, mitochondria will experience their own cycle of autophagy, specifically known as mitophagy. This process coordinates the continuous removal of irreversibly damaged or dysfunctional mitochondria to ensure a balance between mitochondrial biogenesis and degradation is maintained within the cell[22]. For instance, the most characterized pathway of mitophagy in skeletal muscle involves the PINK1/PARKIN mediated response. In the presence of dysfunctional mitochondria, PTEN-induced kinase 1 (PINK1) will accumulate on the outer mitochondrial membrane (OMM), triggering parkin RBR E3 ubiquitin Protein Ligase (PARKIN) phosphorylation. Activated PARKIN will tag proteins on the OMM with ubiquitin, which will mark them as recognizable targets for degradation. One of the proteins responsible for selectively targeting this tagged cargo is the adapter protein p62. The binding of this protein will act as a signal and an adapter to recruit the autophagosomal protein LC3. Once p62 and LC3 have interacted, an autophagosome will form around the damaged/dysfunctional mitochondria. The autophagosome will be delivered to the lysosome, forming an autolysosome, where the contents will be degraded and recycled[22–26]. Although the research that has been conducted on this pathway is abundant, there remains gaps in the literature when trying to understand the exact mechanisms during conditions such as muscle disuse or aging. However, continuously pursuing these pathways can encourage the development of promising treatments to help manage the symptoms of autophagy/mitophagy morphologies in a field that significantly lacks effective therapies.

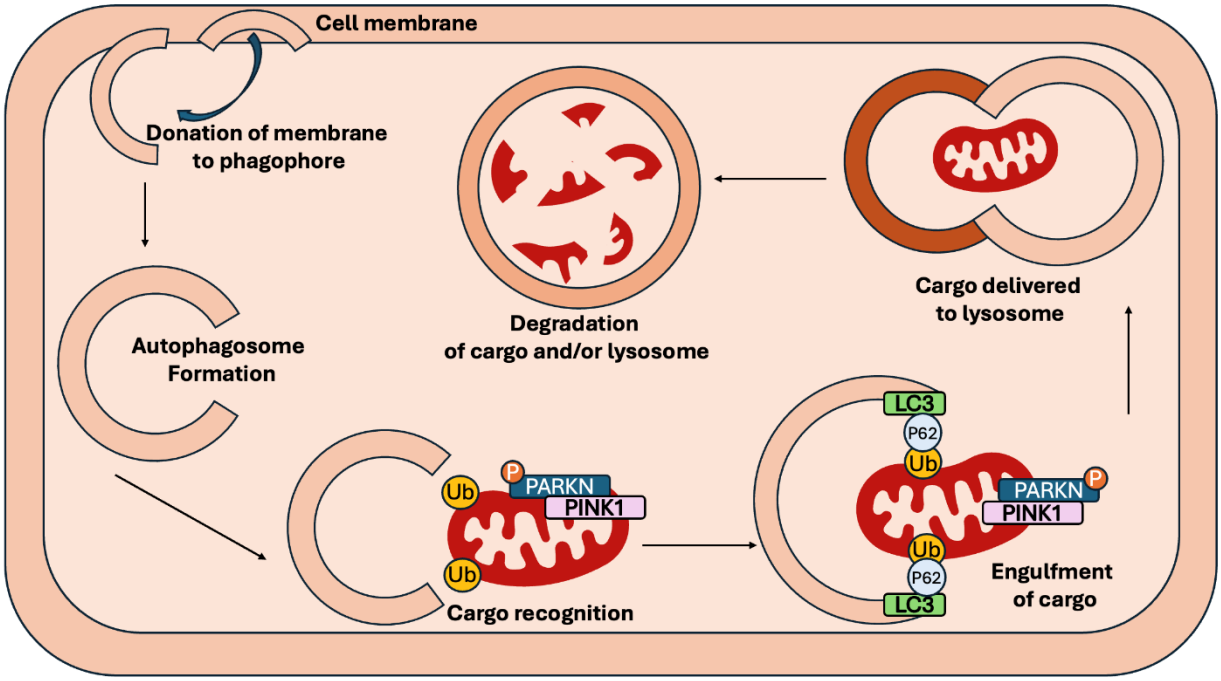

Figure 2 – Graphical illustration of the steps of mitophagy/autophagy within the cell. During autophagy, a portion of the cell membrane is donated to form a phagophore. This structure will eventually form into an autophagosome as the phagophore engulfs cytoplasmic components. As mitochondria become dysfunctional, PTEN-induced kinase 1 (PINK1) will accumulate on the outer mitochondrial membrane (OMM), triggering parkin RBR E3 ubiquitin Protein Ligase (PARKIN) phosphorylation. Activated PARKIN will tag proteins on the OMM with ubiquitin, which will mark them as recognizable targets for degradation. One of the proteins responsible for selectively targeting this tagged cargo is the adapter protein p62. The binding of this protein will act as a signal and an adapter to recruit the autophagosomal protein LC3. Once p62 and LC3 have interacted, an autophagosome will form around the damaged/dysfunctional mitochondria. The autophagosome will be delivered to the lysosome, forming an autolysosome, where the contents will be degraded and recycled.

2.2 Skeletal muscle disorders and mitochondria

Skeletal muscle disorders are typically described as the progressive loss of muscle size and an increase in weakness/exercise intolerance. Clinical conditions such as cancer cachexia, sarcopenia, Duchenne muscular dystrophy and Huntington's disease all fall under this description. Likewise, we observe the presence of mitochondrial dysfunction in almost every feature of muscle wasting in these diseases[27]. Mitochondrial morphologies can vary depending on which organ is being affected. With regards to skeletal muscle, mitochondrial damage is associated with an increase in reactive oxygen species (ROS) production, calcium imbalance, dysfunctional unfolded protein response (UPR), mitochondrial DNA mutations and mitophagy imbalance. Muscle biopsies reveal dysfunctional mitochondria that share these traits and exhibit a fractured and abnormally large mitochondrial structure filled with globular inclusions and lipids, indicating a reduction in substrate utilization and abnormal mitochondrial proliferation[28]. Due to the complexity of skeletal muscle disorders and their symptoms, it is difficult to suggest that the onset of these mitochondrial morphologies is the direct cause of the excessive muscle wasting that is observed. However, although there is no specific treatment, maintaining mitochondrial health to minimize the effects of these diseases should be a main priority.

2.3 Importance of exercise

Since mitochondria serve such an important role in the preservation of skeletal muscle health, it is important that mitochondrial function is maintained to help reduce rates of muscle atrophy during periods of prolonged stress. The most efficient way to achieve this goal is to promote mitochondrial biogenesis by engaging in regular physical activity. It has been demonstrated that aerobic and resistance exercise training can greatly increase the health of the mitochondrial pool by increasing their number and quality. The increase in mitochondrial content has been associated with the increase in mtDNA gene expression that occurs following a bout of exercise, along with the increase in mitochondrial fusion protein MFN2, which promotes the elongation of the reticulum. Mitochondrial quality is thought to be improved

via the increased content of proteins involved in the ETC, thus improving substrate utilization and ATP production[29–34]. Although exercise is an effective therapy for maintaining skeletal muscle health, individuals who are chronically bedridden, injured, or sick cannot benefit from the same results of engaging in regular physical activity. Therefore, continuing to refine our understanding of these stress response pathways can lead to future advancements when attempting to effectively treat mitochondrial dysfunctions in skeletal muscle disorders that are equal to or similar than exercise training for physically compromised individuals.

3.0 Mitochondrial Stress Response Pathways

Independent of the autophagy/mitophagy pathways, there remain additional systems in place that significantly contribute to cell survivability. One system described as the Integrated Stress Response (ISR), is a highly evolutionarily conserved pathway that ultimately decides the fate of a cell's life during periods of prolonged stress. Although this pathway operates on a whole cell scale, the downstream consequences of its physiological stress adaptations have a direct impact on mitochondrial homeostasis. Aside from the ISR, another mitochondrial quality control pathway known as the Mitochondrial Unfolded Protein Response (UPR^{mt}) has been shown to be activated alongside the ISR. This unfolded protein response has also been observed to occur in other organelles such as the endoplasmic reticulum (UPR^{er}). Despite the similarities between these pathways, the downstream targets and changes in global gene content differ vastly between organelles[13,14,34–43]. Although different stress responses have been identified in skeletal muscle, it remains unclear what exact mechanisms are involved and how these adaptive responses can be affected in different scenarios such as prolonged muscle disuse.

3.1 Integrated stress response

The ISR is activated in response to cellular stress with the main goal of attenuating global protein translation while simultaneously triggering the translation of specific downstream gene targets to help create a cellular environment that promotes the protection of the cell and its contents. The first step

is the activation of eukaryotic translation initiation factor subunit alpha (eIF2α) stress sensing kinases, those of which respond to their own very distinct cellular stressors (Figure 3). Currently, there are four well documented kinases that are known to be activated during the ISR. These include Protein kinase RNA-dependent (PKR), heme regulated inhibitor kinase (HRI), general control nonderepressible 2 (GCN2) and PKR-like ER kinase (PERK). Activation of PKR has been observed to be triggered by double-stranded RNA during viral infection[44], whereas HRI is activated during heme deprivation and mitochondrial stress[35,45,46]. The kinase PERK has been observed to specifically localize to the ER membrane and is activated in response to ER stress[47]. Lastly, GCN2 is known to be activated during amino acid deprivation and elevated ROS production[48–51].

Under normal conditions, the protein translation initiation pathway in eukaryotes consists of several different steps. The first step involves the eIF2B complex replenishing eIF2 with GTP to facilitate the formation of the ternary complex (TC). The TC, consisting of eIF2, GTP and Met-tRNA will combine with eIF1, eIF3, eIF5, eIF1A and the 40S ribosomal subunit to form the 43S preinitiation complex (PIC). Secondly, mRNA is recruited to the PIC by the eIF4F complex, allowing the recognition and binding of 5'cap structure, enabling the PIC to scan the 5' end to the AUG initiation codon, ultimately forming the 48S preinitiation complex. Thirdly, upon recognition of the AUG, GTP is hydrolyzed by eIF2 which commits the 40S ribosome to translation initiation. This leads to the recruitment of the 60S subunit and dissociation of eIF2-bound with GDP, eIF3, eIF1A, eIF4F, eIF5 and eIF1, ultimately forming the 80S ribosomal initiation complex. Once this step is complete, the 80S ribosome initiates translation of polypeptide synthesis. Lastly, GDP is exchanged for GTP by eIF2B, allowing the eIF2 complex to prepare for another cycle of protein translation[37,52,53].

However, in the presence of stressful stimuli, this pathway operates quite differently. Like mentioned previously, GDP needs to be replaced with GTP by eIF2B for eIF2 to continue initiating translation. This process is essentially halted upon activation of stress sensor kinases PKR, HRI, GCN2, and PERK, which are responsible for phosphorylating the alpha subunit of eIF2 at serine 51. The

phosphorylation of this complex acts as an inhibitor for eIF2B by conformationally changing its structure, preventing the exchange of GDP to GTP. Inhibition of the eIF2B complex drastically reduces the formation of ternary complexes, ultimately reducing global protein synthesis. Although CAP-dependent translation essentially stops, the translation of mRNAs containing upstream open reading frames (uORF) in their 5' untranslated regions (UTR) increase dramatically. It is estimated that 50% of human and mouse mRNAs contain at least one uORF, but only certain proteins are shown to be upregulated during the ISR signaling pathway[37]. Some well characterized proteins that have been consistently observed to be upregulated during the ISR involve transcription factors (TFs) such as ATF4, ATF5, CHOP, CEBPA, and CEBPB[54]. Once these proteins are translated, they will activate accordingly to the present stressor and initiate the production of downstream proteins that will aid in the recovery and repair of the cell. The goal of this selective upregulation is to halt unnecessary protein synthesis while simultaneously increasing gene expression of the appropriate cellular machinery to assist in minimizing damage until the stressor is no longer present.

Unfortunately, the ISR is not a perfect system that completely protects the cell indefinitely. For instance, the ISR can invoke different responses depending on the duration, intensity, location and type of stressor. It has been observed that prolonged or excessive stress can prompt the ISR to direct the cell to undergo programmed cell death and apoptosis[37]. This process is largely triggered by the transcription factor CHOP, which is responsible for upregulating pro-apoptotic proteins such as BIM, PUMA, and death receptor 4/5 (DR4, DR5), while simultaneously downregulating anti-apoptotic proteins like BCL-XL, and BCL2[55,56]. Although CHOP is associated with initiating these cell death pathways, its activation is largely dependent on its dimerization with other transcription factors like ATF3, ATF4 and ATF5. Therefore, the downstream targets of these proteins are greatly influenced by the presence of these dimerization partners. Specifically, the ATF4-CHOP-PPP1R15A axis of the ISR promotes cell death during periods of chronic ISR activation[57]. Despite the growing body of evidence describing the important mechanisms of the ISR, it remains unclear as to what specific conditions need to be met to induce certain

responses. Like mentioned previously, different outcomes occur depending on the duration and severity of stress that is present. These outcomes become even more complicated when you compare responses between different cell types like hepatocytes, neurons or myofibers. The complexity of this crucial pathway highlights the importance of the continuing investigation between specific stressors such as muscle disuse in the context of skeletal muscle and mitochondrial health.

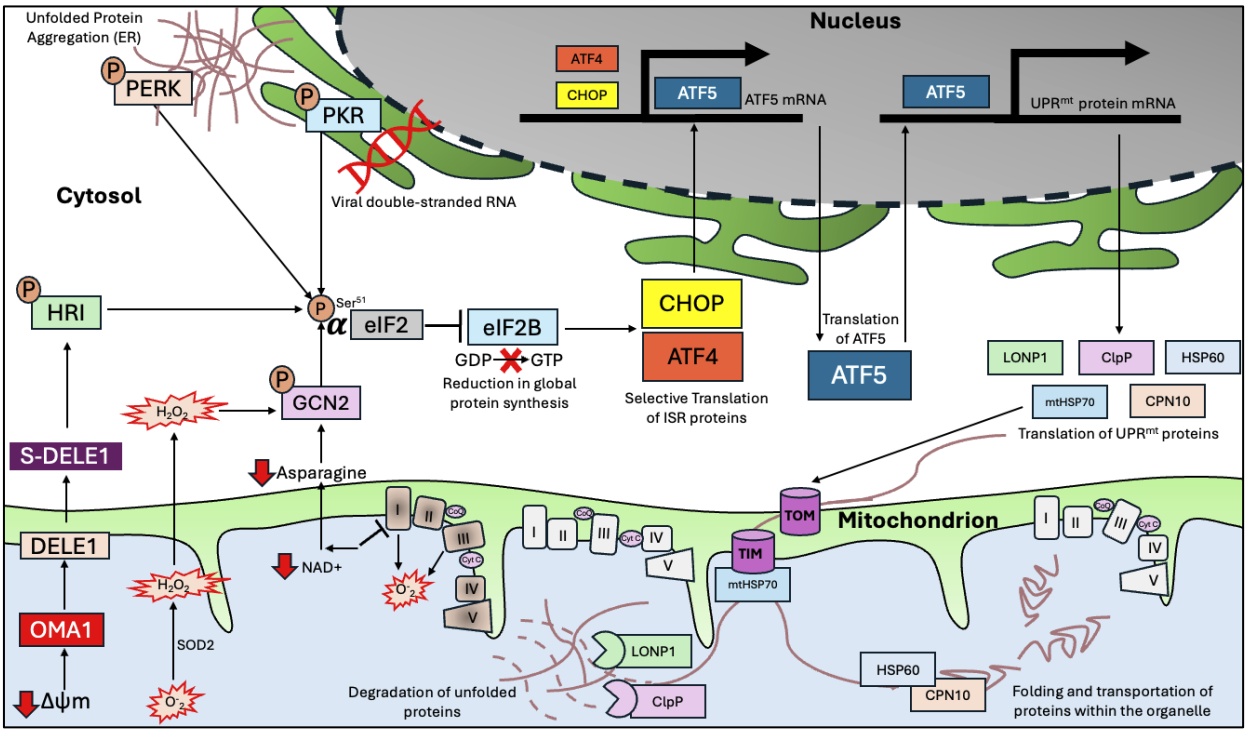

Figure 3. The Role of ATF5 during the ISR/UPR^{mt}. Mitochondrial stress triggers the activation of ER sensor kinases resulting in the subsequent phosphorylation of the alpha subunit of the eIF2 complex. Phosphorylation of this subunit causes the inhibition of the eIF2B complex, resulting in the selective translation of TFs involved in UPR^{mt} protein synthesis. Newly translated chaperones, proteases and antioxidants will then enter the mitochondria via protein important machinery and carry out their specific roles involved in protein degradation, folding/unfolding and alleviating excess mtROS accumulation.

3.1.1 ATF5 and the ISR

Activating transcription factor 5 (ATF5) is a stress responsive bZIP transcription factor that plays a major role during the ISR and differentiation pathways. Members of the bZIP family possess an amphipathic leucine zipper that allows hetero- and homodimerization via a coiled-coil domain along with a basic N-terminal section to facilitate DNA binding. Other members of this family include proteins ATF4, CHOP, CREB, FOS and Nrf-2. Specifically, ATF5 has been hypothesized to be very lenient with its binding capabilities, suggesting a large list of hetero- and homodimer partners and subsequent downstream targets[58]. The structure of ATF5 also includes a mitochondrial targeting sequence (MTS), nuclear export sequence (NES) and a nuclear localization sequence (NLS), allowing it to translocate between different cell compartments[14]. Before translation, the ATF5 gene possesses the ability to form two different mRNA variants known as ATF5α and ATF5β. Like mentioned previously, ATF5α possess an uORF in its 5'UTR, whereas ATF5β does not, allowing ATF5α to be preferentially upregulated during stress[58,59]. Evidence suggests that transcriptional activation of ATF5 is reliant on upstream ATF4 and CHOP initiation in response to cellular stress[60–62]. However, since the function of ATF5 relies on homo/heterodimerizing with other TFs, it is possible that the reduction of ATF5 content that is observed in these studies could be due to the lack of binding partners, leading to a reduction in ATF5 activity/stability, resulting in its swift degradation via Cdc34 and Rad6 E3 ligases. Using this logic, we could hypothesize that ATF5 content is largely reliant on the presence of binding partners as opposed to its content being strictly dictated by upstream transcriptional activation of other bZIP TFs like ATF4 or CHOP. Once translated, ATF5 responds to various cellular stressors such as heat shock, UPR^{er} and the UPR^{mt}. Although ATF5 has been observed to be upregulated during the UPR^{er}, studies have shown that the role of ATF5 in the presence of ER stress does not result in the upregulation of UPR^{er} chaperones or proteases, suggesting that ATF5 is primarily involved in regulating the mitochondrial UPR[63,64]. Activated ATF5 will then translocate to the nucleus with other dimerization partners and initiate the transcription of downstream proteases, chaperones and antioxidants[58]. The main goal of ATF5 and its family members is to alter the cells transcriptional

programming by upregulating proteins that are responsible for maintenance and repair until the stress is no longer present. However, ATF5 has also been reported to be involved in apoptotic pathways via CHOP mediated induction[65]. This suggests that the roles of ATF5 could extend outside the ISR, depending on the dimerization partners it interacts with.

3.2 Mitochondrial Unfolded Protein Response

The main goal of UPR^{mt} activation is to facilitate an adaptive response during prolonged periods of stress by upregulating mitochondrial specific chaperones, proteases and antioxidants. The UPR^{mt} is often activated in response to a mitochondrial proteostasis imbalance that is mainly the result of a large accumulation of irreversibly damaged and/or unfolded/misfolded proteins within the mitochondria. Just like how the ISR is activated by various types of stressors, the UPR^{mt} has its own set of activators[13,14,38–43,66]. For example, excess reactive oxygen species (ROS) production has been shown to activate the UPR^{mt} in *Caenorhabditis elegans and HeLa ovarian carcinoma cells*[67,68]. Toxins produced by bacterial infections have been shown to damage mitochondrial proteins, leading to UPR^{mt} activation[69]. Researchers have also demonstrated that inhibiting protein quality control mechanisms such as chaperone and protease activity causes UPR^{mt} activation[70]. Likewise, the absence of mitochondrial inner import proteins TIM-17 and TIM-23 was demonstrated to activate the UPR^{mt} by disrupting mitochondrial proteostasis via interfering with mitochondrial protein import[71]. It has also been demonstrated that 8-weeks of treadmill running was able to upregulate protein levels of LONP1 and ClpP in skeletal muscle of C57BL/6 mice. These levels were then further elevated when treadmill running was combined with a high fat diet[72]. Additionally, a recent paper revealed that UPR^{mt} mRNA levels were upregulated in skeletal muscle of C57BL6/N mice after an acute exercise protocol[73].

Regardless of the stressor, activation of the UPR^{mt} involves upregulation of mitochondrial protein quality control proteins. The type of protein that is selected, along with the amount that is upregulated, will largely depend on the type of stressor that is present. For example, chaperones like

HSP60, HSP70 and CPN10 (HSP10) are responsible for assisting in posttranslational transportation, folding and refolding of ER and mitochondrial proteins. Proteases like LONP1 and ClpP are responsible for degrading and recycling irreversibly damaged proteins that were either misfolded or unfolded upon translation[13,14,38–43,66]. Antioxidants like NQO1, HO1, Catalase and Glutathione Reductase aim to reduce the damage caused by excess ROS production by either quenching them directly via electron donation, repairing the damaged molecules that are affected or by interacting with gene pathways involved in ROS regulation, like the Nrf2-Keap1 axis[74,75]. Ultimately, the duration of the stressor and the effectiveness of the UPR^{mt} will determine the fate of the mitochondria. It is still undefined within the literature as to what threshold of stress the UPR^{mt} needs to become active or what level/duration of stress to become ineffective.

Much like the ISR, this topic becomes even more convoluted when you try and compare the effectiveness of the UPR^{mt} in different types of cells. For example, high levels of mitochondrial chaperone Hsp60 is associated with an advanced tumor progression in pancreatic cancer, whereas knockdown of Hsp60 decreases cell proliferation in this model[76]. High levels of the mitochondrial chaperone Hsp10 is also associated with a reduced overall survival in various cancers such as astrocytoma[77] and nasopharyngeal carcinoma[78]. Likewise, the chaperone mtHsp70 is observed to be upregulated in melanoma[79], whereas the knockdown inhibits the proliferation of various cancer lines[76,80,81]. Similar to chaperones, mitochondrial proteases LONP1 and ClpP have both been observed to be upregulated in the presence of cancer and knockdown of these proteins is associated with reduced proliferation and increased host survival[82,83]. Despite the evidence suggesting that high levels of UPR^{mt} protein content supports cancer growth and survival, other studies suggest that a heightened UPR^{mt} has a protective effect and the absence of specific mitochondrial UPR proteins can amplify negative outcomes. For instance, a study by Ozcan et al. revealed that therapeutic oral administration of chemical chaperones PBA and TUDCA normalized hyperglycemia, restored insulin sensitivity and enhanced insulin action in the liver, muscle and adipose tissue in male mice[84]. Another study administered a UPR^{mt} agonist (nicotinamide riboside) in NP cells isolated from rat lumbar intervertebral discs. They observed that an upregulated UPR^{mt} was able

to induce mitophagy to inhibit apoptosis, alleviating disc degeneration[85]. Despite the varying results in response to UPR^{mt} activation, it appears the physiological mechanisms are relatively consistent. Although many questions remain unanswered, uncovering the mechanisms of the UPR^{mt} in the context of muscle physiology could potentially lead to significant advancements in understanding how the UPR^{mt} operates varying stressful environments.

3.2.1 ATF5 and the UPR^{mt}

Since ATF5 has both a mitochondrial targeting sequence (MTS) and a nuclear localization sequence (NLS), it is heavily involved in mitochondrial-nuclear retrograde signaling during the UPR^{mt}[14,64,86]. Like previously mentioned, various forms of mitochondrial dysfunction can activate the UPR^{mt} and subsequent upregulation of ATF5 expression. Known inducers of ATF5 transcripts include accumulation of unfolded proteins in the mitochondria[87], inhibition of ETC activity and impaired mitochondrial proteostasis[88]. Upon activation, ATF5 has been observed to upregulate the expression of mitochondrial chaperones and proteases such as mtHsp70, Hsp60, Hsp27 and LONP1, along with inducing CPN10 and ClpP during the UPR^{mt}[14,64,86]. A study conducted by Fiorese et al. revealed that when ATFS-1 (the worm homologue of ATF5) was replaced by mammalian ATF5 in ATFS-1 KO *C. elegans,* UPR^{mt} chaperones and proteases were upregulated in response to mitochondrial stress. The same study also identified the presence of an MTS on ATF5, revealing that ATF5 localizes to the mitochondria in the absence of stress and translocates to the nucleus in the presence of mitochondrial stress. Likewise, knockdown of ATF5 in HEK293T cells reduced expression of Hsp60, mtHsp70 and LONP1, along with a subsequent reduction in mitochondrial respiration[64]. A study conducted by Slavin et al. revealed that ATF5 KO mice exhibited a blunted UPR^{mt} gene expression after a bout of acute exercise training[73]. Additionally, doxycycline induced activation of the UPR^{mt} was shown to be driven in an ATF5-dependent manner in mouse cardiac muscle cells. Suggesting that ATF5 and the mammalian UPR^{mt} could be potential therapeutic targets to help prevent ischemia-reperfusion injury[63]. Similarly, knockdown of ATF5 in

cardiomyocytes blunts the upregulation of UPR^{mt} proteins and decreased mitochondrial respiration in the presence of isoproterenol administration[89]. Another study observed that upregulation of ATF5 facilitates the UPR^{mt} to help protect nucleus pulposus cells from IL-1β administration[85]. Although there has been sufficient research conducted on ATF5 with regards to the UPR^{mt} and its activators in multiple models, there remains a severe lack of literature discussing ATF5 and its role in skeletal muscle, specifically during exercise or skeletal muscle.

3.3 Antioxidant Response and the UPR^{mt}

Much like chaperones and proteases, antioxidants also play a major role during the UPR^{mt}. Although antioxidants don't often directly interact with unfolded/misfolded proteins, they aim to reduce the damage caused by excess ROS production by either quenching them directly via electron donation, repairing the damaged molecules that are affected or by interacting with gene pathways involved in ROS regulation[74,75]. It is well documented that mitochondrial ROS (mtROS) production increases during periods of mitochondrial stress[90,91]. This increase in mtROS corresponds with an upregulation of antioxidants to assist in quenching and removing these damaging molecules to help reduce oxidative stress. This antioxidant system assists the UPR^{mt} to minimize mitochondrial damage until the stress is relieved. For example, antioxidant proteins such as catalase and glutathione peroxidase are known scavengers of excess mtROS and have been shown to be upregulated in tandem with UPR^{mt} proteins[41,73,85,92–94]. Other notable antioxidant related proteins that have been observed to be upregulated during the UPR^{mt} include NQO1, HO1, MnSOD[73], along with SIRT3[95] and Nrf-2[41].

Specifically, Nrf-2 is considered a master transcription factor involved in managing oxidative stress and upregulation of this protein is known to alleviate various diseases such as cancer, diabetes and inflammation[96]. Under basal conditions, Nrf-2 stability is extremely low and is quickly degraded via the ubiquitin-proteasome system. Its degradation is managed by its main regulator Kelch-like ECH-associated protein 1 (KEAP1). KEAP1 is a dimeric protein that sequesters Nrf-2 in the cytosol by acting as an adaptor

for the E3 ubiquitin ligase complex cullin 3 (Cul3), allowing the ubiquitination and constant degradation of Nrf-2 by the 26S proteasome. However, in the presence of a stressful stimuli that increases oxidative stress, cysteine residues on KEAP1 are altered, allowing Nrf-2 to dissociate and remain in the cytosol. Separated Nrf-2 can then translocate into the nucleus where it can heterodimerize with other proteins of the bZIP family. Upon heterodimerization, Nrf-2 will stabilize and bind to specific antioxidant responsive elements (AREs) to promote the subsequent upregulation of downstream antioxidant proteins[74,97]. The transcriptional activation of Nrf-2 has been demonstrated to play a significant role in regulating mitochondrial physiology and homeostasis. For example, Nrf-2 encoded proteins HO-1 and NQO1 have been observed to aid in the maintenance and removal of damaged mitochondria and promote mitochondrial biogenesis by activating Nrf-1 expression. Specifically, the main role of HO-1 is to break down heme into biliverdin, iron and carbon monoxide (CO). Increased CO binds to cytochrome c oxidase (COX), ultimately reducing cellular respiration and increasing hydrogen peroxide production (H_2O_2). Upregulated H_2O_2 levels promote the activation of the PI3K-AKT pathway, leading to the activation and nuclear translocation of Nrf-2, promoting further binding of AREs and subsequent upregulation of other antioxidant proteins. Activation of AKT can also phosphorylate Nrf-1, promoting its nuclear translocation and subsequent activation of mitochondrial biogenesis pathways[98]. Additionally, the main role of NQO1 is to catalyze toxic quinones into hydroquinones, preventing the formation of dangerous semiquinones that could potentially form other ROS molecules, ultimately reducing the potential for further mitochondrial protein damage[99]. Although these antioxidant pathways have become well documented within the literature, the interaction between Nrf-2 and its downstream targets with UPR^{mt} related proteins remains insufficient.

3.3.1 ISR and Nrf-2 Relationship

Like previously mentioned, Nrf-2 heterodimerizes with other bZIP proteins to initiate translation of downstream antioxidant proteins. However, the amount partners that interact with Nrf-2

during gene induction is controversial, suggesting that other dimerization partners may exist. For instance, Nrf-2 is known to heterodimerize with transcription factors SP-1, c-JUN and ATF4[74]. Specifically, ATF4 has been confirmed to bind with Nrf-2 via co-immunoprecipitation and mammalian two-hybrid assays. The researchers provided evidence that this interaction regulated cadmium-induced HO-1 gene expression in mouse hepatoma cells[100]. Although the association between Nrf-2 and members of the ATF/CREB family has not been previously reported, there is a strong likelihood that these proteins may often interact based off the fact they both belong to the same family of bZIP transcription factors. Building off this hypothesis, it is not unreasonable to assume that Nrf-2 and members of the ATF family form bZIP dimers with their leucine zipper structures to initiate downstream translation of ISR/UPR proteins[100]. Interestingly, it has been demonstrated that Nrf-2 phosphorylation can be induced by the ISR sensor kinase PERK, leading to its activation. This kinase also initiates the upregulation and activation of the ATF4-CHOP pathway during ER stress[101]. Likewise, ATF5 is classified under the ATF/bZIP family and protein sequence comparison reveals that both human and mouse ATF5 domains share a 55% similarity with ATF4, a known binding partner of Nrf-2[86]. Although there have been no reports observing the interaction between ATF5 and Nrf-2, a strong argument can be made that ATF5 could potentially bind with Nrf-2, much like ATF4.

3.4 Other Roles of ATF5 in Various Cell Types

Despite being heavily involved in the UPR^{mt}, the roles of ATF5 have expanded within the past decade, with many studies revealing its responsibilities in various survival pathways in different cell types. Specifically, the presence of ATF5 has been observed in cell types such as cardiac tissue[63,102], neurons[103], kidney cells[104], adipose tissue[105], hepatocytes[80,106,107] and osteoblasts[108]. In cardiac tissue, it was observed that PGC-1α and ATF5 form a signaling axis to initiate a protective role in transverse aortic constriction-induced cardiac hypertrophy and oxidative stress via partial activation of the UPRmt[102]. With regards to neuronal cells, ATF5 is highly expressed in neural stem and progenitor cells. This has resulted in a large

body of research dedicated to understanding its role during neurogenesis. Likewise, it was discovered that regulated levels of ATF5 is required for the progression of neural progenitor cells to neurons, suggesting that ATF5 plays a causal role in regulating neuronal differentiation[103]. In the presence of diabetic kidney disease, suppression of ATF5 reduced oxidative stress and apoptosis during tubulointerstitial injury, suggesting that high levels of ATF5 expression can also be detrimental during certain pathological conditions. In adipose tissue, ATF5 forms a complex with transcription factor *C/EBP*β and p300. The p300-dependent acetylation of ATF5 upregulates that transactivation of C/EBP*α* via C/EBP*β*, resulting in adipocyte differentiation[105]. Hepatocytes are another cell-type where ATF5 is highly expressed. Researchers revealed that arsenite-induced CHOP protein expression was reduced in the absence of ATF5 expression in human hepatoma HepG2 cells[80]. These findings reveal ATF5 could be a potential regulator of CHOP-induced apoptosis in this cell model. Lastly, a study conducted by Leong et al. revealed that ATF5 is downregulated during osteogenic differentiation. This finding was not observed in pre-osteoblastic cells, suggesting that ATF5 has a specific role in regulating the osteogenic differentiation of adult stem cells by acting as a negative regulator[108]. This finding could provide insight into controlling adult stem cell differentiation, leading to potential implications for regenerative medicine.

Although ATF5 has been demonstrated to promote survival in normal cell models, it has been hypothesised that ATF5 could play a negative roll in the progression of many types of cancer lines. Expression of ATF5 is highly upregulated in various forms of cancer such as breast, lung, ovarian, pancreatic, and rectal carcinoma[58]. Additionally, ATF5 has been the most investigated in glioma brain tumors[109]. A common theme amongst these cancer models reveals that ATF5 expression is inversely correlated with overall patient/cell survival, and inhibition of ATF5 activity promotes healthy cell survival and reductions in tumor growth[58]. For example, a study by Nukuda et al. observed that ATF5 upregulated the invasiveness of breast cancer cell lines, while siRNA knockdown of ATF5 reduced it[110]. Another study revealed that ATF5 promotes lung cancer development, poorer patient prognosis and increases the resistance to cancer treatment[111]. Additionally, interfering with ATF5 activity via transient transfection of

dnATF5 substantially increased apoptotic activity, along with a downregulation of anti-apoptotic protein BCL-2 expression in ovarian cancer cells[112]. Likewise, ATF5 overexpression is associated with the development of pancreatic cancer and has been shown to induce BCL-2 expression and inhibit BAX, promoting the survival of these cells[113]. Interestingly, although ATF5 has been observed to promote cancer progression in previous models, ATF5 may elicit tumor suppressive roles in hepatocellular carcinomas (HCCs). Previous studies revealed that ATF5 expression was significantly reduced in HCCs when compared to normal hepatic tissue and overexpression of ATF5 resulted in a 50% reduction in cancer growth compared to controls[114]. Although there is a substantial amount of research observing ATF5 in various cell types and cancer, there remains gaps within the literature with regards to skeletal muscle physiology, specifically in the presence of muscle disuse, cancer cachexia or sarcopenia.

4.0. Sex-Specific Adaptations of the ISR/UPR^{mt}

In recent years, a growing body of literature has been conducted on researching the differences between sex specific and sex related adaptations to chronic stress, diseases and genetic disorders. Some examples of these pathologies include depression[115], epilepsy[116], myopathies[117], and organ failure or dysfunction[118]. These illnesses are often characterized by sex-specific differences in severity and adaptation responses. Specifically, it has been observed that females are significantly more prone to developing muscle weakness during prolonged hospital visits[119]. It was also reported that female mice experienced higher catabolic and autophagy signaling in response to chronic muscle disuse compared to male controls[120]. A study conducted by Oliveira et al. revealed that female mice exhibit a greater expression of lysosomal and autophagy proteins after 7 days of denervation. However, despite this enhanced autophagic capacity, female mice experienced a decrease in mitophagy flux following denervation and a subsequent increase in the accumulation of dysfunctional organelles. This decrease in mitophagy was associated with the preservation of COX activity following denervation, most likely due to the accumulation of dysfunctional mitochondria[121]. A study revealed the presence of sexually dimorphic

mechanisms to proteasome activation in the presence of doxycycline treatment in the central nervous system of male/female mice. Female mice exhibited a greater baseline proteasome activation when compared to male matched controls. This response was also consistent in the presence of doxycycline treatment via significantly reducing the presence of K48Ub-linked proteins in the brain of males, but not in females[122]. With regards to the ISR and UPR^{mt}, limited data has been conducted on sex-specific adaptations of ISR/UPR^{mt} activation, especially in skeletal muscle in the presence of chronic muscle disuse. One study observed that ATF4 expression was significantly upregulated in the CNS of female mice with doxycycline treatment when compared to male controls[122]. Interestingly, a study revealed that misfolded protein accumulation within the mitochondrial intermembrane space (IMS) induced the UPR^{mt} via activation of estrogen receptor alpha (ERα) in a familial ALS disease mouse model. Since females have a greater abundance of ERα content and activity, researchers observed a significant sex difference in IMS-UPR^{mt} activation in female mice spinal cords compared to male matched controls[123]. These findings highlight the importance of identifying sex-specific stress adaptations of the ISR/UPR^{mt}. Since these pathways act as a defence mechanism to cellular stress, it is likely that many sex differences remain undiscovered in other pathological conditions such as extreme muscle atrophy. Exploring the sex differences of these crucial stress response pathways can lead to future advancements for designing efficient medical interventions for patients.

RESEARCH OBJECTIVES

Based on the literature mentioned above, the objectives of my thesis were to:

1. Examine the effect of denervation-induced chronic muscle disuse on ATF5 related UPR^{mt} downstream and upstream targets in skeletal muscle of wild-type (WT) and ATF5 deficient (ATF5 KO) mice;
2. Observe the response of mitophagy related proteins in mice lacking ATF5;
3. Evaluate the change in mitochondrial content after denervation in ATF5 KO mice;
4. Compare the quality of the mitochondrial pool between these conditions;
5. Monitor any sex-specific adaptations of UPR^{mt} protein markers in male/female WT and ATF5 KO mice;

HYPOTHESES

We hypothesized that:

1. ATF5 deficient mice would exhibit a reduced UPR^{mt} in response to denervation when compared to their WT controls;
2. ATF5 deficient mice would observe a heightened mitophagy response when compared to WT controls;
3. Mitochondrial content would be reduced in ATF5 KO mice when compared to WT controls;
4. Mitochondrial quality would be reduced in ATF5 KO mice when compared to WT controls;
5. There will be a difference in UPR^{mt} protein makers between sexes in WT and ATF5 KO mice;

CHAPTER 2: MANUSCRIPT

ATF5 IS REQUIRED FOR THE NORMAL STRESS RESPONSE DURING SKELETAL MUSCLE DENERVATION

Jared Kuthe and David A. Hood

Muscle Health Research Centre, School of Kinesiology and Health Science, York University, Toronto, Ontario, M3J 1P3, Canada

To whom correspondence should be addressed:

David A. Hood, PhD. (dhood@yorku.ca)
Muscle Health Research Centre
School of Kinesiology and Health Science
York University, Toronto, ON M3J 1P3, Canada

ABSTRACT

Chronic muscle disuse induces significant muscle atrophy, a decrease in mitochondrial content and an increase in organelle dysfunction. The main line of defence in response to these consequences includes the Integrated Stress Response (ISR) and the Mitochondrial Unfolded Protein Response (UPR^{mt}). These pathways aim to restore cellular homeostasis by reducing global protein synthesis while simultaneously activating specific transcription factors such as ATF5 to induce changes in gene expression. The objective of the current study is to better characterize the possible regulatory role of ATF5 on the UPR^{mt} during mitochondrial stress brought about by chronic muscle disuse, induced by denervation. Denervation resulted in a significant decrease in muscle mass in all hindlimb muscle groups. These results were supported by the significant increase in total p62, LC3I/II, and Beclin1 protein levels, along with a significant elevation in mitochondrial ROS production. ISR activation was confirmed by significant increases in ATF4, CHOP and total eIF2α protein levels in WT animals, but was significantly blunted in the absence of ATF5. Likewise, certain proteins of the UPR^{mt} were impaired in ATF5 KO mice following denervation. Antioxidant proteins NQO1 and HO1 were significantly lower in ATF5 KO mice compared to WT controls. However, mitochondrial content, estimated using COX activity and SDH staining, was higher in the absence of ATF5. This was accompanied by an increase in mitochondrial quality, shown by an elevation in mitochondrial respiration. In conclusion, the lack of ATF5 appears to negatively affect the normal ISR, UPR^{mt} and antioxidant response in the presence of denervation.

Introduction

Skeletal muscle comprises 40% of total body mass and is necessary for controlling locomotion, regulating metabolism, and preserving quality of life[1,2]. However, an increased prevalence of inactivity during injury, illness or prolonged muscle disuse can result in the significant loss of muscle mass and strength[1,3–5]. One cause for this decrease in muscle mass is thought to be the result of the accumulation of dysfunctional mitochondria within skeletal muscle cells during these circumstances[1,3–5]. Mitochondria are organelles that are abundant in mammalian eukaryotic cells and have various responsibilities such as cellular energy production, apoptosis, calcium signaling, and responding to cellular stressors[6]. However, when mitochondria experience abnormal amounts of stress, these pathways become dysfunctional. These defects lead to decreased energy production in the form of ATP, increased levels of mitochondrial reactive oxygen species (mtROS) and accumulation of mutated mitochondrial DNA (mtDNA), all of which can contribute to the deterioration of muscle mass[6]. Thus, maintaining mitochondrial homeostasis is critical for preserving the optimal health of skeletal muscle.

Mitochondria are comprised of roughly 1200 proteins that are nuclear-encoded, with 13 more representing gene products encoded by mtDNA[7,8]. This large import demand of nuclear-encoded proteins requires a precise and complex communication system to ensure that processes like transcription, translation, translocation, folding/unfolding, and degradation are being balanced in response to different cellular conditions[7,8]. The integrated stress response (ISR), endoplasmic reticulum unfolded protein response (UPR^{ER}), and the mitochondrial unfolded protein response (UPR^{mt}) are the main systems responsible for reacting to different levels of cytosolic stress and mitochondrial proteostasis imbalances[7–16].These pro-survival pathways act to restore cellular homeostasis or induce programmed cell death if the stressor cannot be relieved[7–16].

The protein known as Activating Transcription Factor 5 (ATF5) has been shown to play a vital role in the ISR and UPR^{mt} during periods of cellular stress[17–27]. ATF5 is a part of the activating transcription

factor/cyclic adenosine monophosphate (cAMP) response element binding protein family and is known to be involved in a wide array of physiological processes in various types of tissue and species[17–27]. Some roles include regulating the transition of neuro-progenitor cells to postmitotic neurons[20], binding to transcription factors during differentiation of pre-adipocytes[21], regulating osteogenic differentiation in adipose-derived stem cells[22], enhancing hepatic functions in stem cell-derived hepatocytes[23], regulating ER stress and apoptosis in pancreatic beta cells[24], and initiating the mitochondrial UPR^{mt} during recovery after heart failure[25]. Additionally, a growing body of evidence suggests that ATF5 is involved in many pro-survival pathways, such as the UPR^{mt}, UPR^{er}, ISR and heat shock response (HSR) in skeletal muscle[17,18,27]. During cytosolic stress, ATF5 enters the nucleus and initiates the transcription of downstream proteases and chaperones that are involved in managing the accumulation of unfolded/misfolded mitochondrial proteins[17–26]. Although this process has been observed in *C. elegans*[18], cancer cells[26], and various organs[20–25], the involvement of ATF5 during the ISR/UPR^{mt} in skeletal muscle lacks extensive research.

The ISR is recognised as the main pathway that ultimately decides the fate of the cell depending on the level and duration of cellular stress. The first reaction involves specialized ISR sensor kinases known as PERK, GCN2, PKR, and HRI, each of which responds to their own distinct environmental and/or physiological stressor[15,16,28]. Once activated, these kinases will phosphorylate the α-subunit of the eukaryotic translation initiation factor 2 (eIF2) complex on Ser^{51} [15,16,28]. The phosphorylation of this subunit reduces gene expression by blocking the eIF2β-mediated exchange of GDP for GTP, resulting in the global attenuation of 5'-Cap-dependent protein synthesis[15,16,28]. During this process, specific downstream transcription factors that do not require Cap recognition, such as Activating Transcription Factor 4 (ATF4), C/EBP Homologous Protein (CHOP) and ATF5, are translated[15,16,28]. Once these proteins have been synthesized within the cytosol, they will form heterodimer pairs with other members of the bZIP family and translocate to the nucleus to initiate the transcription of downstream ISR proteins that are involved in the UPR^{mt} [15,16,28].

The UPR^{mt} coincides with the ISR to help mediate mitochondrial recovery and is thought to be reliant on the expression of ATF5 and its downstream targets[7,8,10,17,18,29–37]. As mentioned previously, the role of ATF5 during the UPR^{mt} is to localize to the nucleus and initiate the transcription of specific genes to assist in alleviating mitochondrial stress[7,8,29,30,32,34]. Previous studies in other cell types have identified some downstream targets of ATF5 include chaperones HSP60, HSP10, HSP27 and mtHSP70, along with proteases LONP1 and ClpP[8,18,32–34]. These proteins are responsible for managing the accumulation of unfolded and misfolded mitochondrial proteins through processes such as refolding, transporting and/or degradation[8,18,32–34]. Evidence also shows that mice lacking ATF5 have a significant decrease in antioxidant capacity, along with an increase in mtROS and a decrease in mitochondrial respiration[17]. These findings suggest that ATF5 plays a protective role during the UPR^{mt} and could potentially be an contributor to mtROS attenuation during periods of metabolic stress.

To create a cellular environment that favours mitochondrial dysfunction and subsequent activation of the UPR^{mt}, a 7-day denervation protocol was employed in the current study. Previous research has shown that denervation leads to enhanced mitophagy, inflammation, oxidative stress and metabolic disturbance in skeletal muscle[3,38–49]. Results have shown an increase in various mitophagy markers, decreased oxygen consumption, increased mtROS production, decreased antioxidant efficiency and impaired energy production after various timepoints of denervation[3,38–49]. Additionally, researchers have also investigated the sex-specific adaptations to denervation and found that female mice exhibited a higher lysosomal content and mitophagy flux compared to males[40,50]. To further explore these phenomena, we investigated whether the absence of ATF5 would have a significant impact on various UPR^{mt} markers and mitochondrial function in skeletal muscle of male and female WT and ATF5 KO mice in the presence of denervation.

Therefore, the purposes of this study was to 1) examine the effect of denervation-induced chronic muscle disuse on ATF5 related UPR^{mt} downstream and upstream targets in skeletal muscle of wild-type (WT) and

ATF5 deficient (ATF5 KO) mice, 2) observe the response of mitophagy related proteins in mice lacking ATF5, 3) evaluate the change in mitochondrial content after denervation in ATF5 KO mice, 4) compare the quality of the mitochondrial pool between these conditions, and 5) monitor any sex-specific adaptations of UPR^{mt} protein markers in male/female WT and ATF5 KO mice. We hypothesized that the absence of ATF5 wouls lead to an attenuation of the UPR^{mt} response, exacerbate the mitophagy signaling pathway, and impair mitochondrial function in skeletal muscle. We also anticipate the presence of a sex-specific UPR^{mt} adaptation to denervation.

Methods

Animals. ATF5 whole-body KO mice were generated by crossing $ATF5^{tm1(KOMP)}$ (Velocigene Project 11,612) heterozygotes in a C57BL6/N background, generously provided by Dr. Stavros Lomvardas from Columbia University, with FVB WT females. Wild-type (WT) and whole-body ATF5 knockout (ATF KO) male and female mice were housed and bred within a vivarium which operates on a 12-hour day and night cycle with open access to food and water. Mice that were 5-7 months of age were separated into either wild-type control (CON) or ATF5 knock-out (KO) groups.

Genotyping. To determine the samples genotype, ear clippings were taken from each animal to make DNA extracts. Each sample is mixed with JumpStart REDTaq polymerase (P0982, Sigma), forward and reverse primers (50 μM) for the WT and ATF5 gene. Samples were then run on 1% agarose gels and visualized using ethidium bromide with the Invitrogen imaging instrument (iBright CL 1500 imaging system, ThermoFisher).

Denervation surgery. Male and female mice (5-7-month/age) underwent a 7-day denervation protocol. Mice were anesthetized using isoflurane and had a 2 to 3 mm section of their sciatic nerve surgically removed from their left hindlimb to induce chronic muscle disuse. The contralateral right hindlimb of the 7-day-denervation animals served as the intra-animal control and were sham-operated. Animals were

housed with open access to food and water for the duration of the protocol. Following denervation surgery, water supplemented with amoxicillin (0.3 mg/L) was provided, and meloxicam injections (0.05% solution in saline) were administered for the first 2 days post-surgery for pain management (first dose: 2mg/kg body weight, second dose: 1mg/kg body weight). After 7 days, mice were anesthetized using isoflurane and tissue samples for the tibialis anterior (TA), extensor digitorum longus (EDL), gastrocnemius (GAS), and soleus (SOL) tissues from both the sham-operated and DEN leg were collected for analysis. Samples were frozen in liquid nitrogen and stored at -80º C for future data analysis. Following tissue removal, the mice were euthanized via cervical dislocation. All animal experiments have been approved by the York University Animal Care Committee under the auspices of the Canadian Council of Animal Care.

Whole muscle protein extracts. Protein extracts were prepared from frozen mouse tissue from ATF5 KO, and WT animals using the Sakamoto muscle extraction procedure. Approximately 25-30 grams of tissue was weighed and mixed with an extraction buffer containing protease and phosphatase inhibitors. The tissues were then homogenized using the Qiagen TissueLyser II at 30Hz for 1-minute intervals until the samples were completely liquified. Samples were then centrifuged at 14,000x gravity for 10 minutes at 4º C and the supernatant fraction was collected and stored at -80 º C for future experimentation.

Western Blotting. To ensure an equal protein concentration across samples, a Bradford assay was performed on the TA and GAS protein extracts from ATF5 KO, and WT mice. Western blot samples were then prepared according to a pipette plan using the mean protein concentration from the Bradford assay procedure. Samples (20 µg) were loaded on 10-15% SDS-PAGE gels and separated by electrophoresis at 120V [3 Amps, and 300 Watts] for 90 to 120 minutes. Samples were then transferred onto a nitrocellulose membrane and inserted into a transfer apparatus for another 105 minutes at 120V [3 Amps, and 300 Watts]. The membranes were then soaked in Ponceau Red until incorporated and rinsed with ddH2O before imaging. Once the desired proteins are cut from the membrane, they were then washed with 1x Tris-Buffered Saline with Tween for 3 minutes (TBS-T). The membranes were then blocked with 5% skim

milk in 1x TBS-T for 1 hour and incubated with the appropriate primary antibodies overnight at 4ºC. The next day, membranes were washed 3 times for 5 minutes and then incubated with the matching secondary antidotes for 1 hr at room temperature. Blots were then washed another 3 times for 5 minutes and imaged using enhanced chemiluminescence with the iBright CL1500 Imaging System. Quantification was performed using ImageJ software and all samples were normalized to their respective ponceau loading control.

Cytochrome c Oxidase activity. Frozen portions of GAS muscle were lysed in enzyme extraction buffer using the Qiagen TissueLyser II and sonicated for 3x3 sec, at 30% power. A buffered test solution containing fully reduced horse heart cytochrome c (C2506-1G, SIGMA) was prepared and incubated at 30°C for 15 minutes, then combined with enzyme extracts. Next, 50µl of the whole muscle homogenate was pipetted into a 96-well plate. Lastly, the maximal oxidation rate of fully reduced cytochrome c was measured by the absorbance at 550 nm at 30ºC using a microplate reader[51].

High-resolution respirometry and ROS emission. High-resolution respirometry (Oxygraph-2 K, Oroboros Instruments) was performed on a section of the sham-operated and denervated GAS. Fibers were mechanically separated in ice-cold biopsy preservation solution buffer (2.77 mM CaK_2EGTA, 7.23 mM K_2EGTA, 7.55 mM Na_2ATP, 6.56 mM $MgCl_2 \cdot 6H_2O$, 20 mM taurine, 15 mM Na_2 phosphocreatine, 20 mM imidazole, 0.5 mM DTT, 50 mM 2-(*N*-morpholino) ethanesulfonic acid hydrate, and pH 7.1), permeabilized in biopsy preservation solution with 40 µg/µl saponin at 4 °C for 30 min, and washed in buffer Z (105 mM K-2-(*N*-morpholino) ethanesulfonic acid, 30 mM KCl, 10 mM KH_2PO_4, 5 mM $MgCl_2 \cdot 6H_2O$, 1 mM EGTA, 5 mg/ml bovine serum albumin, and pH 7.4). Fibers were then incubated in the chamber with oxygenated buffer Z supplemented with 10 µM of Amplex-Red to measure ROS production as well as 1 µM blebbistatin (catalog no.: B592500; Toronto Research Chemicals) to prevent tetanus of the muscle and 25 U/ml Cu/Zn SOD1 to convert O_2^- to H_2O_2 and 2 mM EGTA. After obtaining background values, substrates were titrated as follows to assess respiration and

ROS production: pyruvate–malate (complex I, state 2), ADP (complex I, state 3), and succinate (complex I and II, state 3).

Histology and cross-sectional area: EDL muscle from CON and DEN hindlimb were extracted from the animal, mounted in Cyromatrix (Thermo Fisher Scientific), frozen in isopentane at the temperature of liquid nitrogen and stored in -80º C for future sectioning. Muscles were then cut into 10 μm cross sections using the cryostat instrument (Lecia CM1950). Cross sections were transferred onto glass slides and incubated with an SDH-staining solution (0.2 M sodium succinate, 0.2 M phosphate buffer, pH 7.4 and nitro blue tetrazolium) at 37 º C for 20 min. Slides were then rinsed with distilled water, and a microscope cover glass was mounted on slides using DPX mountant for histology (catalog no: 06522; Sigma). Photos of muscles sections were taken using a Samsung Galaxy S10e smartphone.

Statistical Analyses. All data collected was analyzed using GraphPad Prism 10.0, and values were expressed as means ± SD. Comparisons between SHAM operated and denervated of WT and ATF5 KO tissue weights were analyzed using a two-way ANOVA with repeated measures. Comparisons between DEN and matched sham-operated samples from WT and ATF5 KO animals were evaluated using two-way ANOVA with repeated measures for all protein, tissue weights, COX activity, respiration, and ROS data. Statistical significance was considered as $p \leq 0.05$.

Results

Seven days of denervation leads to a reduction in muscle mass in ATF5 KO and WT male/female mice. The ATF5 KO mouse model was confirmed via DNA genotyping based on the presence of the mutant ATF5 gene and the absence of the WT gene (Fig. 1A). To confirm the effectiveness of the 7-day denervation protocol, we measured the wet weight of the denervated and sham-operated GAS and SOL of young male and female mice. Upon denervation, every group experienced a similar loss of muscle mass in the both the SOL and GAS muscle groups ($P<0.05$) (Fig. 1B-C). Both male ($P<0.0001$) and female ($P<0.001$) ATF5 KO mice had significantly less total bodyweight when compared to their WT controls.

Male KO mice exhibited the greatest reduction, revealing a 35% reduction in weight compared to 22% in females (Fig. 1D). Interestingly, there was a significant effect of genotype when comparing epididymal fat in male WT and KO mice ($P<0.0001$) (Fig. 1E). Results suggest that female mice could be more resilient to the phenotype changes brought upon by absence of ATF5 when compared to male matched controls.

Mitochondrial content after seven days of denervation in WT and ATF5 KO male/female mice. To observe the effect of chronic muscle disuse on mitochondrial content in ATF5 KO mice, we visualized the effect of denervation on SDH histochemical staining (Fig. 2B) and cytochrome c oxidase activity (Fig. 2A). Denervated muscle displayed an observable reduction in SDH stain intensity in WT mice. However, this reduction was not observed in KO mice. Likewise, our results revealed a reduction in COX enzyme activity in response to denervation within the WT group, with an attenuation observed in KO mice for both male and female groups ($P<0.05$). Male WT mice experienced a 32% reduction in COX enzyme activity in response to denervation, with KO counterparts experiencing a 10% reduction (Fig. 2B). Likewise, we observed a 26% reduction in COX enzyme activity in female WT mice, with only an 8% reduction in KO counterparts. Results could suggest that the absence of ATF5 can greatly affect mitochondrial adaptations to denervation.

High resolution respirometry and ROS emissions of WT and ATF5 KO mice. To assess the quality of the mitochondrial pool in ATF5 KO mice, we performed high resolution respirometry and ROS emission analysis. There were no significant changes in mitochondrial respiration in WT mice in response to denervation when normalized to COX activity (Fig. 3A-C). Consistent with SDH staining and COX activity levels, ATF5 KO mice preserved mitochondrial respiration post-denervation in all groups. This was displayed by a 29% increase in P+M/ADP supported respiration ($P<0.05$) (Fig. 3B) and a 43% increase in succinate supported respiration ($P<0.05$) (Fig. 3C) in knockout mice post denervation. This increase in respiration after denervation in the KO group resulted in a 27% greater abundance of P+M-

supported respiration, along with a 12% and 23% increase in P+M/ADP and succinate-supported respiration post denervation when compared to WT denervated controls, respectively. When normalized to COX activity, an increase in ROS emission was observed during P+M supported respiration ($P<0.05$), with a trending increase across all other active respiratory states in WT mice in response to denervation. Likewise, a significant increase was observed in ATF5 KO mice in all groups ($P<0.05$) (Fig. 3D-F). The results suggest that although KO mice express a greater abundance of mitochondrial content compared to WT mice, the quality of the mitochondrial pool is comparable in the presence of denervation.

Mitophagy-related protein expression response to denervation in young WT and ATF5 KO mice. To observe the response of mitophagy-related proteins in mice lacking ATF5, we evaluated various mitophagy and autophagy protein markers in the TA of WT and ATF5 KO male/female mice. There was no significant change in basal mitophagy protein levels between genotypes in sham-operated TA in all groups. However, we observed a significant elevation of P62 ($P<0.01$) and Beclin1 ($P<0.05$) protein expression ranging from 26 to 75% in both WT and KO groups in response to 7 days of denervation (Fig. 4A-B). These findings were consistent with previous studies that investigated the mitophagy response during various time points of denervation[3,38–49]. Female WT mice experienced a 75% increase in P62 protein expression ($P<0.0001$) in response to denervation, with male WT mice experiencing a 58% increase ($P<0.001$). Likewise, a 48% increase in Beclin1 protein expression ($P<0.0005$) was observed in female WT mice, with a similar increase of 49% in male WT mice ($P<0.05$). Female WT mice experienced an 84% increase in LC3 I protein expression ($P<0.0001$) compared to the 53% increase observed in male WT mice ($P=0.055$). This same trend was observed with LC3 II expression, revealing an 85% ($P<0.001$) and 41% increase in female and male WT mice, respectively. Despite this difference in LC3 upregulation, the ratio between LC3 I and II was similar between all groups. This difference between male and female protein expression was absent in the ATF5 KO groups. The results suggest that ATF5 KO male and female mice could exhibit a different mitophagy/autophagy response in the presence of denervation.

ISR related protein expression in response to denervation in young WT and ATF5 KO mice. To assess the upstream activation of the ISR after 7 days of denervation in the absence of ATF5, the protein expression of ATF4, CHOP, t-eIF2α and p-eIF2α was measured in the TA of WT and ATF5 KO male/female mice (Fig. 5A-D). In previous studies, the transcription factors ATF4 and CHOP have been shown to be upregulated in response to denervation[42]. Likewise, our data revealed increases ranging from 53 to 84% in ATF4 ($P<0.01$) (Fig. 5A), CHOP ($P<0.0001$) (Fig. 5B) and t-eIF2α ($P<0.001$) (Fig.5D) after 7 days of denervation in all groups. However, there were no significant effect of denervation on phosphorylated eIF2α (Fig5C). The upregulation of ATF4 appears to be blunted in ATF5 KO male mice ($P<0.01$), with a similar trend in female mice in response to denervation. Likewise, CHOP protein expression in denervated hindlimbs was blunted in both male ($P<0.001$) and female KO mice ($P<0.01$). This response was also observed with total eIF2α in female KO mice (0.05), with a similar trend in male KO mice ($P<0.11$). When normalized to total eIF2α, phosphorylated eIF2α was higher in the sham-operated hindlimbs of female WT mice ($P<0.01$), with a similar trend in KO sham-operated hindlimbs ($P=0.053$). This trend was not observed in male WT mice but was elevated in male KO sham-operated hindlimbs ($P<0.05$). The data suggest that the absence of ATF5 could impact the protein levels of other transcription factors involved in ISR activation during chronic muscle disuse.

UPR^{mt} related protein expression in response to denervation in young WT and ATF5 KO mice. We measured the protein content of downstream UPR^{mt} targets during denervation in WT and ATF5 KO male/female mice (Fig. 6A-E). A trending increase in protease LONP1 ($P=0.12$) was observed in male WT mice with no significant changes in the KO group. Female WT mice experienced a 49% increase in LONP1 content ($P<0.01$), but this response was blunted in female KO animals ($P<0.05$) (Fig.6A). Similarly, no significant changes in chaperone mtHSP70 expression were observed in male WT mice in response to denervation, while both WT and KO female mice experienced a 58% ($P<0.01$) and 40% increase ($P<0.05$), respectively. The protein levels of chaperone HSP60 were upregulated in both male and female WT mice post denervation by 36% and 43%, respectively ($P<0.05$). This response was

attenuated in the KO groups for both sexes (Fig.6C). Consistent with proteins LONP1 and mtHSP70, there was no significant increase in both protease ClpP (Fig.6D) and chaperone CPN10 in male WT mice post denervation (Fig.6E). Meanwhile, elevated levels of ClpP ($P<0.05$) and CPN10 ($P<0.01$) were observed in denervated hindlimbs of WT female mice. When we compared the fold change of the UPR^{mt} between genotypes post denervation, male KO mice exhibited a blunted ClpP ($P<0.05$) and CPN10 (31%) response. Likewise, female KO experienced a reduced LONP1 ($P<0.05$), CPN10 ($P=0.083$), mtHSP70 (31%) and HSP60 (34%) response to denervation. The results suggest that the absence of ATF5 could lead to an impaired UPR^{mt} during periods of chronic muscle disuse. Additionally, much like the autophagy/mitophagy response in female mice, the results suggest the presence of a sex-specific UPR^{mt} during chronic muscle disuse.

Antioxidant related protein expression and COX enzyme activity in denervation in young WT and ATF5 KO mice. Evidence suggests that ATF5 may play an important role during metabolic processes and regulating antioxidant expression[17]. Thus, we wanted to investigate how the absence of ATF5 would impact the total protein content of antioxidant markers in the presence of denervation (Fig. 7A-E). The protein content of Nrf-2 was measured in male and female ATF5 KO mice in response to denervation (Fig.7A). A trending upregulation of Nrf-2 protein expression ($P=0.067$) was observed in female WT mice, which was not as pronounced in male WT controls. Interestingly, male KO mice experienced a 38% increase in Nrf-2 expression, almost matching the 40% and 35% increase in female WT and KO mice, respectively (Fig.7A). The protein expression of NQO1 was increased by 38% in WT male mice in response to denervation ($P<0.05$). This response was lower in both sham-operated and denervated hindlimbs by 90% ($P<0.001$) and 75% ($P<0.0001$) in male KO mice, respectively. Likewise, we observed a 63% decrease ($P<0.01$) in NQO1 expression in sham-operated hindlimbs and a 51% ($P<0.01$) decrease in denervated hindlimbs in female KO mice. The protein expression of antioxidant catalase (Fig.7D) was increased by 36% ($P<0.05$) and 63% ($P<0.001$) in both male and female WT mice in response to denervation, respectively. This response was similar in both male and female KO mice ($P<0.001$).

However, basal levels of catalase appear to be significantly lower in the sham-operated hindlimbs of male KO animals ($P<0.05$). Likewise, the protein expression of glutathione reductase was elevated by 29% ($P=0.0503$) and 30% ($P<0.0001$) in both male and female WT mice in response to denervation, respectively (Fig. 7E). This trend was also observed in KO animals with a 35% ($P<0.05$) increase in male and a 20% ($P<0.001$) increase in female denervated hindlimbs. The results suggest that female mice not only exhibit biological differences in mitophagy and UPR^{mt} activation compared to males but may also possess variances in antioxidant expression in response to chronic muscle disuse. Additionally, the ablation of ATF5 could negatively alter total antioxidant-related protein content, which is further exacerbated in the presence of denervation.

Lysosomal protein content in response to denervation in WT and ATF5 KO mice. To assess differences in lysosomal protein content, immature/mature cathepsin B and LAMP1 were measured in ATF5 KO mice in response to denervation (Fig.8 A-B). The protein expression of immature cathepsin B was increased by 66% in both male ($P<0.001$) and female WT mice ($P<0.0001$) in response to denervation (Fig.8A). This response was blunted in both male ($P<0.01$) and female ($P<0.05$) KO animals. The protein expression of mature cathepsin B protein levels was elevated by 42% ($P=0.059$) and 56% ($P<0.01$) in both male and female WT animals, respectively. This response was further elevated in both male and female KO animals revealing a 73% increase in male ($P<0.05$) and a 65% increase ($P<0.001$) increase in female denervated hindlimbs. The ratio of mature to immature cathepsin B was significantly higher in the sham-operated legs of female KO mice when comparted to WT sham-operated controls ($P<0.05$). Denervation induced a significant upregulation of LAMP1 protein expression in male KO mice ($P<0.05$), with a trending increase in male WT mice ($P=0.07$) (Fig.8B). This response was not observed in the female cohort. The results suggest that the absence of ATF5 reduces the induction of certain lysosomal markers in the presence of chronic muscle disuse in a sex-specific manner.

Discussion

Phenotype differences between sex and genotypes

Mice subjected to 7 days of denervation experienced a significant loss in normalized and raw wet muscle weight (mg) in most muscle groups (Fig.S2E-H). However, this reduction in skeletal muscle does not explain the drastic difference in bodyweight between genotypes that we are observing. A previous paper revealed that the level of ATF5 expression in mice directly correlated with adiposity[21]. This finding is supported by the significant difference in epididymal fat deposits we have observed in our male KO mice model. Additionally, the amount of muscle per gram of bodyweight was substantially higher in KO mice. This observation is most likely the result of the significant difference in bodyweight and adipose tissue affecting the normalized values in the KO cohort. The results suggest that although KO mice appear to experience a greater reduction in raw muscle weight post denervation, the substantially lower adiposity could lead to a greater muscle to bodyweight ratio when compared to WT mice.

Mitochondrial Content

In previous literature, the increased levels of COX activity in ATF5 KO mice were thought to be the result of elevated peroxisome proliferator-activated receptor-gamma coactivator 1-alpha (PGC-1α) protein concentrations[17]. PGC-1α is widely known for its major role in mitochondrial biogenesis and has been shown to facilitate the increase in genes associated with the UPR[3,44,52]. This could be the reason why we observed higher COX enzyme activity levels and sustained levels of denervation-induced UPR^{mt} protein content in ATF5 KO mice. Another study demonstrated that nuclear MNRR1 triggers the UPR^{mt} through the regulation of ATF5 transcription and overexpression of MNRR1 induces the UPR^{mt} in cybrid cells[53]. Much like PGC-1α, MNRR1 is a regulator of mitochondrial function and is responsible for directly binding to and activating cytochrome *c* oxidase (COX). One hypothesis could be that, along with PGC-1α, MNRR1 could also be highly expressed in ATF5 KO mice, resulting in a further increase in COX

activity and SDH protein levels. Future research could involve exploring the relationship between MNRR1 and downstream ATF5 expression during chronic muscle disuse.

Relationship between mitochondrial respiration and ROS production in ATF5 KO animals

Currently, there is a severe lack of literature investigating the relationship between mitochondrial respiration and ROS emission with the ISR/UPR^{mt} pathway during chronic muscle disuse. Thus, we sought to investigate whether the absence of ATF5 would negatively affect mitochondrial quality post-denervation. When normalized to COX activity levels, mitochondrial respiration was not significantly altered in WT animals post denervation. This result was consistent with previous literature that revealed male WT mice experienced no significant change across all states of respiration after 7 days of denervation[40]. However, an increase in respiration was observed post-denervation in ATF5 KO mice. Interestingly, when normalized to COX activity levels, ROS emission levels were consistent in all groups post denervation, despite ATF5 KO mice exhibiting greater respiration rates. Additionally, there were no observable differences between basal respiration and ROS production between genotypes. The results suggest that the absence of ATF5 could increase the quality of the mitochondrial pool, resulting in an increase in mitochondrial content and subsequent increase in respiration during chronic muscle disuse. Whether this adaptation is overall beneficial for cell survival and overall health remains unclear.

Relationship between autophagy/mitophagy and lysosomal protein expression with ATF5

Previous literature has shown that ATF5 plays an important role in various mitophagy-related pathways [53,55]. Despite this relationship, we did not observe any significant findings in any mitophagy/autophagy markers between WT and ATF5 KO mice in response to denervation. Although we observed a significant blunting of P62 and LC3II in female KO mice, there was still a significant effect of denervation in all groups regardless of genotype. It also appears the absence of ATF5 could further elevate LC3 I and II in male KO mice. However, the ratio of LC3 II to I was not significantly different between genotypes. Currently, there is insufficient data suggesting that the absence of ATF5 affects the mitophagy/autophagy

response to chronic muscle disuse in skeletal muscle. Likewise, further research is required to completely understand the relationship between the ISR/UPR^{mt} and autophagy/mitophagy related pathways in male and female mice during chronic muscle disuse. Additionally, lysosomal protease cathepsin B (immature) was observed to be blunted in KO mice post denervation. However, the ratio of mature to immature cathepsin B was higher in KO animals. This suggests that a greater abundance of immature cathepsin B is being cleaved into its active state within the lysosomes of KO animals. Future research could involve measuring mitophagy/autophagy flux in ATF5 KO mice by blocking lysosomal degradation via colchicine to assess changes in autophagy and lysosomal markers like LC3-II, P62 and cathepsin B in skeletal muscle during chronic muscle disuse.

ATF5 and the ISR

Activation of the ISR was observed after 7 days of denervation via upregulation of ATF4, CHOP and total eIF2α protein content in WT mice regardless of sex. Unfortunately, we were unable to measure total protein content levels of ATF5 due to the lack of an effective commercially available primary antibody. Currently, there are no reliable data investigating the role of ATF5 in the presence of chronic muscle disuse in mammalian cells. Despite this absence of research, we can still draw informed conclusions based on other ISR markers that have been measured in similar models. For instance, a study conducted by Memme et al. observed an upregulation of ATF4 and CHOP in response to 7 days of denervation, matching our current research findings. Additionally, a recent paper measured nuclear translocation of ATF4 in response to acute exercise, along with mRNA levels of ATF5 and CHOP. Researchers observed an upregulation of nuclear ATF4 protein expression after acute exercise but no subsequent downstream upregulation of ATF5 mRNA[58]. This finding was supported by a previous paper that found no changes in ATF5 mRNA levels in response to acute exercise training[17]. Similarly, chronic contractile activity (CCA) was observed to have a significant impact on ATF4 and CHOP activation throughout a 7-day time course, highlighting the effectiveness of ISR activation in both exercise and muscle disuse models[59]. Although it is widely agreed

upon that ISR activation is integral for cellular survival, the duration/intensity of stress that is necessary for sufficient ISR activation is still largely debated.

We observed that ATF5 KO mice experienced a blunted ISR via a reduced expression of ATF4 and CHOP in response to denervation in both male and female KO mice. It was previously thought that ATF5 was primarily a downstream target of ATF4 and CHOP during the ISR in mammalian cells. However, our data suggest that ATF5 content could largely be reliant on the presence of binding partners as opposed to its content being strictly dictated by the upstream transcriptional activation of other bZIP proteins like ATF4 or CHOP. For instance, transcription factors of the bZIP family like ATF4, CHOP and Nrf-2 that fail to heterodimerize with one another are continuously degraded within the cell in the absence of cellular stress[60–62]. Knowing this, one could suggest that when ATF5 is ablated, the availability of potential binding partners amongst bZIP proteins is reduced, leading to a reduction in heterodimerization rate. This reduction in potential dimerization partners could be a main contributor to the blunted ISR that were observed in our KO animals in response to denervation. Further research could be dedicated to understanding the relationship between ATF5 and other members of the bZIP family during periods of chronic muscle disuse via measuring protein stability and rate of nuclear translocation.

ATF5 and the UPR^{mt}

Although ATF5 is known for upregulating various UPR^{mt} genes in response to cellular stress, the basal protein content of various chaperones and proteases in ATF5 KO mice was not significantly affected in any group. Much like ATF5, transcription factors ATF4, C/EBPα/β and CHOP are also responsible for transcribing UPR^{mt} related proteins such as HSP60, HSP10, mtHSP70, ClpP and LONP1[28]. Therefore, the current level of UPR^{mt} related proteins that we observed in our ATF5 KO model could be the biproduct of other transcription factors heterodimerizing to compensate for the lack of available ATF5. Interestingly, it appears that male WT mice experience a substantially reduced UPR^{mt} when compared to female WT controls with respect to proteins LONP1 and mtHSP70. The genes for ATF5[26], LONP1[63], mtHSP70[64],

HSP60[65], ClpP[66] and CPN10[67] are all located on non-sex-related chromosomes in both mice and humans. Although existing research on sex-specific adaptations of the UPR^{mt} remain scarce, a noteworthy study revealed that misfolded protein accumulation within the intermembrane space induced the UPR^{mt} via activation of estrogen receptor alpha (ERα) in a familial ALS disease mouse model. Since females have a greater abundance of ERα content and activity, researchers observed a significant sex difference in UPR^{mt} activation in female mice spinal cord tissues compared to male controls[68]. Since these pathways act as a defence mechanism to cellular stress, it is likely that many sex differences remain undiscovered in other pathological conditions, such as extreme muscle atrophy. These findings highlight the importance of identifying sex-specific stress adaptations of the UPR^{mt}.

ATF5 and Antioxidant Expression

Although antioxidants do not often directly interact with unfolded/misfolded proteins, they aim to reduce the damage caused by excess ROS production by either quenching them directly via electron donation, repairing the damaged molecules that are affected or by interacting with gene pathways involved in ROS regulation. Likewise, superoxide is rapidly converted to hydrogen peroxide (H_2O_2) and excess amounts can trigger membrane depolarization (Fig. 9) and stimulate mitochondrial fragmentation[69]. Basal levels of antioxidant proteins NQO1 and HO1 have been previously shown to be reduced in skeletal muscle of ATF5 KO mice[17,45]. Likewise, our ATF5 KO model experienced a significant blunting in these proteins, both basally and post-denervation. Interestingly, despite the upregulation of Nrf-2 protein, downstream protein contents of NQO1 and HO1 were still significantly blunted in KO animals. This suggests the presence of another mechanism of action that could interfere with antioxidant protein expression in ATF5 KO animals. One hypothesis involves the dimerization capabilities between Nrf-2 and ATF5. Like previously mentioned, Nrf-2 heterodimerizes with other bZIP proteins to initiate transcription of downstream antioxidant proteins. However, the number of partners that interact with Nrf-2 during gene induction is controversial, suggesting that other dimerization partners may exist. For instance, Nrf-2 is known to heterodimerize with transcription factors SP-1, c-JUN and ATF4[70]. Likewise, ATF5 is classified

under the ATF/bZIP family and protein sequence comparison reveals that both human and mouse ATF5 domains share a 55% similarity with ATF4[19]. Knowing this, it is not unreasonable to assume that Nrf-2 and other members of the ATF family, like ATF5, form bZIP dimers with their leucine zipper structures to initiate downstream translation of antioxidant proteins[71]. Although there have been no reports observing the interaction between ATF5 and Nrf-2, an argument can be made that ATF5 could potentially bind with Nrf-2, much like ATF4. Future experiments could involve investigating the binding capabilities between Nrf-2 and other members of the bZIP family during periods of chronic muscle disuse to observe the effect on downstream antioxidant targets.

Conclusion

In summary, our data suggest that the absence of ATF5 preserves mitochondrial quantity and quality in skeletal muscle during chronic muscle disuse. This was observed by the preservation of COX activity, SDH staining intensity and mitochondrial respiration, with no differences in ROS production post-denervation. Additionally, denervation resulted in an elevation of mitophagy/autophagy and lysosomal markers in both genotypes. The absence of ATF5 blunted the ISR via reductions in ATF4 and CHOP, which was accompanied by a reduced rate of activation of certain UPR^{mt} markers such as LONP1, ClpP and CPN10 in male and female KO mice. Lastly, ATF5 appears to be necessary to maintain normal antioxidant capacity both basally and during muscle denervation (Table 2). Whether the presence of a whole body ATF5 KO model is beneficial for overall skeletal muscle health remains uncertain. Future experiments could include a muscle specific ATF5 KO model to assess differences in adaptation responses to muscle disuse.

References (Manuscript)

1. Sartori, R., Romanello, V., & Sandri, M. (2021). Mechanisms of muscle atrophy and hypertrophy: Implications in health and disease. *Nature Communications*, *12*(1), 330. https://doi.org/10.1038/s41467-020-20123-1
2. Triolo, M., & Hood, D. A. (2019). Mitochondrial breakdown in skeletal muscle and the emerging role of the lysosomes. *Archives of Biochemistry and Biophysics*, *661*, 66–73. https://doi.org/10.1016/j.abb.2018.11.004
3. Vainshtein, A., Desjardins, E. M., Armani, A., Sandri, M., & Hood, D. A. (2015). PGC-1α modulates denervation-induced mitophagy in skeletal muscle. *Skeletal Muscle*, *5*(1), 9. https://doi.org/10.1186/s13395-015-0033-y
4. Chen, X., Ji, Y., Liu, R., Zhu, X., Wang, K., Yang, X., Liu, B., Gao, Z., Huang, Y., Shen, Y., Liu, H., & Sun, H. (2023). Mitochondrial dysfunction: Roles in skeletal muscle atrophy. *Journal of Translational Medicine*, *21*(1), 503. https://doi.org/10.1186/s12967-023-04369-z
5. Peterson, C. M., Johannsen, D. L., & Ravussin, E. (2012). Skeletal Muscle Mitochondria and Aging: A Review. *Journal of Aging Research*, *2012*, 1–20. https://doi.org/10.1155/2012/194821
6. Osellame, L. D., Blacker, T. S., & Duchen, M. R. (2012). Cellular and molecular mechanisms of mitochondrial function. *Best Practice & Research Clinical Endocrinology & Metabolism*, *26*(6), 711–723. https://doi.org/10.1016/j.beem.2012.05.003
7. Zhou, Z., Fan, Y., Zong, R., & Tan, K. (2022). The mitochondrial unfolded protein response: A multitasking giant in the fight against human diseases. *Ageing Research Reviews*, *81*, 101702. https://doi.org/10.1016/j.arr.2022.101702
8. Inigo, J. R., & Chandra, D. (2022). The mitochondrial unfolded protein response (UPRmt): Shielding against toxicity to mitochondria in cancer. *Journal of Hematology & Oncology*, *15*(1), 98. https://doi.org/10.1186/s13045-022-01317-0
9. Costa-Mattioli, M., & Walter, P. (2020). The integrated stress response: From mechanism to disease. *Science*, *368*(6489), eaat5314. https://doi.org/10.1126/science.aat5314
10. Li, C., Li, N., Zhang, Z., Song, Y., Li, J., Wang, Z., Bo, H., & Zhang, Y. (2023). The specific mitochondrial unfolded protein response in fast- and slow-twitch muscles of high-fat diet-induced insulin-resistant rats. *Frontiers in Endocrinology*, *14*, 1127524. https://doi.org/10.3389/fendo.2023.1127524
11. Harding, H. P., Zhang, Y., & Ron, D. (1999). Protein translation and folding are coupled by an endoplasmic-reticulum-resident kinase. *Nature*, *397*(6716), 271–274. https://doi.org/10.1038/16729
12. Pakos-Zebrucka, K., Koryga, I., Mnich, K., Ljujic, M., Samali, A., & Gorman, A. M. (2016). The integrated stress response. *EMBO Reports*, *17*(10), 1374–1395. https://doi.org/10.15252/embr.201642195
13. Zhao, Q. (2002). A mitochondrial specific stress response in mammalian cells. *The EMBO Journal*, *21*(17), 4411–4419. https://doi.org/10.1093/emboj/cdf445
14. Zhang, G., Wang, X., Li, C., Li, Q., An, Y. A., Luo, X., Deng, Y., Gillette, T. G., Scherer, P. E., & Wang, Z. V. (2021). Integrated Stress Response Couples Mitochondrial Protein Translation With Oxidative Stress Control. *Circulation*, *144*(18), 1500–1515. https://doi.org/10.1161/CIRCULATIONAHA.120.053125
15. Ryoo, H. D. (2024). The integrated stress response in metabolic adaptation. *Journal of Biological Chemistry*, *300*(4), 107151. https://doi.org/10.1016/j.jbc.2024.107151
16. Kalinin, A., Zubkova, E., & Menshikov, M. (2023). Integrated Stress Response (ISR) Pathway: Unraveling Its Role in Cellular Senescence. *International Journal of Molecular Sciences*, *24*(24), 17423. https://doi.org/10.3390/ijms242417423

17. Slavin, M. B., Kumari, R., & Hood, D. A. (2022). ATF5 is a regulator of exercise-induced mitochondrial quality control in skeletal muscle. *Molecular Metabolism*, *66*, 101623. https://doi.org/10.1016/j.molmet.2022.101623
18. Fiorese, C. J., Schulz, A. M., Lin, Y.-F., Rosin, N., Pellegrino, M. W., & Haynes, C. M. (2016). The Transcription Factor ATF5 Mediates a Mammalian Mitochondrial UPR. *Current Biology*, *26*(15), 2037–2043. https://doi.org/10.1016/j.cub.2016.06.002
19. Paerhati, P., Liu, J., Jin, Z., Jakoš, T., Zhu, S., Qian, L., Zhu, J., & Yuan, Y. (2022). Advancements in Activating Transcription Factor 5 Function in Regulating Cell Stress and Survival. *International Journal of Molecular Sciences*, *23*(13), 7129. https://doi.org/10.3390/ijms23137129
20. Angelastro, J. M., Ignatova, T. N., Kukekov, V. G., Steindler, D. A., Stengren, G. B., Mendelsohn, C., & Greene, L. A. (2003). Regulated Expression of ATF5 Is Required for the Progression of Neural Progenitor Cells to Neurons. *The Journal of Neuroscience*, *23*(11), 4590–4600. https://doi.org/10.1523/JNEUROSCI.23-11-04590.2003
21. Zhao, Y., Zhang, Y.-D., Zhang, Y.-Y., Qian, S.-W., Zhang, Z.-C., Li, S.-F., Guo, L., Liu, Y., Wen, B., Lei, Q.-Y., Tang, Q.-Q., & Li, X. (2014). P300-Dependent Acetylation of Activating Transcription Factor 5 Enhances C/EBPβ Transactivation of C/EBPα during 3T3-L1 Differentiation. *Molecular and Cellular Biology*, *34*(3), 315–324. https://doi.org/10.1128/MCB.00956-13
22. Leong, D. T., Abraham, M. C., Gupta, A., Lim, T., Chew, F. T., & Hutmacher, D. W. (2012). ATF5, a possible regulator of osteogenic differentiation in human adipose-derived stem cells. *Journal of Cellular Biochemistry*, *113*(8), 2744–2753. https://doi.org/10.1002/jcb.24150
23. Nakamori, D., Takayama, K., Nagamoto, Y., Mitani, S., Sakurai, F., Tachibana, M., & Mizuguchi, H. (2016). Hepatic maturation of human iPS cell-derived hepatocyte-like cells by ATF5, c/EBPα, and PROX1 transduction. *Biochemical and Biophysical Research Communications*, *469*(3), 424–429. https://doi.org/10.1016/j.bbrc.2015.12.007
24. Ma, J., Liu, Y., Valladolid-Acebes, I., Recio-López, P., Peng, G., Li, J., Berggren, P.-O., Juntti-Berggren, L., & Tong, N. (2023). ATF5 is a regulator of ER stress and β-cell apoptosis in different mouse models of genetic- and diet-induced obesity and diabetes mellitus. *Cellular Signalling*, *102*, 110535. https://doi.org/10.1016/j.cellsig.2022.110535
25. Wang, Y. T., Lim, Y., McCall, M. N., Huang, K.-T., Haynes, C. M., Nehrke, K., & Brookes, P. S. (2019). Cardioprotection by the mitochondrial unfolded protein response requires ATF5. *American Journal of Physiology-Heart and Circulatory Physiology*, *317*(2), H472–H478. https://doi.org/10.1152/ajpheart.00244.2019
26. Sears, T. K., & Angelastro, J. M. (2017). The transcription factor ATF5: Role in cellular differentiation, stress responses, and cancer. *Oncotarget*, *8*(48), 84595–84609. https://doi.org/10.18632/oncotarget.21102
27. Brearley-Sholto, M. C., Loczenski-Brown, D. M., Jones, S., Daniel, Z. C. T. R., Ebling, F. J. P., Parr, T., & Brameld, J. M. (2021). Effect of AAV-mediated overexpression of ATF5 and downstream targets of an integrated stress response in murine skeletal muscle. *Scientific Reports*, *11*(1), 19796. https://doi.org/10.1038/s41598-021-99432-4
28. Wang, Y., Li, J., Zhang, Z., Wang, R., Bo, H., & Zhang, Y. (2023). Exercise Improves the Coordination of the Mitochondrial Unfolded Protein Response and Mitophagy in Aging Skeletal Muscle. *Life*, *13*(4), 1006. https://doi.org/10.3390/life13041006
29. Slavin, M. B., Memme, J. M., Oliveira, A. N., Moradi, N., & Hood, D. A. (2022). Regulatory networks coordinating mitochondrial quality control in skeletal muscle. *American Journal of Physiology-Cell Physiology*, *322*(5), C913–C926. https://doi.org/10.1152/ajpcell.00065.2022
30. Apablaza, P., Bórquez, J. C., Mendoza, R., Silva, M., Tapia, G., Espinosa, A., Troncoso, R., Videla, L. A., Juretić, N., & Del Campo, A. (2023). Exercise Induces an Augmented Skeletal Muscle Mitochondrial Unfolded Protein Response in a Mouse Model of Obesity Produced by a High-Fat

Diet. *International Journal of Molecular Sciences*, *24*(6), 5654. https://doi.org/10.3390/ijms24065654
31. Rath, E., Berger, E., Messlik, A., Nunes, T., Liu, B., Kim, S. C., Hoogenraad, N., Sans, M., Sartor, R. B., & Haller, D. (2012). Induction of dsRNA-activated protein kinase links mitochondrial unfolded protein response to the pathogenesis of intestinal inflammation. *Gut*, *61*(9), 1269–1278. https://doi.org/10.1136/gutjnl-2011-300767
32. Shpilka, T., & Haynes, C. M. (2018). The mitochondrial UPR: Mechanisms, physiological functions and implications in ageing. *Nature Reviews Molecular Cell Biology*, *19*(2), 109–120. https://doi.org/10.1038/nrm.2017.110
33. Zhu, L., Zhou, Q., He, L., & Chen, L. (2021). Mitochondrial unfolded protein response: An emerging pathway in human diseases. *Free Radical Biology and Medicine*, *163*, 125–134. https://doi.org/10.1016/j.freeradbiomed.2020.12.013
34. Richards, B. J., Slavin, M., Oliveira, A. N., Sanfrancesco, V. C., & Hood, D. A. (2023). Mitochondrial protein import and UPRmt in skeletal muscle remodeling and adaptation. *Seminars in Cell & Developmental Biology*, *143*, 28–36. https://doi.org/10.1016/j.semcdb.2022.01.002
35. Ron, D., & Walter, P. (2007). Signal integration in the endoplasmic reticulum unfolded protein response. *Nature Reviews Molecular Cell Biology*, *8*(7), 519–529. https://doi.org/10.1038/nrm2199
36. Gallot, Y. S., & Bohnert, K. R. (2021). Confounding Roles of ER Stress and the Unfolded Protein Response in Skeletal Muscle Atrophy. *International Journal of Molecular Sciences*, *22*(5), 2567. https://doi.org/10.3390/ijms22052567
37. Kny, M., & Fielitz, J. (2022). Hidden Agenda—The Involvement of Endoplasmic Reticulum Stress and Unfolded Protein Response in Inflammation-Induced Muscle Wasting. *Frontiers in Immunology*, *13*, 878755. https://doi.org/10.3389/fimmu.2022.878755
38. Triolo, M., Bhattacharya, D., & Hood, D. A. (2022). Denervation induces mitochondrial decline and exacerbates lysosome dysfunction in middle-aged mice. *Aging*, *14*(22), 8900–8913. https://doi.org/10.18632/aging.204365
39. Triolo, M., Slavin, M., Moradi, N., & Hood, D. A. (2022). Time-dependent changes in autophagy, mitophagy and lysosomes in skeletal muscle during denervation-induced disuse. *The Journal of Physiology*, *600*(7), 1683–1701. https://doi.org/10.1113/JP282173
40. Oliveira, A. N., Memme, J. M., Wong, J., & Hood, D. A. (2024). Dimorphic effect of TFE3 in determining mitochondrial and lysosomal content in muscle following denervation. *Skeletal Muscle*, *14*(1), 7. https://doi.org/10.1186/s13395-024-00339-1
41. O′Leary, M. F. N., Vainshtein, A., Carter, H. N., Zhang, Y., & Hood, D. A. (2012). Denervation-induced mitochondrial dysfunction and autophagy in skeletal muscle of apoptosis-deficient animals. *American Journal of Physiology-Cell Physiology*, *303*(4), C447–C454. https://doi.org/10.1152/ajpcell.00451.2011
42. Memme, J. M., Oliveira, A. N., & Hood, D. A. (2022). P53 regulates skeletal muscle mitophagy and mitochondrial quality control following denervation-induced muscle disuse. *Journal of Biological Chemistry*, *298*(2), 101540. https://doi.org/10.1016/j.jbc.2021.101540
43. Hyatt, H., Deminice, R., Yoshihara, T., & Powers, S. K. (2019). Mitochondrial dysfunction induces muscle atrophy during prolonged inactivity: A review of the causes and effects. *Archives of Biochemistry and Biophysics*, *662*, 49–60. https://doi.org/10.1016/j.abb.2018.11.005
44. Kang, C., Goodman, C. A., Hornberger, T. A., & Ji, L. L. (2015). PGC-1α overexpression by *in vivo* transfection attenuates mitochondrial deterioration of skeletal muscle caused by immobilization. *The FASEB Journal*, *29*(10), 4092–4106. https://doi.org/10.1096/fj.14-266619

45. Adhihetty, P. J., O'Leary, M. F. N., Chabi, B., Wicks, K. L., & Hood, D. A. (2007). Effect of denervation on mitochondrially mediated apoptosis in skeletal muscle. *Journal of Applied Physiology*, *102*(3), 1143–1151. https://doi.org/10.1152/japplphysiol.00768.2006
46. Trevino, M. B., Zhang, X., Standley, R. A., Wang, M., Han, X., Reis, F. C. G., Periasamy, M., Yu, G., Kelly, D. P., Goodpaster, B. H., Vega, R. B., & Coen, P. M. (2019). Loss of mitochondrial energetics is associated with poor recovery of muscle function but not mass following disuse atrophy. *American Journal of Physiology-Endocrinology and Metabolism*, *317*(5), E899–E910. https://doi.org/10.1152/ajpendo.00161.2019
47. Powers, S. K., Lynch, G. S., Murphy, K. T., Reid, M. B., & Zijdewind, I. (2016). Disease-Induced Skeletal Muscle Atrophy and Fatigue. *Medicine & Science in Sports & Exercise*, *48*(11), 2307–2319. https://doi.org/10.1249/MSS.0000000000000975
48. Singh, K., & Hood, D. A. (2011). Effect of denervation-induced muscle disuse on mitochondrial protein import. *American Journal of Physiology-Cell Physiology*, *300*(1), C138–C145. https://doi.org/10.1152/ajpcell.00181.2010
49. Zhang, X., Trevino, M. B., Wang, M., Gardell, S. J., Ayala, J. E., Han, X., Kelly, D. P., Goodpaster, B. H., Vega, R. B., & Coen, P. M. (2018). Impaired Mitochondrial Energetics Characterize Poor Early Recovery of Muscle Mass Following Hind Limb Unloading in Old Mice. *The Journals of Gerontology: Series A*, *73*(10), 1313–1322. https://doi.org/10.1093/gerona/gly051
50. Triolo, M., Oliveira, A. N., Kumari, R., & Hood, D. A. (2022). The influence of age, sex, and exercise on autophagy, mitophagy, and lysosome biogenesis in skeletal muscle. *Skeletal Muscle*, *12*(1), 13. https://doi.org/10.1186/s13395-022-00296-7
51. Carafoli, E., Margreth, A., & Buffa, P. (1964). Early biochemical changes in mitochondria from denervated muscle and their relation to the onset of atrophy. *Experimental and Molecular Pathology*, *3*(2), 171–181. https://doi.org/10.1016/0014-4800(64)90050-4
52. Wu, J., Ruas, J. L., Estall, J. L., Rasbach, K. A., Choi, J. H., Ye, L., Boström, P., Tyra, H. M., Crawford, R. W., Campbell, K. P., Rutkowski, D. T., Kaufman, R. J., & Spiegelman, B. M. (2011). The Unfolded Protein Response Mediates Adaptation to Exercise in Skeletal Muscle through a PGC-1α/ATF6α Complex. *Cell Metabolism*, *13*(2), 160–169. https://doi.org/10.1016/j.cmet.2011.01.003
53. Aras, S., Purandare, N., Gladyck, S., Somayajulu-Nitu, M., Zhang, K., Wallace, D. C., & Grossman, L. I. (2020). Mitochondrial Nuclear Retrograde Regulator 1 (MNRR1) rescues the cellular phenotype of MELAS by inducing homeostatic mechanisms. *Proceedings of the National Academy of Sciences*, *117*(50), 32056–32065. https://doi.org/10.1073/pnas.2005877117
54. Memme, J. M., Sanfrancesco, V. C., & Hood, D. A. (2023). Activating transcription factor 4 regulates mitochondrial content, morphology, and function in differentiating skeletal muscle myotubes. *American Journal of Physiology-Cell Physiology*, *325*(1), C224–C242. https://doi.org/10.1152/ajpcell.00080.2023
55. Liou, Y.-H., Personnaz, J., Jacobi, D., Knudsen, N. H., Chalom, M. M., Starost, K. A., Nnah, I. C., & Lee, C.-H. (2022). Hepatic Fis1 regulates mitochondrial integrated stress response and improves metabolic homeostasis. *JCI Insight*, *7*(4), e150041. https://doi.org/10.1172/jci.insight.150041
56. Gkirtzimanaki, K., Kabrani, E., Nikoleri, D., Polyzos, A., Blanas, A., Sidiropoulos, P., Makrigiannakis, A., Bertsias, G., Boumpas, D. T., & Verginis, P. (2018). IFNα Impairs Autophagic Degradation of mtDNA Promoting Autoreactivity of SLE Monocytes in a STING-Dependent Fashion. *Cell Reports*, *25*(4), 921-933.e5. https://doi.org/10.1016/j.celrep.2018.09.001
57. Bird, L. E., Xu, B., Hobbs, A. D., Ziegler, A. R., Scott, N. E., Newton, P., Thomas, D. R., Edgington-Mitchell, L. E., & Newton, H. J. (2025). Coxiella burnetii manipulates the lysosomal protease cathepsin B to facilitate intracellular success. *Nature Communications*, *16*(1), 3844. https://doi.org/10.1038/s41467-025-59283-3

58. Sanfrancesco, V. C., & Hood, D. A. (2025). Acute contractile activity induces the activation of the mitochondrial integrated stress response and the transcription factor ATF4. *Journal of Applied Physiology*, *138*(3), 857–871. https://doi.org/10.1152/japplphysiol.00307.2024
59. Memme, J. M., Oliveira, A. N., & Hood, D. A. (2016). Chronology of UPR activation in skeletal muscle adaptations to chronic contractile activity. *American Journal of Physiology-Cell Physiology*, *310*(11), C1024–C1036. https://doi.org/10.1152/ajpcell.00009.2016
60. Hogan, M. R., Cockram, G. P., & Lu, R. (2006). Cooperative interaction of Zhangfei and ATF4 in transactivation of the cyclic AMP response element. *FEBS Letters*, *580*(1), 58–62. https://doi.org/10.1016/j.febslet.2005.11.046
61. Teske, B. F., Fusakio, M. E., Zhou, D., Shan, J., McClintick, J. N., Kilberg, M. S., & Wek, R. C. (2013). CHOP induces activating transcription factor 5 (ATF5) to trigger apoptosis in response to perturbations in protein homeostasis. *Molecular Biology of the Cell*, *24*(15), 2477–2490. https://doi.org/10.1091/mbc.e13-01-0067
62. Tonelli, C., Chio, I. I. C., & Tuveson, D. A. (2018). Transcriptional Regulation by Nrf2. *Antioxidants & Redox Signaling*, *29*(17), 1727–1745. https://doi.org/10.1089/ars.2017.7342
63. Amerik, A. Yu., Petukhova, G. V., Grigorenko, V. G., Lykov, I. P., Yarovoi, S. V., Lipkin, V. M., & Gorbalenya, A. E. (1994). Cloning and sequence analysis of cDNA for a human homolog of eubacterial ATP-dependent Lon proteases. *FEBS Letters*, *340*(1–2), 25–28. https://doi.org/10.1016/0014-5793(94)80166-5
64. Domanico, S. Z., DeNagel, D. C., Dahlseid, J. N., Green, J. M., & Pierce, S. K. (1993). Cloning of the gene encoding peptide-binding protein 74 shows that it is a new member of the heat shock protein 70 family. *Molecular and Cellular Biology*, *13*(6), 3598–3610. https://doi.org/10.1128/MCB.13.6.3598
65. Tang, Y., Zhou, Y., Fan, S., & Wen, Q. (2022). The multiple roles and therapeutic potential of HSP60 in cancer. *Biochemical Pharmacology*, *201*, 115096. https://doi.org/10.1016/j.bcp.2022.115096
66. Andresen, B. S., Corydon, T. J., Wilsbech, M., Bross, P., Schroeder, L. D., Hindkjær, T. F., Bolund, L., & Gregersen, N. (2000). Characterization of mouse Clpp protease cDNA, gene, and protein. *Mammalian Genome*, *11*(4), 275–280. https://doi.org/10.1007/s003350010052
67. Rospert, S., Junne, T., Glick, B. S., & Schatz, G. (1993). Cloning and disruption of the gene encoding yeast mitochondrial chaperonin 10, the homolog of *E. coli* groES. *FEBS Letters*, *335*(3), 358–360. https://doi.org/10.1016/0014-5793(93)80419-U
68. Riar, A. K., Burstein, S. R., Palomo, G. M., Arreguin, A., Manfredi, G., & Germain, D. (2017). Sex specific activation of the ERα axis of the mitochondrial UPR (UPRmt) in the G93A-SOD1 mouse model of familial ALS. *Human Molecular Genetics*, *26*(7), 1318–1327. https://doi.org/10.1093/hmg/ddx049
69. Chen, M.-M., Li, Y., Deng, S.-L., Zhao, Y., Lian, Z.-X., & Yu, K. (2022). Mitochondrial Function and Reactive Oxygen/Nitrogen Species in Skeletal Muscle. *Frontiers in Cell and Developmental Biology*, *10*, 826981. https://doi.org/10.3389/fcell.2022.826981
70. Panieri, E., Pinho, S. A., Afonso, G. J. M., Oliveira, P. J., Cunha-Oliveira, T., & Saso, L. (2022). NRF2 and Mitochondrial Function in Cancer and Cancer Stem Cells. *Cells*, *11*(15), 2401. https://doi.org/10.3390/cells11152401
71. He, C. H., Gong, P., Hu, B., Stewart, D., Choi, M. E., Choi, A. M. K., & Alam, J. (2001). Identification of Activating Transcription Factor 4 (ATF4) as an Nrf2-interacting Protein. *Journal of Biological Chemistry*, *276*(24), 20858–20865. https://doi.org/10.1074/jbc.M101198200

References (Review of Literature)

1. Frontera, W. R., & Ochala, J. (2015). Skeletal Muscle: A Brief Review of Structure and Function. *Calcified Tissue International*, *96*(3), 183–195. https://doi.org/10.1007/s00223-014-9915-y
2. Periasamy, M., Herrera, J. L., & Reis, F. C. G. (2017). Skeletal Muscle Thermogenesis and Its Role in Whole Body Energy Metabolism. *Diabetes & Metabolism Journal*, *41*(5), 327. https://doi.org/10.4093/dmj.2017.41.5.327
3. Ottenheijm, C. A. C., & Granzier, H. (2010). Lifting the Nebula: Novel Insights into Skeletal Muscle Contractility. *Physiology*, *25*(5), 304–310. https://doi.org/10.1152/physiol.00016.2010
4. Gordon, A. M., Homsher, E., & Regnier, M. (2000). Regulation of Contraction in Striated Muscle. *Physiological Reviews*, *80*(2), 853–924. https://doi.org/10.1152/physrev.2000.80.2.853
5. Schiaffino, S., & Reggiani, C. (2011). Fiber Types in Mammalian Skeletal Muscles. *Physiological Reviews*, *91*(4), 1447–1531. https://doi.org/10.1152/physrev.00031.2010
6. Schiaffino, S. (2018). Muscle fiber type diversity revealed by anti-myosin heavy chain antibodies. *The FEBS Journal*, *285*(20), 3688–3694. https://doi.org/10.1111/febs.14502
7. Williamson, D. L., Gallagher, P. M., Carroll, C. C., Raue, U., & Trappe, S. W. (2001). Reduction in hybrid single muscle fiber proportions with resistance training in humans. *Journal of Applied Physiology*, *91*(5), 1955–1961. https://doi.org/10.1152/jappl.2001.91.5.1955
8. Protasoni, M., & Zeviani, M. (2021). Mitochondrial Structure and Bioenergetics in Normal and Disease Conditions. *International Journal of Molecular Sciences*, *22*(2), 586. https://doi.org/10.3390/ijms22020586
9. Osellame, L. D., Blacker, T. S., & Duchen, M. R. (2012). Cellular and molecular mechanisms of mitochondrial function. *Best Practice & Research Clinical Endocrinology & Metabolism*, *26*(6), 711–723. https://doi.org/10.1016/j.beem.2012.05.003
10. Susin, S. A., Lorenzo, H. K., Zamzami, N., Marzo, I., Snow, B. E., Brothers, G. M., Mangion, J., Jacotot, E., Costantini, P., Loeffler, M., Larochette, N., Goodlett, D. R., Aebersold, R., Siderovski, D. P., Penninger, J. M., & Kroemer, G. (1999). Molecular characterization of mitochondrial apoptosis-inducing factor. *Nature*, *397*(6718), 441–446. https://doi.org/10.1038/17135
11. Duchen, M. R. (2000). Mitochondria and calcium: From cell signalling to cell death. *The Journal of Physiology*, *529*(1), 57–68. https://doi.org/10.1111/j.1469-7793.2000.00057.x
12. Brand, M. D., Affourtit, C., Esteves, T. C., Green, K., Lambert, A. J., Miwa, S., Pakay, J. L., & Parker, N. (2004). Mitochondrial superoxide: Production, biological effects, and activation of uncoupling proteins. *Free Radical Biology and Medicine*, *37*(6), 755–767. https://doi.org/10.1016/j.freeradbiomed.2004.05.034
13. Zhou, Z., Fan, Y., Zong, R., & Tan, K. (2022). The mitochondrial unfolded protein response: A multitasking giant in the fight against human diseases. *Ageing Research Reviews*, *81*, 101702. https://doi.org/10.1016/j.arr.2022.101702
14. Inigo, J. R., & Chandra, D. (2022). The mitochondrial unfolded protein response (UPRmt): Shielding against toxicity to mitochondria in cancer. *Journal of Hematology & Oncology*, *15*(1), 98. https://doi.org/10.1186/s13045-022-01317-0
15. Chinnery, P. F., & Hudson, G. (2013). Mitochondrial genetics. *British Medical Bulletin*, *106*(1), 135–159. https://doi.org/10.1093/bmb/ldt017
16. Zhang, P., Chen, X., & Fan, M. (2007). Signaling mechanisms involved in disuse muscle atrophy. *Medical Hypotheses*, *69*(2), 310–321. https://doi.org/10.1016/j.mehy.2006.11.043
17. Valenzuela, P. L., Morales, J. S., Pareja-Galeano, H., Izquierdo, M., Emanuele, E., De La Villa, P., & Lucia, A. (2018). Physical strategies to prevent disuse-induced functional decline in the elderly. *Ageing Research Reviews*, *47*, 80–88. https://doi.org/10.1016/j.arr.2018.07.003
18. Dirks, M. L., Wall, B. T., Van De Valk, B., Holloway, T. M., Holloway, G. P., Chabowski, A., Goossens, G. H., & Van Loon, L. J. C. (2016). One Week of Bed Rest Leads to Substantial

Muscle Atrophy and Induces Whole-Body Insulin Resistance in the Absence of Skeletal Muscle Lipid Accumulation. *Diabetes*, *65*(10), 2862–2875. https://doi.org/10.2337/db15-1661
19. Von Haehling, S., Morley, J. E., & Anker, S. D. (2010). An overview of sarcopenia: Facts and numbers on prevalence and clinical impact. *Journal of Cachexia, Sarcopenia and Muscle*, *1*(2), 129–133. https://doi.org/10.1007/s13539-010-0014-2
20. Pišot, R., Marusic, U., Biolo, G., Mazzucco, S., Lazzer, S., Grassi, B., Reggiani, C., Toniolo, L., Di Prampero, P. E., Passaro, A., Narici, M., Mohammed, S., Rittweger, J., Gasparini, M., Gabrijelčič Blenkuš, M., & Šimunič, B. (2016). Greater loss in muscle mass and function but smaller metabolic alterations in older compared with younger men following 2 wk of bed rest and recovery. *Journal of Applied Physiology*, *120*(8), 922–929. https://doi.org/10.1152/japplphysiol.00858.2015
21. Doherty, T. J. (2003). Invited Review: Aging and sarcopenia. *Journal of Applied Physiology*, *95*(4), 1717–1727. https://doi.org/10.1152/japplphysiol.00347.2003
22. Chatzinikita, E., Maridaki, M., Palikaras, K., Koutsilieris, M., & Philippou, A. (2023). The Role of Mitophagy in Skeletal Muscle Damage and Regeneration. *Cells*, *12*(5), 716. https://doi.org/10.3390/cells12050716
23. Levine, B., Mizushima, N., & Virgin, H. W. (2011). Autophagy in immunity and inflammation. *Nature*, *469*(7330), 323–335. https://doi.org/10.1038/nature09782
24. Yorimitsu, T., & Klionsky, D. J. (2005). Autophagy: Molecular machinery for self-eating. *Cell Death & Differentiation*, *12*(S2), 1542–1552. https://doi.org/10.1038/sj.cdd.4401765
25. Kim, Y., & Hood, D. A. (2017). Regulation of the autophagy system during chronic contractile activity-induced muscle adaptations. *Physiological Reports*, *5*(14), e13307. https://doi.org/10.14814/phy2.13307
26. Wang, S., Long, H., Hou, L., Feng, B., Ma, Z., Wu, Y., Zeng, Y., Cai, J., Zhang, D., & Zhao, G. (2023). The mitophagy pathway and its implications in human diseases. *Signal Transduction and Targeted Therapy*, *8*(1), 304. https://doi.org/10.1038/s41392-023-01503-7
27. Chen, T.-H., Koh, K.-Y., Lin, K. M.-C., & Chou, C.-K. (2022). Mitochondrial Dysfunction as an Underlying Cause of Skeletal Muscle Disorders. *International Journal of Molecular Sciences*, *23*(21), 12926. https://doi.org/10.3390/ijms232112926
28. Tarnopolsky, M. A., & Raha, S. (2005). Mitochondrial Myopathies: Diagnosis, Exercise Intolerance, and Treatment Options: *Medicine & Science in Sports & Exercise*, *37*(12), 2086–2093. https://doi.org/10.1249/01.mss.0000177341.89478.06
29. Padilha, C. S., Borges, F. H., Costa Mendes Da Silva, L. E., Frajacomo, F. T. T., Jordao, A. A., Duarte, J. A., Cecchini, R., Guarnier, F. A., & Deminice, R. (2017). Resistance exercise attenuates skeletal muscle oxidative stress, systemic pro-inflammatory state, and cachexia in Walker-256 tumor-bearing rats. *Applied Physiology, Nutrition, and Metabolism*, *42*(9), 916–923. https://doi.org/10.1139/apnm-2016-0436
30. Ballarò, R., Beltrà, M., De Lucia, S., Pin, F., Ranjbar, K., Hulmi, J. J., Costelli, P., & Penna, F. (2019). Moderate exercise in mice improves cancer plus chemotherapy-induced muscle wasting and mitochondrial alterations. *The FASEB Journal*, *33*(4), 5482–5494. https://doi.org/10.1096/fj.201801862R
31. Connor, M. K., Irrcher, I., & Hood, D. A. (2001). Contractile Activity-induced Transcriptional Activation of Cytochrome c Involves Sp1 and Is Proportional to Mitochondrial ATP Synthesis in C2C12 Muscle Cells. *Journal of Biological Chemistry*, *276*(19), 15898–15904. https://doi.org/10.1074/jbc.M100272200
32. Adhihetty, P. J., Irrcher, I., Joseph, A., Ljubicic, V., & Hood, D. A. (2003). Plasticity of Skeletal Muscle Mitochondria in Response to Contractile Activity. *Experimental Physiology*, *88*(1), 99–107. https://doi.org/10.1113/eph8802505

33. Erlich, A. T., Brownlee, D. M., Beyfuss, K., & Hood, D. A. (2018). Exercise induces TFEB expression and activity in skeletal muscle in a PGC-1α-dependent manner. *American Journal of Physiology-Cell Physiology*, *314*(1), C62–C72. https://doi.org/10.1152/ajpcell.00162.2017
34. Wang, Y., Li, J., Zhang, Z., Wang, R., Bo, H., & Zhang, Y. (2023). Exercise Improves the Coordination of the Mitochondrial Unfolded Protein Response and Mitophagy in Aging Skeletal Muscle. *Life*, *13*(4), 1006. https://doi.org/10.3390/life13041006
35. Wang, X., & Zhang, G. (2025). The mitochondrial integrated stress response: A novel approach to anti-aging and pro-longevity. *Ageing Research Reviews*, *103*, 102603. https://doi.org/10.1016/j.arr.2024.102603
36. Ryoo, H. D. (2024). The integrated stress response in metabolic adaptation. *Journal of Biological Chemistry*, *300*(4), 107151. https://doi.org/10.1016/j.jbc.2024.107151
37. Kalinin, A., Zubkova, E., & Menshikov, M. (2023). Integrated Stress Response (ISR) Pathway: Unraveling Its Role in Cellular Senescence. *International Journal of Molecular Sciences*, *24*(24), 17423. https://doi.org/10.3390/ijms242417423
38. Shpilka, T., & Haynes, C. M. (2018). The mitochondrial UPR: Mechanisms, physiological functions and implications in ageing. *Nature Reviews Molecular Cell Biology*, *19*(2), 109–120. https://doi.org/10.1038/nrm.2017.110
39. Zhu, L., Zhou, Q., He, L., & Chen, L. (2021). Mitochondrial unfolded protein response: An emerging pathway in human diseases. *Free Radical Biology and Medicine*, *163*, 125–134. https://doi.org/10.1016/j.freeradbiomed.2020.12.013
40. Richards, B. J., Slavin, M., Oliveira, A. N., Sanfrancesco, V. C., & Hood, D. A. (2023). Mitochondrial protein import and UPRmt in skeletal muscle remodeling and adaptation. *Seminars in Cell & Developmental Biology*, *143*, 28–36. https://doi.org/10.1016/j.semcdb.2022.01.002
41. Slavin, M. B., Memme, J. M., Oliveira, A. N., Moradi, N., & Hood, D. A. (2022). Regulatory networks coordinating mitochondrial quality control in skeletal muscle. *American Journal of Physiology-Cell Physiology*, *322*(5), C913–C926. https://doi.org/10.1152/ajpcell.00065.2022
42. Gallot, Y. S., & Bohnert, K. R. (2021). Confounding Roles of ER Stress and the Unfolded Protein Response in Skeletal Muscle Atrophy. *International Journal of Molecular Sciences*, *22*(5), 2567. https://doi.org/10.3390/ijms22052567
43. Kny, M., & Fielitz, J. (2022). Hidden Agenda—The Involvement of Endoplasmic Reticulum Stress and Unfolded Protein Response in Inflammation-Induced Muscle Wasting. *Frontiers in Immunology*, *13*, 878755. https://doi.org/10.3389/fimmu.2022.878755
44. Dey, M., Trieselmann, B., Locke, E. G., Lu, J., Cao, C., Dar, A. C., Krishnamoorthy, T., Dong, J., Sicheri, F., & Dever, T. E. (2005). PKR and GCN2 Kinases and Guanine Nucleotide Exchange Factor Eukaryotic Translation Initiation Factor 2B (eIF2B) Recognize Overlapping Surfaces on eIF2α. *Molecular and Cellular Biology*, *25*(8), 3063–3075. https://doi.org/10.1128/MCB.25.8.3063-3075.2005
45. Chen, J.-J., & London, I. M. (1995). Regulation of protein synthesis by heme-regulated eIF-2α kinase. *Trends in Biochemical Sciences*, *20*(3), 105–108. https://doi.org/10.1016/S0968-0004(00)88975-6
46. Chatzinikita, E., Maridaki, M., Palikaras, K., Koutsilieris, M., & Philippou, A. (2023). The Role of Mitophagy in Skeletal Muscle Damage and Regeneration. *Cells*, *12*(5), 716. https://doi.org/10.3390/cells12050716
47. Harding, H. P., Zhang, Y., & Ron, D. (1999). Protein translation and folding are coupled by an endoplasmic-reticulum-resident kinase. *Nature*, *397*(6716), 271–274. https://doi.org/10.1038/16729
48. Dever, T. E., Chen, J. J., Barber, G. N., Cigan, A. M., Feng, L., Donahue, T. F., London, I. M., Katze, M. G., & Hinnebusch, A. G. (1993). Mammalian eukaryotic initiation factor 2 alpha kinases

functionally substitute for GCN2 protein kinase in the GCN4 translational control mechanism of yeast. *Proceedings of the National Academy of Sciences*, *90*(10), 4616–4620. https://doi.org/10.1073/pnas.90.10.4616
49. Delfinis, L. J., Khajehzadehshoushtar, S., & Perry, C. G. R. (2025). Perspectives on the interpretation of mitochondrial responses during skeletal muscle disuse-induced atrophy. *The Journal of Physiology*, JP284160. https://doi.org/10.1113/JP284160
50. Crawford, R. A., Ashe, M. P., Hubbard, S. J., & Pavitt, G. D. (2022). Cytosolic aspartate aminotransferase moonlights as a ribosome-binding modulator of Gcn2 activity during oxidative stress. *eLife*, *11*, e73466. https://doi.org/10.7554/eLife.73466
51. Shenton, D., Smirnova, J. B., Selley, J. N., Carroll, K., Hubbard, S. J., Pavitt, G. D., Ashe, M. P., & Grant, C. M. (2006). Global Translational Responses to Oxidative Stress Impact upon Multiple Levels of Protein Synthesis. *Journal of Biological Chemistry*, *281*(39), 29011–29021. https://doi.org/10.1074/jbc.M601545200
52. Komar, A. A., & Merrick, W. C. (2020). A Retrospective on eIF2A—and Not the Alpha Subunit of eIF2. *International Journal of Molecular Sciences*, *21*(6), 2054. https://doi.org/10.3390/ijms21062054
53. Moon, S. L., Sonenberg, N., & Parker, R. (2018). Neuronal Regulation of eIF2α Function in Health and Neurological Disorders. *Trends in Molecular Medicine*, *24*(6), 575–589. https://doi.org/10.1016/j.molmed.2018.04.001
54. Young, S. K., & Wek, R. C. (2016). Upstream Open Reading Frames Differentially Regulate Gene-specific Translation in the Integrated Stress Response. *Journal of Biological Chemistry*, *291*(33), 16927–16935. https://doi.org/10.1074/jbc.R116.733899
55. Ghosh, A. P., Klocke, B. J., Ballestas, M. E., & Roth, K. A. (2012). CHOP Potentially Co-Operates with FOXO3a in Neuronal Cells to Regulate PUMA and BIM Expression in Response to ER Stress. *PLoS ONE*, *7*(6), e39586. https://doi.org/10.1371/journal.pone.0039586
56. Liu, K., Shi, Y., Guo, X., Wang, S., Ouyang, Y., Hao, M., Liu, D., Qiao, L., Li, N., Zheng, J., & Chen, D. (2014). CHOP mediates ASPP2-induced autophagic apoptosis in hepatoma cells by releasing Beclin-1 from Bcl-2 and inducing nuclear translocation of Bcl-2. *Cell Death & Disease*, *5*(7), e1323–e1323. https://doi.org/10.1038/cddis.2014.276
57. Han, J., Back, S. H., Hur, J., Lin, Y.-H., Gildersleeve, R., Shan, J., Yuan, C. L., Krokowski, D., Wang, S., Hatzoglou, M., Kilberg, M. S., Sartor, M. A., & Kaufman, R. J. (2013). ER-stress-induced transcriptional regulation increases protein synthesis leading to cell death. *Nature Cell Biology*, *15*(5), 481–490. https://doi.org/10.1038/ncb2738
58. Sears, T. K., & Angelastro, J. M. (2017). The transcription factor ATF5: Role in cellular differentiation, stress responses, and cancer. *Oncotarget*, *8*(48), 84595–84609. https://doi.org/10.18632/oncotarget.21102
59. Vinson, C., Myakishev, M., Acharya, A., Mir, A. A., Moll, J. R., & Bonovich, M. (2002). Classification of Human B-ZIP Proteins Based on Dimerization Properties. *Molecular and Cellular Biology*, *22*(18), 6321–6335. https://doi.org/10.1128/mcb.22.18.6321-6335.2002
60. Zhou, D., Palam, L. R., Jiang, L., Narasimhan, J., Staschke, K. A., & Wek, R. C. (2008). Phosphorylation of eIF2 Directs ATF5 Translational Control in Response to Diverse Stress Conditions. *Journal of Biological Chemistry*, *283*(11), 7064–7073. https://doi.org/10.1074/jbc.m708530200
61. Greene, L. A., Zhou, Q., Siegelin, M. D., & Angelastro, J. M. (2023). Targeting Transcription Factors ATF5, CEBPB and CEBPD with Cell-Penetrating Peptides to Treat Brain and Other Cancers. *Cells*, *12*(4), 581. https://doi.org/10.3390/cells12040581
62. Fusakio, M. E., Willy, J. A., Wang, Y., Mirek, E. T., Al Baghdadi, R. J. T., Adams, C. M., Anthony, T. G., & Wek, R. C. (2016). Transcription factor ATF4 directs basal and stress-induced gene

expression in the unfolded protein response and cholesterol metabolism in the liver. *Molecular Biology of the Cell*, *27*(9), 1536–1551. https://doi.org/10.1091/mbc.e16-01-0039
63. Wang, Y. T., Lim, Y., McCall, M. N., Huang, K.-T., Haynes, C. M., Nehrke, K., & Brookes, P. S. (2019). Cardioprotection by the mitochondrial unfolded protein response requires ATF5. *American Journal of Physiology-Heart and Circulatory Physiology*, *317*(2), H472–H478. https://doi.org/10.1152/ajpheart.00244.2019
64. Fiorese, C. J., Schulz, A. M., Lin, Y.-F., Rosin, N., Pellegrino, M. W., & Haynes, C. M. (2016). The Transcription Factor ATF5 Mediates a Mammalian Mitochondrial UPR. *Current Biology*, *26*(15), 2037–2043. https://doi.org/10.1016/j.cub.2016.06.002
65. Teske, B. F., Fusakio, M. E., Zhou, D., Shan, J., McClintick, J. N., Kilberg, M. S., & Wek, R. C. (2013). CHOP induces activating transcription factor 5 (ATF5) to trigger apoptosis in response to perturbations in protein homeostasis. *Molecular Biology of the Cell*, *24*(15), 2477–2490. https://doi.org/10.1091/mbc.e13-01-0067
66. Ji, Y., Jiang, Q., Chen, B., Chen, X., Li, A., Shen, D., Shen, Y., Liu, H., Qian, X., Yao, X., & Sun, H. (2025). Endoplasmic reticulum stress and unfolded protein response: Roles in skeletal muscle atrophy. *Biochemical Pharmacology*, *234*, 116799. https://doi.org/10.1016/j.bcp.2025.116799
67. Runkel, E. D., Liu, S., Baumeister, R., & Schulze, E. (2016). Correction: Surveillance-Activated Defenses Block the ROS-Induced Mitochondrial Unfolded Protein Response. *PLOS Genetics*, *12*(10), e1006377. https://doi.org/10.1371/journal.pgen.1006377
68. Sutandy, F. X. R., Gößner, I., Tascher, G., & Münch, C. (2023). A cytosolic surveillance mechanism activates the mitochondrial UPR. *Nature*, *618*(7966), 849–854. https://doi.org/10.1038/s41586-023-06142-0
69. Pellegrino, M. W., Nargund, A. M., Kirienko, N. V., Gillis, R., Fiorese, C. J., & Haynes, C. M. (2014). Mitochondrial UPR-regulated innate immunity provides resistance to pathogen infection. *Nature*, *516*(7531), 414–417. https://doi.org/10.1038/nature13818
70. Yoneda, T., Benedetti, C., Urano, F., Clark, S. G., Harding, H. P., & Ron, D. (2004). Compartment-specific perturbation of protein handling activates genes encoding mitochondrial chaperones. *Journal of Cell Science*, *117*(18), 4055–4066. https://doi.org/10.1242/jcs.01275
71. Rainbolt, T. K., Atanassova, N., Genereux, J. C., & Wiseman, R. L. (2013). Stress-Regulated Translational Attenuation Adapts Mitochondrial Protein Import through Tim17A Degradation. *Cell Metabolism*, *18*(6), 908–919. https://doi.org/10.1016/j.cmet.2013.11.006
72. Apablaza, P., Bórquez, J. C., Mendoza, R., Silva, M., Tapia, G., Espinosa, A., Troncoso, R., Videla, L. A., Juretić, N., & Del Campo, A. (2023). Exercise Induces an Augmented Skeletal Muscle Mitochondrial Unfolded Protein Response in a Mouse Model of Obesity Produced by a High-Fat Diet. *International Journal of Molecular Sciences*, *24*(6), 5654. https://doi.org/10.3390/ijms24065654
73. Slavin, M. B., Kumari, R., & Hood, D. A. (2022). ATF5 is a regulator of exercise-induced mitochondrial quality control in skeletal muscle. *Molecular Metabolism*, *66*, 101623. https://doi.org/10.1016/j.molmet.2022.101623
74. Panieri, E., Pinho, S. A., Afonso, G. J. M., Oliveira, P. J., Cunha-Oliveira, T., & Saso, L. (2022). NRF2 and Mitochondrial Function in Cancer and Cancer Stem Cells. *Cells*, *11*(15), 2401. https://doi.org/10.3390/cells11152401
75. Poljsak, B., Šuput, D., & Milisav, I. (2013). Achieving the Balance between ROS and Antioxidants: When to Use the Synthetic Antioxidants. *Oxidative Medicine and Cellular Longevity*, *2013*, 1–11. https://doi.org/10.1155/2013/956792
76. Zhou, C., Sun, H., Zheng, C., Gao, J., Fu, Q., Hu, N., Shao, X., Zhou, Y., Xiong, J., Nie, K., Zhou, H., Shen, L., Fang, H., & Lyu, J. (2018). Oncogenic HSP60 regulates mitochondrial oxidative phosphorylation to support Erk1/2 activation during pancreatic cancer cell growth. *Cell Death & Disease*, *9*(2), 161. https://doi.org/10.1038/s41419-017-0196-z

77. Fan, W., Fan, S.-S., Feng, J., Xiao, D., Fan, S., & Luo, J. (2017). Elevated expression of HSP10 protein inhibits apoptosis and associates with poor prognosis of astrocytoma. *PLOS ONE*, *12*(10), e0185563. https://doi.org/10.1371/journal.pone.0185563
78. Feng, J., Zhan, Y., Zhang, Y., Zheng, H., Wang, W., & Fan, S. (2019). Increased expression of heat shock protein (HSP) 10 and HSP70 correlates with poor prognosis of nasopharyngeal carcinoma. *Cancer Management and Research*, *Volume 11*, 8219–8227. https://doi.org/10.2147/CMAR.S218427
79. Wu, P.-K., Hong, S.-K., Veeranki, S., Karkhanis, M., Starenki, D., Plaza, J. A., & Park, J.-I. (2013). A Mortalin/HSPA9-Mediated Switch in Tumor-Suppressive Signaling of Raf/MEK/Extracellular Signal-Regulated Kinase. *Molecular and Cellular Biology*, *33*(20), 4051–4067. https://doi.org/10.1128/MCB.00021-13
80. Starenki, D., Hong, S.-K., Lloyd, R. V., & Park, J.-I. (2015). Mortalin (GRP75/HSPA9) upregulation promotes survival and proliferation of medullary thyroid carcinoma cells. *Oncogene*, *34*(35), 4624–4634. https://doi.org/10.1038/onc.2014.392
81. Liu, L.-X., Lu, J.-C., Zeng, H.-Y., Cai, J.-B., Zhang, P.-F., Guo, X.-J., Huang, X.-Y., Dong, R.-Z., Zhang, C., Kang, Q., Zou, H., Zhang, X.-Y., Zhang, L., Zhang, X.-W., Ke, A.-W., & Shi, G.-M. (2019). Mortalin stabilizes CD151-depedent tetraspanin-enriched microdomains and implicates in the progression of hepatocellular carcinoma. *Journal of Cancer*, *10*(25), 6199–6206. https://doi.org/10.7150/jca.36301
82. Luo, J., Zeng, B., Tao, C., Lu, M., & Ren, G. (2020). ClpP regulates breast cancer cell proliferation, invasion and apoptosis by modulating the Src/PI3K/Akt signaling pathway. *PeerJ*, *8*, e8754. https://doi.org/10.7717/peerj.8754
83. Quirós, P. M., Español, Y., Acín-Pérez, R., Rodríguez, F., Bárcena, C., Watanabe, K., Calvo, E., Loureiro, M., Fernández-García, M. S., Fueyo, A., Vázquez, J., Enríquez, J. A., & López-Otín, C. (2014). ATP-Dependent Lon Protease Controls Tumor Bioenergetics by Reprogramming Mitochondrial Activity. *Cell Reports*, *8*(2), 542–556. https://doi.org/10.1016/j.celrep.2014.06.018
84. Özcan, U., Yilmaz, E., Özcan, L., Furuhashi, M., Vaillancourt, E., Smith, R. O., Görgün, C. Z., & Hotamisligil, G. S. (2006). Chemical Chaperones Reduce ER Stress and Restore Glucose Homeostasis in a Mouse Model of Type 2 Diabetes. *Science*, *313*(5790), 1137–1140. https://doi.org/10.1126/science.1128294
85. Xu, W.-N., Zheng, H.-L., Yang, R.-Z., Sun, Y.-F., Peng, B.-R., Liu, C., Song, J., Jiang, S.-D., & Zhu, L.-X. (2024). The mitochondrial UPR induced by ATF5 attenuates intervertebral disc degeneration via cooperating with mitophagy. *Cell Biology and Toxicology*, *40*(1), 16. https://doi.org/10.1007/s10565-024-09854-9
86. Paerhati, P., Liu, J., Jin, Z., Jakoš, T., Zhu, S., Qian, L., Zhu, J., & Yuan, Y. (2022). Advancements in Activating Transcription Factor 5 Function in Regulating Cell Stress and Survival. *International Journal of Molecular Sciences*, *23*(13), 7129. https://doi.org/10.3390/ijms23137129
87. Zhao, Q. (2002). A mitochondrial specific stress response in mammalian cells. *The EMBO Journal*, *21*(17), 4411–4419. https://doi.org/10.1093/emboj/cdf445
88. Dogan, S. A., Pujol, C., Maiti, P., Kukat, A., Wang, S., Hermans, S., Senft, K., Wibom, R., Rugarli, E. I., & Trifunovic, A. (2014). Tissue-Specific Loss of DARS2 Activates Stress Responses Independently of Respiratory Chain Deficiency in the Heart. *Cell Metabolism*, *19*(3), 458–469. https://doi.org/10.1016/j.cmet.2014.02.004
89. Smyrnias, I., Gray, S. P., Okonko, D. O., Sawyer, G., Zoccarato, A., Catibog, N., López, B., González, A., Ravassa, S., Díez, J., & Shah, A. M. (2019). Cardioprotective Effect of the Mitochondrial Unfolded Protein Response During Chronic Pressure Overload. *Journal of the American College of Cardiology*, *73*(14), 1795–1806. https://doi.org/10.1016/j.jacc.2018.12.087
90. Hayashi, T., Kudo, T., Fujita, R., Fujita, S., Tsubouchi, H., Fuseya, S., Suzuki, R., Hamada, M., Okada, R., Muratani, M., Shiba, D., Suzuki, T., Warabi, E., Yamamoto, M., & Takahashi, S.

(2021). Nuclear factor E2-related factor 2 (NRF2) deficiency accelerates fast fibre type transition in soleus muscle during space flight. *Communications Biology*, *4*(1), 787. https://doi.org/10.1038/s42003-021-02334-4
91. Sena, L. A., & Chandel, N. S. (2012). Physiological Roles of Mitochondrial Reactive Oxygen Species. *Molecular Cell*, *48*(2), 158–167. https://doi.org/10.1016/j.molcel.2012.09.025
92. Weydert, C. J., & Cullen, J. J. (2010). Measurement of superoxide dismutase, catalase and glutathione peroxidase in cultured cells and tissue. *Nature Protocols*, *5*(1), 51–66. https://doi.org/10.1038/nprot.2009.197
93. Safakli, R. N., Gray, S. P., Bernardi, N., & Smyrnias, I. (2025). Unveiling a novel signalling pathway involving NRF2 and PGAM5 in regulating the mitochondrial unfolded protein response in stressed cardiomyocytes. *The International Journal of Biochemistry & Cell Biology*, *178*, 106704. https://doi.org/10.1016/j.biocel.2024.106704
94. Palmeira, C. M., Teodoro, J. S., Amorim, J. A., Steegborn, C., Sinclair, D. A., & Rolo, A. P. (2019). Mitohormesis and metabolic health: The interplay between ROS, cAMP and sirtuins. *Free Radical Biology and Medicine*, *141*, 483–491. https://doi.org/10.1016/j.freeradbiomed.2019.07.017
95. Kenny, T. C., Hart, P., Ragazzi, M., Sersinghe, M., Chipuk, J., Sagar, M. A. K., Eliceiri, K. W., LaFramboise, T., Grandhi, S., Santos, J., Riar, A. K., Papa, L., D'Aurello, M., Manfredi, G., Bonini, M. G., & Germain, D. (2017). Selected mitochondrial DNA landscapes activate the SIRT3 axis of the UPRmt to promote metastasis. *Oncogene*, *36*(31), 4393–4404. https://doi.org/10.1038/onc.2017.52
96. Yamamoto, M., Kensler, T. W., & Motohashi, H. (2018). The KEAP1-NRF2 System: A Thiol-Based Sensor-Effector Apparatus for Maintaining Redox Homeostasis. *Physiological Reviews*, *98*(3), 1169–1203. https://doi.org/10.1152/physrev.00023.2017
97. Champsi, S., & Hood, D. A. (2025). Sulforaphane treatment mimics contractile activity-induced mitochondrial adaptations in muscle myotubes. *American Journal of Physiology-Cell Physiology*, *328*(2), C335–C354. https://doi.org/10.1152/ajpcell.00669.2024
98. Itoh, K., Ye, P., Matsumiya, T., Tanji, K., & Ozaki, T. (2015). Emerging functional cross-talk between the Keap1-Nrf2 system and mitochondria. *Journal of Clinical Biochemistry and Nutrition*, *56*(2), 91–97. https://doi.org/10.3164/jcbn.14-134
99. Ross, D., & Siegel, D. (2021). The diverse functionality of NQO1 and its roles in redox control. *Redox Biology*, *41*, 101950. https://doi.org/10.1016/j.redox.2021.101950
100. He, C. H., Gong, P., Hu, B., Stewart, D., Choi, M. E., Choi, A. M. K., & Alam, J. (2001). Identification of Activating Transcription Factor 4 (ATF4) as an Nrf2-interacting Protein. *Journal of Biological Chemistry*, *276*(24), 20858–20865. https://doi.org/10.1074/jbc.M101198200
101. Zong, Z.-H., Du, Z.-X., Li, N., Li, C., Zhang, Q., Liu, B.-Q., Guan, Y., & Wang, H.-Q. (2012). Implication of Nrf2 and ATF4 in differential induction of CHOP by proteasome inhibition in thyroid cancer cells. *Biochimica et Biophysica Acta (BBA) - Molecular Cell Research*, *1823*(8), 1395–1404. https://doi.org/10.1016/j.bbamcr.2012.06.001
102. Zhang, B., Tan, Y., Zhang, Z., Feng, P., Ding, W., Wang, Q., Liang, H., Duan, W., Wang, X., Yu, S., Liu, J., Yi, D., Sun, Y., & Yi, W. (2020). Novel PGC-1α/ATF5 Axis Partly Activates UPRmt and Mediates Cardioprotective Role of Tetrahydrocurcumin in Pathological Cardiac Hypertrophy. *Oxidative Medicine and Cellular Longevity*, *2020*, 1–21. https://doi.org/10.1155/2020/9187065
103. Angelastro, J. M., Ignatova, T. N., Kukekov, V. G., Steindler, D. A., Stengren, G. B., Mendelsohn, C., & Greene, L. A. (2003). Regulated Expression of ATF5 Is Required for the Progression of Neural Progenitor Cells to Neurons. *The Journal of Neuroscience*, *23*(11), 4590–4600. https://doi.org/10.1523/JNEUROSCI.23-11-04590.2003
104. Liu, Y., Zhang, L., Zhang, S., Liu, J., Li, X., Yang, K., Yang, D., Liu, Y., Sun, L., Liu, F., & Xiao, L. (2023). ATF5 regulates tubulointerstitial injury in diabetic kidney disease via mitochondrial

unfolded protein response. *Molecular Medicine*, *29*(1), 57. https://doi.org/10.1186/s10020-023-00651-4
105. Zhao, Y., Zhang, Y.-D., Zhang, Y.-Y., Qian, S.-W., Zhang, Z.-C., Li, S.-F., Guo, L., Liu, Y., Wen, B., Lei, Q.-Y., Tang, Q.-Q., & Li, X. (2014). P300-Dependent Acetylation of Activating Transcription Factor 5 Enhances C/EBPβ Transactivation of C/EBPα during 3T3-L1 Differentiation. *Molecular and Cellular Biology*, *34*(3), 315–324. https://doi.org/10.1128/MCB.00956-13
106. Nakamori, D., Takayama, K., Nagamoto, Y., Mitani, S., Sakurai, F., Tachibana, M., & Mizuguchi, H. (2016). Hepatic maturation of human iPS cell-derived hepatocyte-like cells by ATF5, c/EBPα, and PROX1 transduction. *Biochemical and Biophysical Research Communications*, *469*(3), 424–429. https://doi.org/10.1016/j.bbrc.2015.12.007
107. Yamazaki, T., Ohmi, A., Kurumaya, H., Kato, K., Abe, T., Yamamoto, H., Nakanishi, N., Okuyama, R., Umemura, M., Kaise, T., Watanabe, R., Okawa, Y., Takahashi, S., & Takahashi, Y. (2010). Regulation of the human CHOP gene promoter by the stress response transcription factor ATF5 via the AARE1 site in human hepatoma HepG2 cells. *Life Sciences*, *87*(9–10), 294–301. https://doi.org/10.1016/j.lfs.2010.07.006
108. Leong, D. T., Abraham, M. C., Gupta, A., Lim, T., Chew, F. T., & Hutmacher, D. W. (2012). ATF5, a possible regulator of osteogenic differentiation in human adipose-derived stem cells. *Journal of Cellular Biochemistry*, *113*(8), 2744–2753. https://doi.org/10.1002/jcb.24150
109. Karpel-Massler, G., Horst, B. A., Shu, C., Chau, L., Tsujiuchi, T., Bruce, J. N., Canoll, P., Greene, L. A., Angelastro, J. M., & Siegelin, M. D. (2016). A Synthetic Cell-Penetrating Dominant-Negative ATF5 Peptide Exerts Anticancer Activity against a Broad Spectrum of Treatment-Resistant Cancers. *Clinical Cancer Research*, *22*(18), 4698–4711. https://doi.org/10.1158/1078-0432.CCR-15-2827
110. Nukuda, A., Endoh, H., Yasuda, M., Mizutani, T., Kawabata, K., & Haga, H. (2016). Role of ATF5 in the invasive potential of diverse human cancer cell lines. *Biochemical and Biophysical Research Communications*, *474*(3), 509–514. https://doi.org/10.1016/j.bbrc.2016.04.131
111. Ishihara, S., Yasuda, M., Ishizu, A., Ishikawa, M., Shirato, H., & Haga, H. (2015). Activating transcription factor 5 enhances radioresistance and malignancy in cancer cells. *Oncotarget*, *6*(7), 4602–4614. https://doi.org/10.18632/oncotarget.2912
112. Chen, A., Qian, D., Wang, B., Hu, M., Lu, J., Qi, Y., & Liu, D. X. (2012). ATF5 Is Overexpressed in Epithelial Ovarian Carcinomas and Interference With Its Function Increases Apoptosis Through the Downregulation of Bcl-2 in SKOV-3 Cells: *International Journal of Gynecological Pathology*, *31*(6), 532–537. https://doi.org/10.1097/PGP.0b013e31824df26b
113. Hu, M., Wang, B., Qian, D., Li, L., Zhang, L., Song, X., & Liu, D. X. (2012). Interference with ATF5 function enhances the sensitivity of human pancreatic cancer cells to paclitaxel-induced apoptosis. *Anticancer Research*, *32*(10), 4385–4394.
114. Gho, J. W.-M., Ip, W.-K., Chan, K. Y.-Y., Law, P. T.-Y., Lai, P. B.-S., & Wong, N. (2008). Re-Expression of Transcription Factor *ATF5* in Hepatocellular Carcinoma Induces G2-M Arrest. *Cancer Research*, *68*(16), 6743–6751. https://doi.org/10.1158/0008-5472.CAN-07-6469
115. Duman, R. S. (2017). Sex-specific disease-associated modules for depression. *Nature Medicine*, *23*(9), 1015–1017. https://doi.org/10.1038/nm.4391
116. Shakeshaft, A., Panjwani, N., Collingwood, A., Crudgington, H., Hall, A., Andrade, D. M., Beier, C. P., Fong, C. Y., Gardella, E., Gesche, J., Greenberg, D. A., Hamandi, K., Koht, J., Lim, K. S., Møller, R. S., Ng, C. C., Orsini, A., Rees, M. I., Rubboli, G., … Pal, D. K. (2022). Sex-specific disease modifiers in juvenile myoclonic epilepsy. *Scientific Reports*, *12*(1), 2785. https://doi.org/10.1038/s41598-022-06324-2
117. Foltz, S., Wu, F., Ghazal, N., Kwong, J. Q., Hartzell, H. C., & Choo, H. J. (2022). Sex differences in the involvement of skeletal and cardiac muscles in myopathic *Ano5*$^{-/-}$ mice. *American*

Journal of Physiology-Cell Physiology, *322*(2), C283–C295. https://doi.org/10.1152/ajpcell.00350.2021
118. Lopez, M.-C., Efron, P. A., Ozrazgat-Baslanti, T., Zhang, J., Cuschieri, J., Maier, R. V., Minei, J. P., Baker, H. V., Moore, F. A., Moldawer, L. L., & Brakenridge, S. C. (2016). Sex-based differences in the genomic response, innate immunity, organ dysfunction, and clinical outcomes after severe blunt traumatic injury and hemorrhagic shock. *Journal of Trauma and Acute Care Surgery*, *81*(3), 478–485. https://doi.org/10.1097/TA.0000000000001113
119. Lipes, J., Mardini, L., & Jayaraman, D. (2013). Sex and Mortality of Hospitalized Adults After Admission to an Intensive Care Unit. *American Journal of Critical Care*, *22*(4), 314–319. https://doi.org/10.4037/ajcc2013225
120. Rosa-Caldwell, M. E., Lim, S., Haynie, W. A., Brown, J. L., Deaver, J. W., Morena Da Silva, F., Jansen, L. T., Lee, D. E., Wiggs, M. P., Washington, T. A., & Greene, N. P. (2021). Female mice may have exacerbated catabolic signalling response compared to male mice during development and progression of disuse atrophy. *Journal of Cachexia, Sarcopenia and Muscle*, *12*(3), 717–730. https://doi.org/10.1002/jcsm.12693
121. Oliveira, A. N., Memme, J. M., Wong, J., & Hood, D. A. (2024). Dimorphic effect of TFE3 in determining mitochondrial and lysosomal content in muscle following denervation. *Skeletal Muscle*, *14*(1), 7. https://doi.org/10.1186/s13395-024-00339-1
122. Jenkins, E. C., O'Connell, M. J., Manfredi, G., & Germain, D. (2021). Doxycycline promotes proteasome fitness in the central nervous system. *Scientific Reports*, *11*(1), 17003. https://doi.org/10.1038/s41598-021-96540-z
123. Riar, A. K., Burstein, S. R., Palomo, G. M., Arreguin, A., Manfredi, G., & Germain, D. (2017). Sex specific activation of the ERα axis of the mitochondrial UPR (UPRmt) in the G93A-SOD1 mouse model of familial ALS. *Human Molecular Genetics*, *26*(7), 1318–1327. https://doi.org/10.1093/hmg/ddx049
124. Sartori, R., Romanello, V., & Sandri, M. (2021). Mechanisms of muscle atrophy and hypertrophy: Implications in health and disease. *Nature Communications*, *12*(1), 330. https://doi.org/10.1038/s41467-020-20123-1
125. Triolo, M., & Hood, D. A. (2019). Mitochondrial breakdown in skeletal muscle and the emerging role of the lysosomes. *Archives of Biochemistry and Biophysics*, *661*, 66–73. https://doi.org/10.1016/j.abb.2018.11.004
126. Vainshtein, A., Desjardins, E. M., Armani, A., Sandri, M., & Hood, D. A. (2015). PGC-1α modulates denervation-induced mitophagy in skeletal muscle. *Skeletal Muscle*, *5*(1), 9. https://doi.org/10.1186/s13395-015-0033-y
127. Chen, X., Ji, Y., Liu, R., Zhu, X., Wang, K., Yang, X., Liu, B., Gao, Z., Huang, Y., Shen, Y., Liu, H., & Sun, H. (2023). Mitochondrial dysfunction: Roles in skeletal muscle atrophy. *Journal of Translational Medicine*, *21*(1), 503. https://doi.org/10.1186/s12967-023-04369-z
128. Peterson, C. M., Johannsen, D. L., & Ravussin, E. (2012). Skeletal Muscle Mitochondria and Aging: A Review. *Journal of Aging Research*, *2012*, 1–20. https://doi.org/10.1155/2012/194821
129. Costa-Mattioli, M., & Walter, P. (2020). The integrated stress response: From mechanism to disease. *Science*, *368*(6489), eaat5314. https://doi.org/10.1126/science.aat5314
130. Li, C., Li, N., Zhang, Z., Song, Y., Li, J., Wang, Z., Bo, H., & Zhang, Y. (2023). The specific mitochondrial unfolded protein response in fast- and slow-twitch muscles of high-fat diet-induced insulin-resistant rats. *Frontiers in Endocrinology*, *14*, 1127524. https://doi.org/10.3389/fendo.2023.1127524
131. Pakos-Zebrucka, K., Koryga, I., Mnich, K., Ljujic, M., Samali, A., & Gorman, A. M. (2016). The integrated stress response. *EMBO Reports*, *17*(10), 1374–1395. https://doi.org/10.15252/embr.201642195

132. Zhang, G., Wang, X., Li, C., Li, Q., An, Y. A., Luo, X., Deng, Y., Gillette, T. G., Scherer, P. E., & Wang, Z. V. (2021). Integrated Stress Response Couples Mitochondrial Protein Translation With Oxidative Stress Control. *Circulation*, *144*(18), 1500–1515. https://doi.org/10.1161/CIRCULATIONAHA.120.053125
133. Ma, J., Liu, Y., Valladolid-Acebes, I., Recio-López, P., Peng, G., Li, J., Berggren, P.-O., Juntti-Berggren, L., & Tong, N. (2023). ATF5 is a regulator of ER stress and β-cell apoptosis in different mouse models of genetic- and diet-induced obesity and diabetes mellitus. *Cellular Signalling*, *102*, 110535. https://doi.org/10.1016/j.cellsig.2022.110535
134. Brearley-Sholto, M. C., Loczenski-Brown, D. M., Jones, S., Daniel, Z. C. T. R., Ebling, F. J. P., Parr, T., & Brameld, J. M. (2021). Effect of AAV-mediated overexpression of ATF5 and downstream targets of an integrated stress response in murine skeletal muscle. *Scientific Reports*, *11*(1), 19796. https://doi.org/10.1038/s41598-021-99432-4
135. Wang, Y., Li, J., Zhang, Z., Wang, R., Bo, H., & Zhang, Y. (2023). Exercise Improves the Coordination of the Mitochondrial Unfolded Protein Response and Mitophagy in Aging Skeletal Muscle. *Life*, *13*(4), 1006. https://doi.org/10.3390/life13041006
136. Rath, E., Berger, E., Messlik, A., Nunes, T., Liu, B., Kim, S. C., Hoogenraad, N., Sans, M., Sartor, R. B., & Haller, D. (2012). Induction of dsRNA-activated protein kinase links mitochondrial unfolded protein response to the pathogenesis of intestinal inflammation. *Gut*, *61*(9), 1269–1278. https://doi.org/10.1136/gutjnl-2011-300767
137. Ron, D., & Walter, P. (2007). Signal integration in the endoplasmic reticulum unfolded protein response. *Nature Reviews Molecular Cell Biology*, *8*(7), 519–529. https://doi.org/10.1038/nrm2199
138. Triolo, M., Bhattacharya, D., & Hood, D. A. (2022). Denervation induces mitochondrial decline and exacerbates lysosome dysfunction in middle-aged mice. *Aging*, *14*(22), 8900–8913. https://doi.org/10.18632/aging.204365
139. Triolo, M., Slavin, M., Moradi, N., & Hood, D. A. (2022). Time-dependent changes in autophagy, mitophagy and lysosomes in skeletal muscle during denervation-induced disuse. *The Journal of Physiology*, *600*(7), 1683–1701. https://doi.org/10.1113/JP282173
140. O′Leary, M. F. N., Vainshtein, A., Carter, H. N., Zhang, Y., & Hood, D. A. (2012). Denervation-induced mitochondrial dysfunction and autophagy in skeletal muscle of apoptosis-deficient animals. *American Journal of Physiology-Cell Physiology*, *303*(4), C447–C454. https://doi.org/10.1152/ajpcell.00451.2011
141. Memme, J. M., Oliveira, A. N., & Hood, D. A. (2022). P53 regulates skeletal muscle mitophagy and mitochondrial quality control following denervation-induced muscle disuse. *Journal of Biological Chemistry*, *298*(2), 101540. https://doi.org/10.1016/j.jbc.2021.101540
142. Hyatt, H., Deminice, R., Yoshihara, T., & Powers, S. K. (2019). Mitochondrial dysfunction induces muscle atrophy during prolonged inactivity: A review of the causes and effects. *Archives of Biochemistry and Biophysics*, *662*, 49–60. https://doi.org/10.1016/j.abb.2018.11.005
143. Kang, C., Goodman, C. A., Hornberger, T. A., & Ji, L. L. (2015). PGC-1α overexpression by *in vivo* transfection attenuates mitochondrial deterioration of skeletal muscle caused by immobilization. *The FASEB Journal*, *29*(10), 4092–4106. https://doi.org/10.1096/fj.14-266619
144. Adhihetty, P. J., O'Leary, M. F. N., Chabi, B., Wicks, K. L., & Hood, D. A. (2007). Effect of denervation on mitochondrially mediated apoptosis in skeletal muscle. *Journal of Applied Physiology*, *102*(3), 1143–1151. https://doi.org/10.1152/japplphysiol.00768.2006
145. Trevino, M. B., Zhang, X., Standley, R. A., Wang, M., Han, X., Reis, F. C. G., Periasamy, M., Yu, G., Kelly, D. P., Goodpaster, B. H., Vega, R. B., & Coen, P. M. (2019). Loss of mitochondrial energetics is associated with poor recovery of muscle function but not mass following disuse atrophy. *American Journal of Physiology-Endocrinology and Metabolism*, *317*(5), E899–E910. https://doi.org/10.1152/ajpendo.00161.2019

146. Powers, S. K., Lynch, G. S., Murphy, K. T., Reid, M. B., & Zijdewind, I. (2016). Disease-Induced Skeletal Muscle Atrophy and Fatigue. *Medicine & Science in Sports & Exercise*, *48*(11), 2307–2319. https://doi.org/10.1249/MSS.0000000000000975
147. Singh, K., & Hood, D. A. (2011). Effect of denervation-induced muscle disuse on mitochondrial protein import. *American Journal of Physiology-Cell Physiology*, *300*(1), C138–C145. https://doi.org/10.1152/ajpcell.00181.2010
148. Zhang, X., Trevino, M. B., Wang, M., Gardell, S. J., Ayala, J. E., Han, X., Kelly, D. P., Goodpaster, B. H., Vega, R. B., & Coen, P. M. (2018). Impaired Mitochondrial Energetics Characterize Poor Early Recovery of Muscle Mass Following Hind Limb Unloading in Old Mice. *The Journals of Gerontology: Series A*, *73*(10), 1313–1322. https://doi.org/10.1093/gerona/gly051
149. Triolo, M., Oliveira, A. N., Kumari, R., & Hood, D. A. (2022). The influence of age, sex, and exercise on autophagy, mitophagy, and lysosome biogenesis in skeletal muscle. *Skeletal Muscle*, *12*(1), 13. https://doi.org/10.1186/s13395-022-00296-7
150. Carafoli, E., Margreth, A., & Buffa, P. (1964). Early biochemical changes in mitochondria from denervated muscle and their relation to the onset of atrophy. *Experimental and Molecular Pathology*, *3*(2), 171–181. https://doi.org/10.1016/0014-4800(64)90050-4
151. Wu, J., Ruas, J. L., Estall, J. L., Rasbach, K. A., Choi, J. H., Ye, L., Boström, P., Tyra, H. M., Crawford, R. W., Campbell, K. P., Rutkowski, D. T., Kaufman, R. J., & Spiegelman, B. M. (2011). The Unfolded Protein Response Mediates Adaptation to Exercise in Skeletal Muscle through a PGC-1α/ATF6α Complex. *Cell Metabolism*, *13*(2), 160–169. https://doi.org/10.1016/j.cmet.2011.01.003
152. Vainshtein, A., Tryon, L. D., Pauly, M., & Hood, D. A. (2015). Role of PGC-1α during acute exercise-induced autophagy and mitophagy in skeletal muscle. *American Journal of Physiology-Cell Physiology*, *308*(9), C710–C719. https://doi.org/10.1152/ajpcell.00380.2014
153. Aras, S., Purandare, N., Gladyck, S., Somayajulu-Nitu, M., Zhang, K., Wallace, D. C., & Grossman, L. I. (2020). Mitochondrial Nuclear Retrograde Regulator 1 (MNRR1) rescues the cellular phenotype of MELAS by inducing homeostatic mechanisms. *Proceedings of the National Academy of Sciences*, *117*(50), 32056–32065. https://doi.org/10.1073/pnas.2005877117
154. Liou, Y.-H., Personnaz, J., Jacobi, D., Knudsen, N. H., Chalom, M. M., Starost, K. A., Nnah, I. C., & Lee, C.-H. (2022). Hepatic Fis1 regulates mitochondrial integrated stress response and improves metabolic homeostasis. *JCI Insight*, *7*(4), e150041. https://doi.org/10.1172/jci.insight.150041
155. Gkirtzimanaki, K., Kabrani, E., Nikoleri, D., Polyzos, A., Blanas, A., Sidiropoulos, P., Makrigiannakis, A., Bertsias, G., Boumpas, D. T., & Verginis, P. (2018). IFNα Impairs Autophagic Degradation of mtDNA Promoting Autoreactivity of SLE Monocytes in a STING-Dependent Fashion. *Cell Reports*, *25*(4), 921-933.e5. https://doi.org/10.1016/j.celrep.2018.09.001
156. Sanfrancesco, V. C., & Hood, D. A. (2025). Acute contractile activity induces the activation of the mitochondrial integrated stress response and the transcription factor ATF4. *Journal of Applied Physiology*, *138*(3), 857–871. https://doi.org/10.1152/japplphysiol.00307.2024
157. Memme, J. M., Oliveira, A. N., & Hood, D. A. (2016). Chronology of UPR activation in skeletal muscle adaptations to chronic contractile activity. *American Journal of Physiology-Cell Physiology*, *310*(11), C1024–C1036. https://doi.org/10.1152/ajpcell.00009.2016
158. Hogan, M. R., Cockram, G. P., & Lu, R. (2006). Cooperative interaction of Zhangfei and ATF4 in transactivation of the cyclic AMP response element. *FEBS Letters*, *580*(1), 58–62. https://doi.org/10.1016/j.febslet.2005.11.046
159. Tonelli, C., Chio, I. I. C., & Tuveson, D. A. (2018). Transcriptional Regulation by Nrf2. *Antioxidants & Redox Signaling*, *29*(17), 1727–1745. https://doi.org/10.1089/ars.2017.7342

160. Amerik, A. Yu., Petukhova, G. V., Grigorenko, V. G., Lykov, I. P., Yarovoi, S. V., Lipkin, V. M., & Gorbalenya, A. E. (1994). Cloning and sequence analysis of cDNA for a human homolog of eubacterial ATP-dependent Lon proteases. *FEBS Letters*, *340*(1–2), 25–28. https://doi.org/10.1016/0014-5793(94)80166-5
161. Domanico, S. Z., DeNagel, D. C., Dahlseid, J. N., Green, J. M., & Pierce, S. K. (1993). Cloning of the gene encoding peptide-binding protein 74 shows that it is a new member of the heat shock protein 70 family. *Molecular and Cellular Biology*, *13*(6), 3598–3610. https://doi.org/10.1128/MCB.13.6.3598
162. Tang, Y., Zhou, Y., Fan, S., & Wen, Q. (2022). The multiple roles and therapeutic potential of HSP60 in cancer. *Biochemical Pharmacology*, *201*, 115096. https://doi.org/10.1016/j.bcp.2022.115096
163. Andresen, B. S., Corydon, T. J., Wilsbech, M., Bross, P., Schroeder, L. D., Hindkjær, T. F., Bolund, L., & Gregersen, N. (2000). Characterization of mouse Clpp protease cDNA, gene, and protein. *Mammalian Genome*, *11*(4), 275–280. https://doi.org/10.1007/s003350010052
164. Rospert, S., Junne, T., Glick, B. S., & Schatz, G. (1993). Cloning and disruption of the gene encoding yeast mitochondrial chaperonin 10, the homolog of *E. coli* groES. *FEBS Letters*, *335*(3), 358–360. https://doi.org/10.1016/0014-5793(93)80419-U
165. Chen, M.-M., Li, Y., Deng, S.-L., Zhao, Y., Lian, Z.-X., & Yu, K. (2022). Mitochondrial Function and Reactive Oxygen/Nitrogen Species in Skeletal Muscle. *Frontiers in Cell and Developmental Biology*, *10*, 826981. https://doi.org/10.3389/fcell.2022.826981
166. Yuhan, L., Khaleghi Ghadiri, M., & Gorji, A. (2024). Impact of NQO1 dysregulation in CNS disorders. *Journal of Translational Medicine*, *22*(1), 4. https://doi.org/10.1186/s12967-023-04802-3
167. Candas, D., & Li, J. J. (2014). MnSOD in Oxidative Stress Response-Potential Regulation *via* Mitochondrial Protein Influx. *Antioxidants & Redox Signaling*, *20*(10), 1599–1617. https://doi.org/10.1089/ars.2013.5305
168. Shen, Y., Zhang, Q., Huang, Z., Zhu, J., Qiu, J., Ma, W., Yang, X., Ding, F., & Sun, H. (2020). Isoquercitrin Delays Denervated Soleus Muscle Atrophy by Inhibiting Oxidative Stress and Inflammation. *Frontiers in Physiology*, *11*, 988. https://doi.org/10.3389/fphys.2020.00988

Figure Legends

Figure 1. Seven days of denervation leads to a reduction in muscle mass in ATF5 KO and WT mice. Whole-body ATF5 KO mouse model was confirmed through DNA genotyping by targeting the ATF5 WT (100 bp) and MUT (400 bp) alleles with designated primer sets (A). Quantification of GAS and SOL muscle weight of WT and ATF5 KO male/female mice normalized to bodyweight (B-C) Comparison of total bodyweight (g) between WT and ATF5 KO male/female mice (D). Comparison of male epididymal fat (fat/bodyweight (g)) between WT and ATF5 KO groups. (WT: n = 18, KO n = 24, WT (males) n = 8-9, WT (females) n = 10-11, KO (males) = 13, KO (females) = 11)) *P < 0.05, **P < 0.01, ***P < 0.001, ****P < 0.0001. Comparisons between CON vs DEN, total bodyweight, and epididymal fat from WT and ATF5 KO animals are evaluated using two-way ANOVA with repeated measures.

Figure 2. Mitochondrial content after seven days of denervation in WT and ATF5 KO male/female mice. Visual qualitative images of SDH staining of male WT and ATF5 KO mice within EDL muscle cross-sections (A). Mitochondrial content was measured by cytochrome c oxidase activity in WT and ATF5 KO male/female mice (B). WT: n = 13, KO n = 16, WT (males) n = 6, WT (females) n = 7, KO (males) = 8, KO (females) = 8. *P < 0.05. Comparisons of COX enzyme activity between CON vs DEN of WT and ATF5 KO animals are evaluated using two-way ANOVA with repeated measures.

Figure 3. High resolution respirometry and ROS emissions of WT and ATF5 KO mice. Oxygen consumption measured for complex I (pyruvate/malate), complex I active (ADP) and complex I+II active (succinate) in male WT and ATF5 KO mice after to seven days of denervation. ROS emissions rates corrected for respiration supported by pyruvate + malate, ADP and succinate in WT and ATF5 KO mice after to seven days of denervation (WT: n = 4, KO n = 4) *P < 0.05, **P < 0.01. Comparisons of respiration and ROS emissions between CON vs DEN of WT and ATF5 KO animals are evaluated using two-way ANOVA with repeated measures.

Figure 4. Mitophagy/autophagy related protein expression in response to denervation in WT and ATF5 KO mice. Western blot and respective quantification of mitophagy/autophagy related proteins in whole muscle TA muscle of WT and KO mice with corresponding ponceau stains. Proteins include P62, Beclin1, and LC3 I/II (A-C). (WT: n = 10, KO n = 13, Males n = , Females n = tbt. *P < 0.05, **P < 0.01, ***P < 0.001, ****P < 0.0001. Comparisons of total protein content between CON vs DEN of WT and ATF5 KO animals are evaluated using two-way ANOVA with repeated measures.

Figure 5. ISR protein content in response to denervation in response to 7 days of denervation in WT and ATF5 KO mice. Western blot and respective quantification of ISR related proteins in whole muscle TA muscle of WT and KO mice with corresponding ponceau stains. Proteins include ATF4, CHOP, p-eIF2 α, and t-eIF2 α (A-D). WT: n = 10, KO n = 13, WT (males) n = 4, WT (females) n = 4-6, KO (males) = 5-6, KO (females) = 4-8. *P < 0.05, **P < 0.01, ***P < 0.001, ****P < 0.0001. Comparisons of total protein content between CON vs DEN of WT and ATF5 KO animals are evaluated using two-way ANOVA with repeated measures.

Figure 6. UPR^{mt} protein content in response to denervation in WT and ATF5 KO mice. Western blot and respective quantification of UPR^{mt} related proteins in whole muscle TA muscle of WT and KO mice with corresponding ponceau stains. Proteins include LONP1, mtHSP70, HSP60, ClpP and CPN10 (A-E). WT: n = 11, KO n = 12, WT (males) n = 4-5, WT (females) n = 4-5, KO (males) = 4-5, KO (females) = 6. *P < 0.05, **P < 0.01. Comparisons of total protein content between CON vs DEN of WT and ATF5 KO animals are evaluated using two-way ANOVA with repeated measures.

Figure 7. Antioxidant protein content in response to denervation in WT and ATF5 KO mice. Western blot and respective quantification of antioxidant related proteins in whole muscle TA muscle of WT and KO mice with corresponding ponceau stains. Proteins include Nrf-2, NQO1, HO1, Catalase and GR (A-E). WT: n = 11, KO n = 12, WT (males) n = 4-5, WT (females) n = 4-5, KO (males) = 4-5, KO (females) = 6. *P < 0.05, **P < 0.01, ***P < 0.001, ****P < 0.0001. Comparisons of total protein content between CON vs DEN of WT and ATF5 KO animals are evaluated using two-way ANOVA with repeated measures.

Figure 8. Lysosomal protein content in response to denervation in WT and ATF5 mice. Western blot and respective quantification of lysosomal related proteins in whole muscle TA muscle of WT and KO mice with corresponding ponceau stains. Proteins include immature/mature Cathepsin B and LAMP1 (A-B). WT: n = 11, KO n = 10, WT (males) n = 4-6, WT (females) n = 5, KO (males) = 5, KO (females) = 5. *P < 0.05, **P < 0.01, ***P < 0.001, ****P < 0.0001. Comparisons of total protein content between CON vs DEN of WT and ATF5 KO animals are evaluated using two-way ANOVA with repeated measures.

Figure 9. Signaling pathways involved in regulating mitochondrial function during the ISR and UPR^{mt}. Mitochondrial stress triggers the activation of ER sensor kinases resulting in the subsequent phosphorylation of the alpha subunit of the eIF2 complex. Phosphorylation of this subunit causes the inhibition of the eIF2B complex, resulting in the selective translation of TFs involved in UPR^{mt} protein synthesis. Newly translated chaperones, proteases and antioxidants will then enter the mitochondria via protein important machinery and carry out their specific roles involved in protein degradation, folding/unfolding and alleviating excess mtROS accumulation.

Figure 10. Results Summary. Overall, mice experienced a significant loss of muscle mass post denervation in all groups. Proteins involved in the ISR/UPR^{mt} and antioxidant, lysosomal, autophagy pathways were all increased in response to denervation in WT mice, with females experiencing a greater degree of activation with certain autophagy and UPR^{mt} related proteins. Mitochondrial content was reduced post denervation, accompanied by an increase in ROS production in WT mice. Mitochondrial content was preserved in ATF5 KO mice post denervation, along with an attenuation of certain proteins involved in the ISR and antioxidant/lysosomal pathways. Male and female KO mice had significantly lower bodyweights compared to WT controls. Specifically, male KO mice had lower levels of adiposity, along with a reduced expression of certain proteins involved in the UPR^{mt}. Male KO mice experienced an enhanced activation of certain autophagy related proteins, whereas female mice experienced an attenuated response with proteins involved in autophagy and the ISR/UPR^{mt} pathway.

Table 1: List of primary/secondary antibodies and concentrations

Protein	Primary Concentration	Secondary Concentration	Company	Catalogue #
Cpn10	1:2000	1:1000 (R)	ENZO	ADI-SPA-110-D
LONP1	1:1000	1:1000 (R)	Cell Signaling	28020S
Parkin	1:1000	1:1000 (M)	Cell Signaling	4211S
HSP60	1:1000	1:1000 (M)	ENZO	ADI-SPA-806-D
mtHSP70	1:1000	1:2000 (M)	ENZO	ADI-SPA-825-D
ClpP	1:1000	1:1000 (R)	abcam	ab124822
LC3-I/II	1:500	1:1000 (R)	Cell Signaling	4108S
P62	1:1000	1:1000 (R)	Cell Signaling	5114S
BECLIN1	1:1000	1:1000 (R)	Cell Signaling	3738S
CHOP	1:500	1:1000 (M)	Cell Signaling	2895S
LAMP1	1:1000	1:1000 (R)	abcam	Ab24170
ATF4	1:1000	1:1000 (M)	Cell Signaling	11815S
NQO1	1:1000	1:1000 (R)	abcam	ab34173
HO-1	1:1000	1:1000 (M)	abcam	ab13248
Nrf-2	1:500	1:1000 (R)	Cell Signaling	12721S
Catalase	1:1000	1:1000 (R)	Cell Signaling	14907S
Glutathione Reductase	1:2000	1:1000 (R)	Santa Cruz	133245
Cathepsin B	1:1000	1:1000 (R)	Cell Signaling	31718S
P-eIF2α	1:1000 (5%BSA)	1:1000 (R)	Cell Signaling	9721S
T-eIF2α	1:1000	1:1000 (R)	Cell Signaling	9722S
Anti-rabbit secondary	---	---	Cell Signaling	7074S
Anti-mouse secondary	---	---	Cell Signaling	7076S

Figure 1. Seven days of denervation leads to a reduction in muscle mass in ATF5 KO and WT.

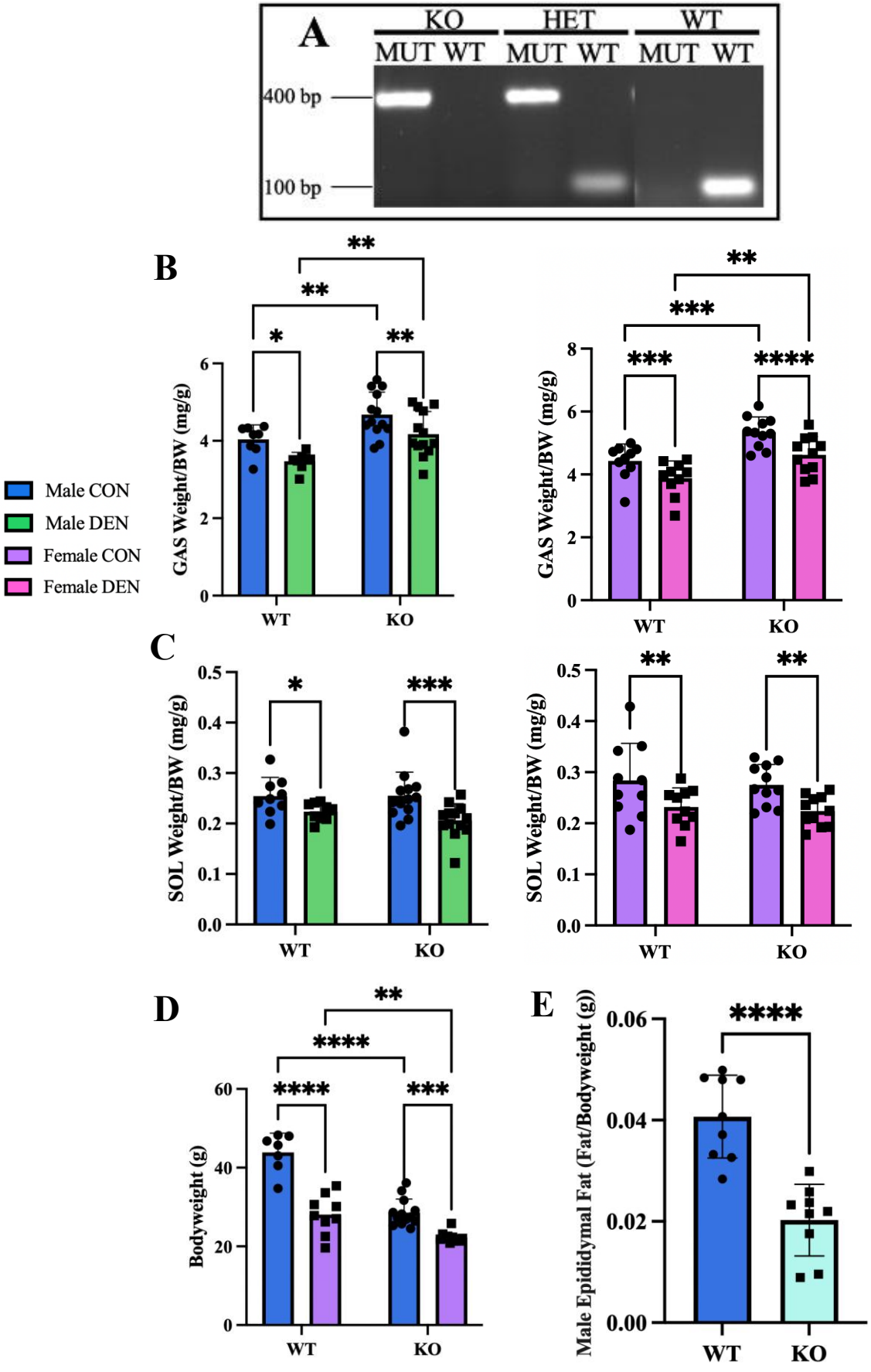

Figure 2. Mitochondrial content after seven days of denervation in WT and ATF5 KO mice.

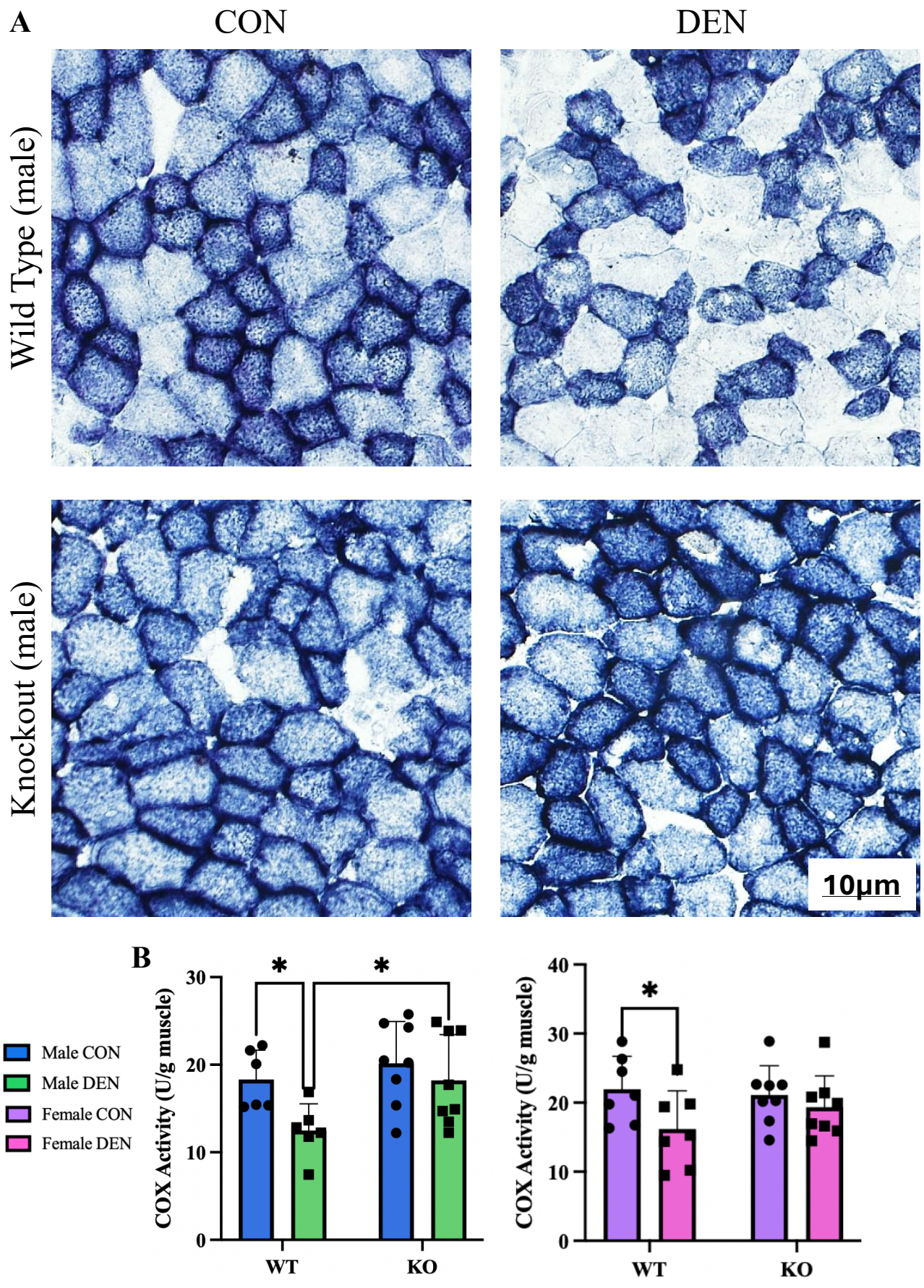

Figure 3. High resolution respirometry and ROS emissions of WT and ATF5 KO mice.

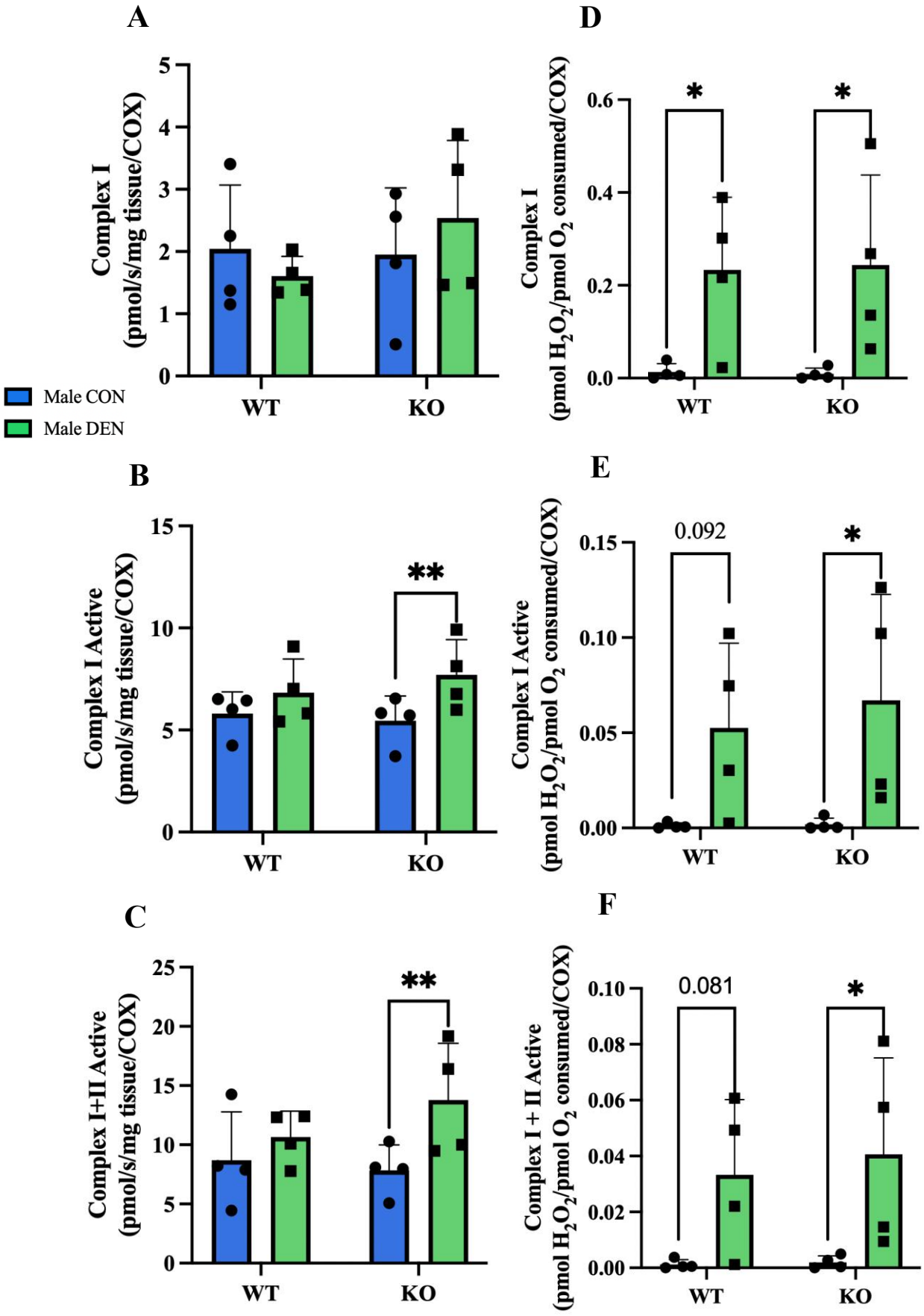

Figure 4. Mitophagy/autophagy related protein expression in response to denervation in WT and ATF5 KO mice.

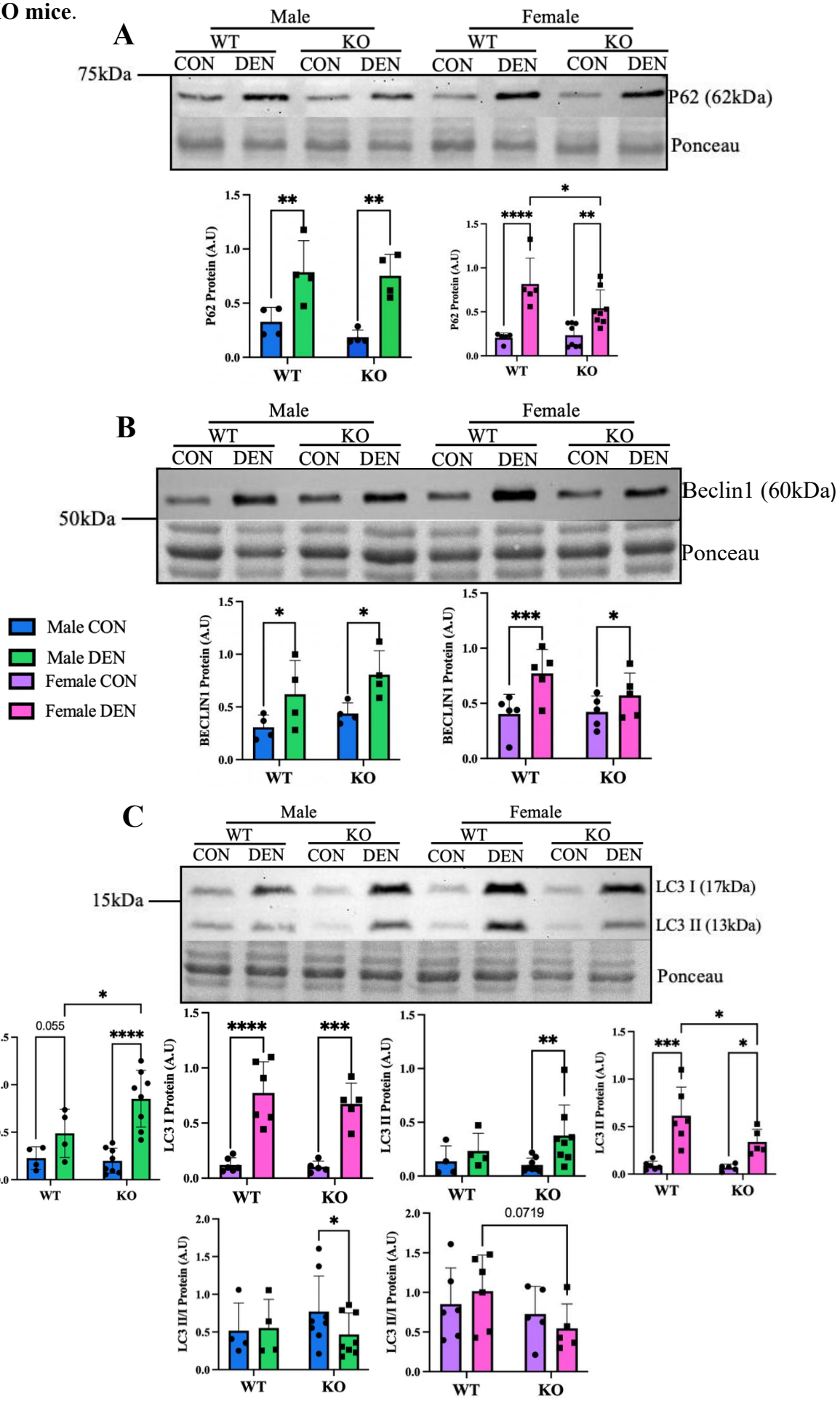

Figure 5. ISR protein content in response to denervation in response to 7 days of denervation in WT and ATF5 KO mice.

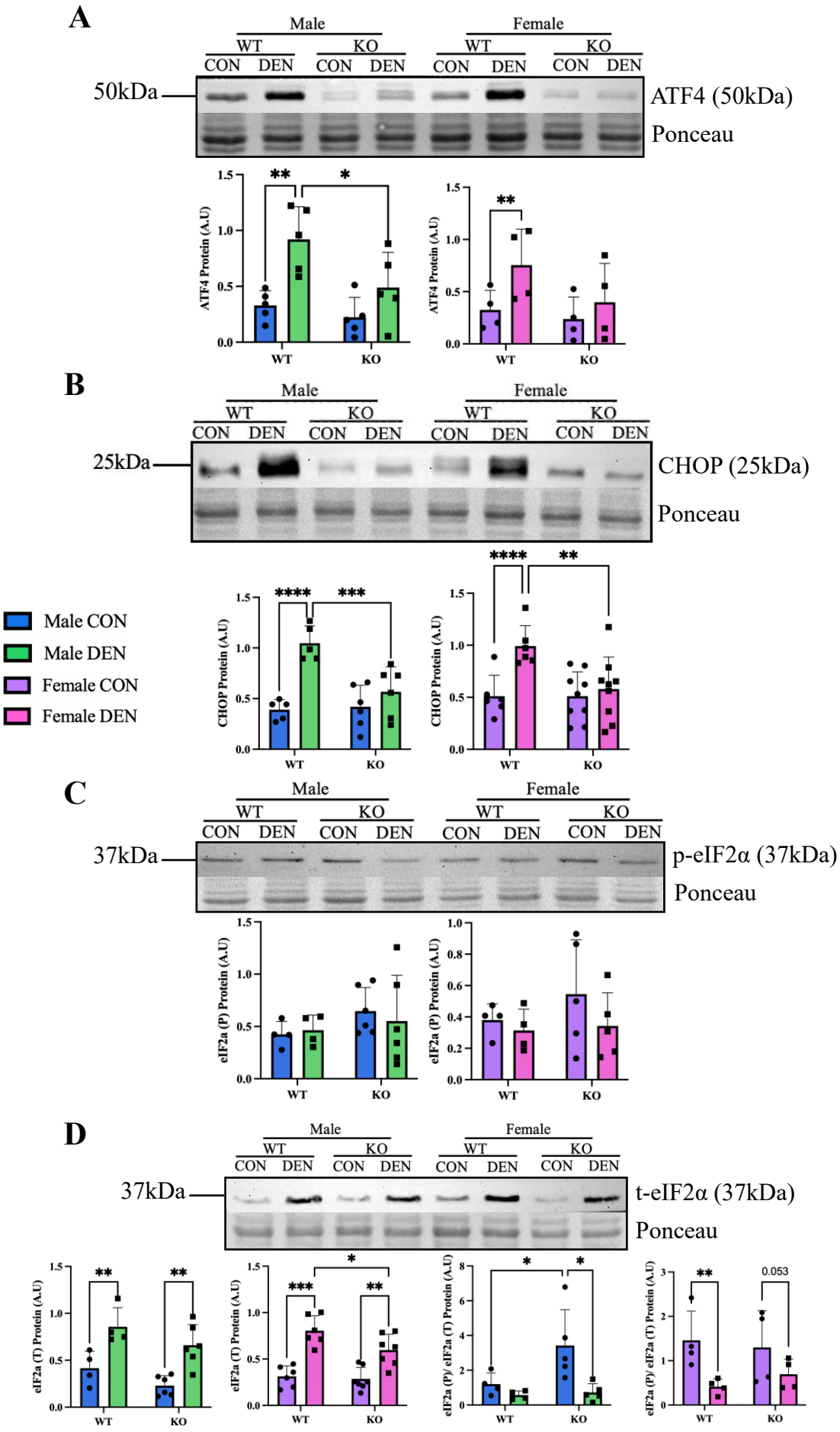

Figure 6. UPR^{mt} protein content in response to denervation in WT and ATF5 KO mice.

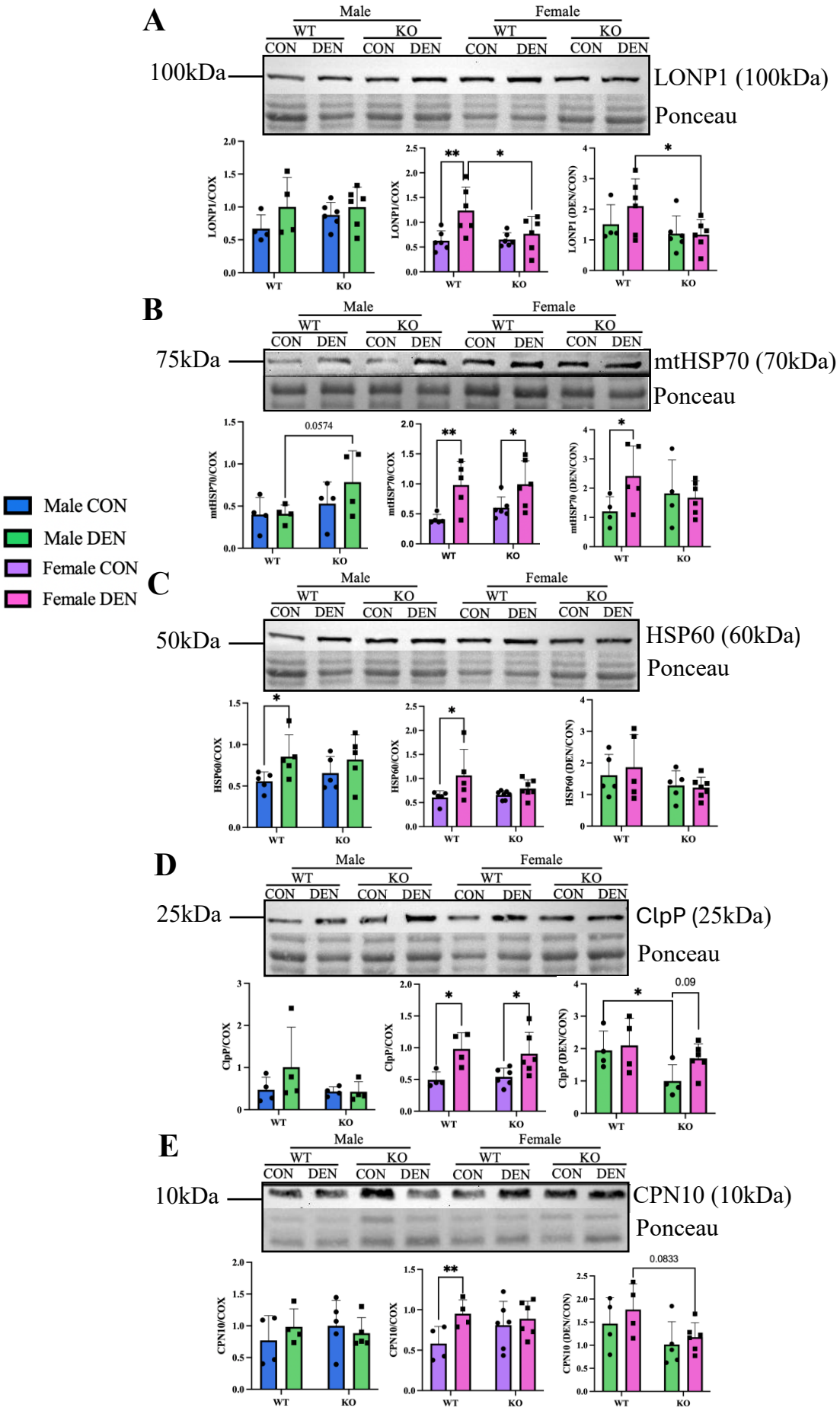

Figure 7. Antioxidant protein content in response to denervation in WT and ATF5 KO mice.

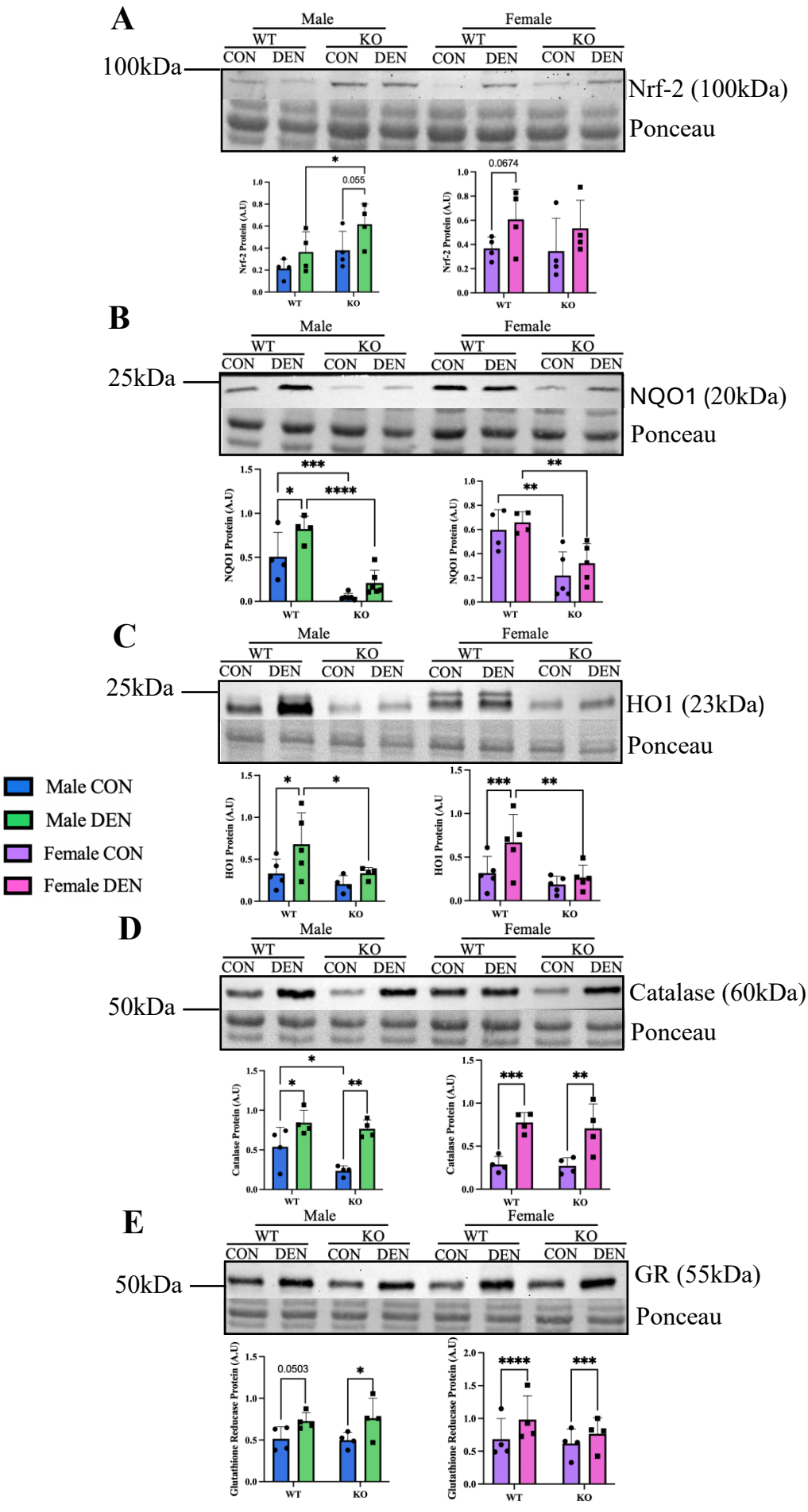

Figure 8. Lysosomal protein content in response to denervation in WT and ATF5 mice.

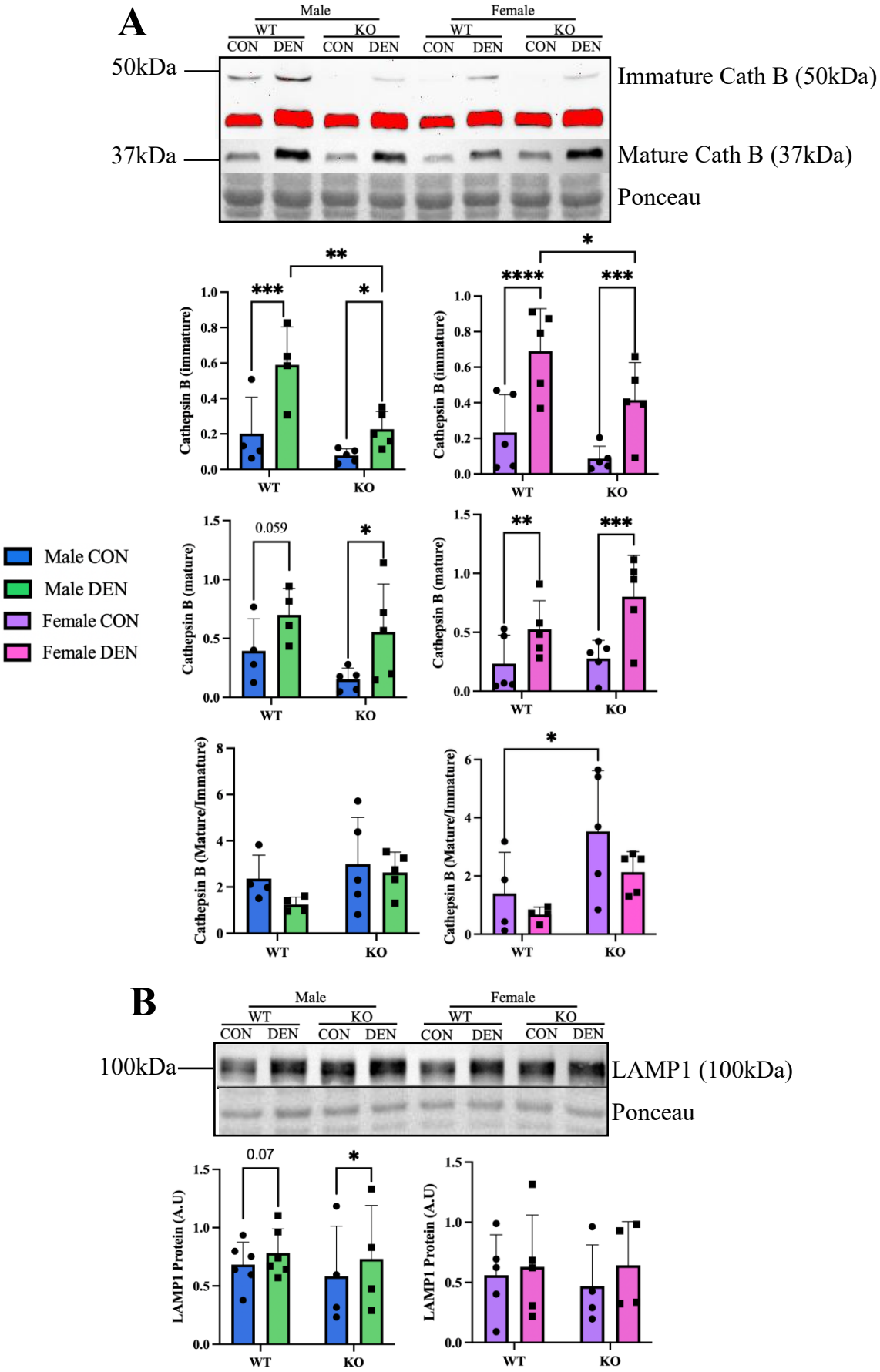

Figure 9. Signaling pathways involved in regulating mitochondrial function during the ISR and UPR^{mt}.

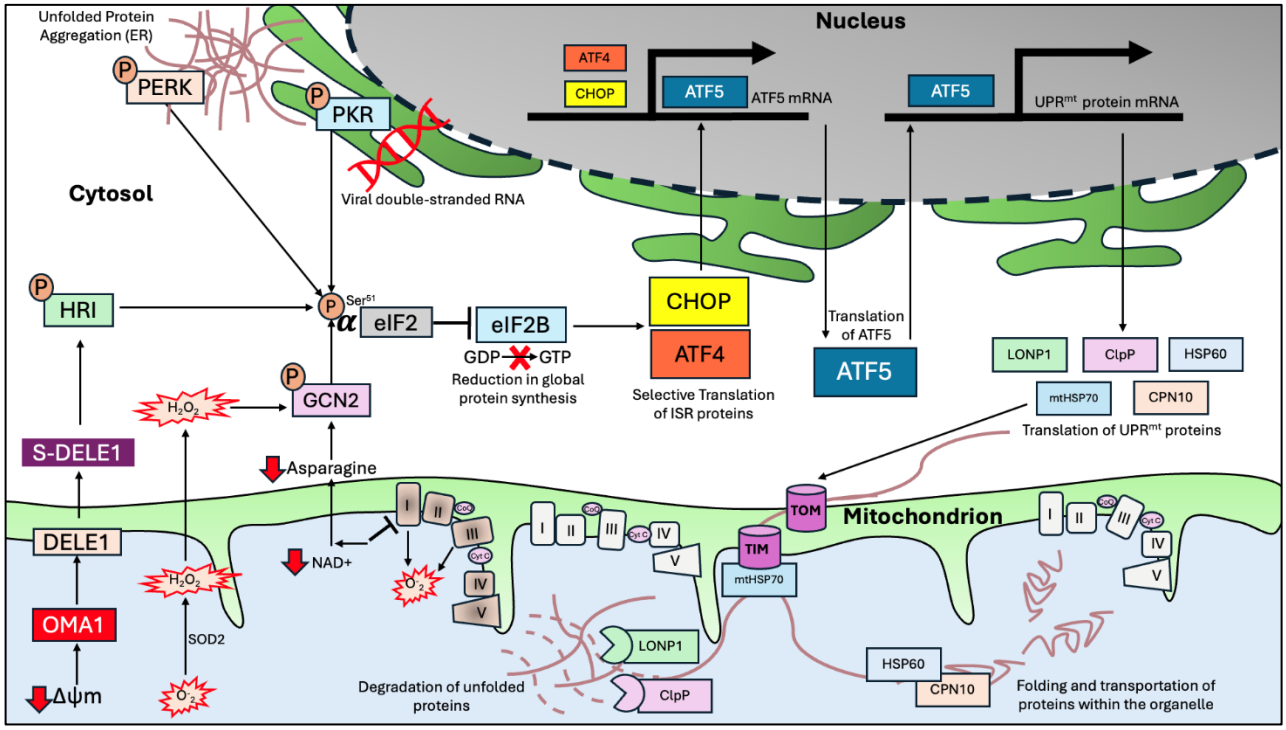

Figure 10. Conclusion schematic of results section.

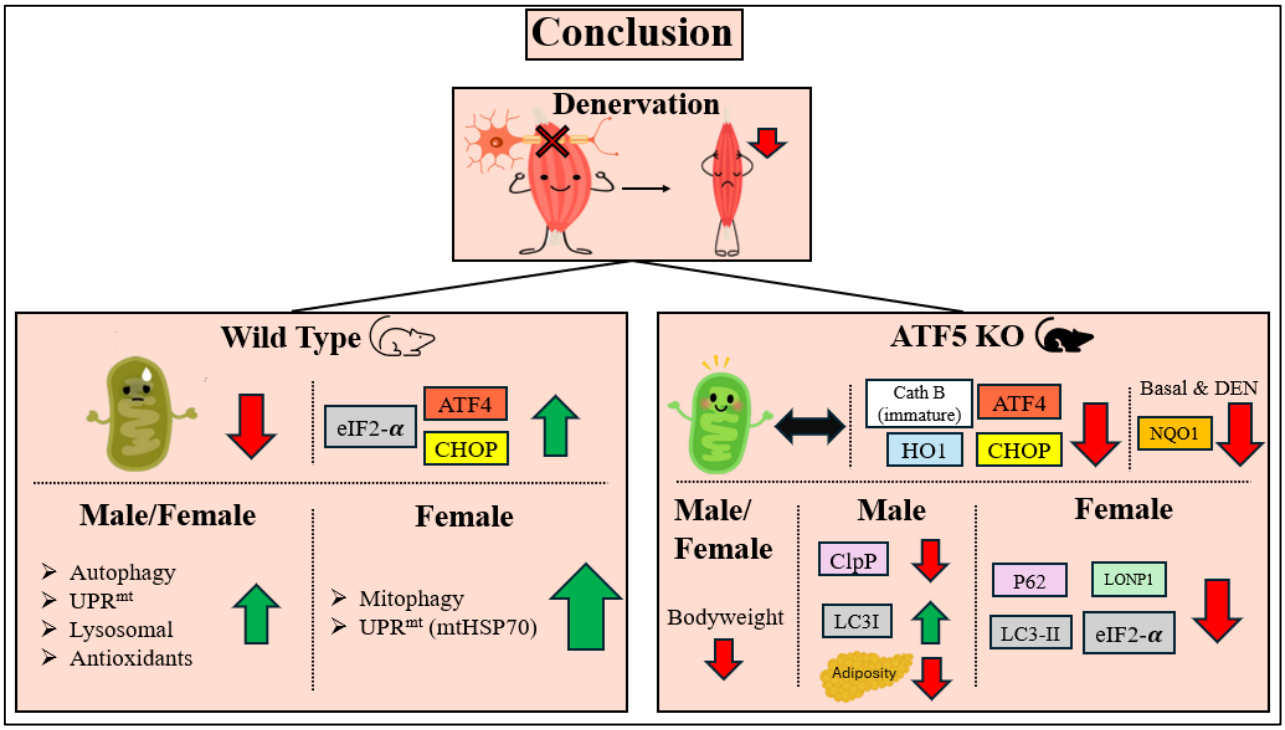

Future Directions

- Explore the relationship between ATF5 and Nrf-2 binding capabilities in an ATF5 KO model during chronic muscle disuse to assess what degree of the antioxidant response is reliant on ATF5;
- Measure mitophagy/autophagy flux in ATF5 KO mice via colchicine to assess changes in autophagy and lysosomal markers;
- Explore an MNRR1 KO model to assess ATF5 expression and its effects on the UPR^{mt} in response to muscle disuse;

Limitations

- Unable to measure total ATF5 protein content in muscle samples due to the lack of an effective commercially available primary antibody;
- Insufficient number of samples to conduct statistical analysis on SDH staining intensity between groups;
- Preliminary data for high-resolution and ROS emission data lacks female WT and KO samples for sex-related comparisons;

APPENDIX A: DATA AND STATISTICAL ANALYSIS

Table 1A. LC3 I Protein Expression in sham-operated and denervated samples of WT/KO male/female mice

	LC3 I Protein Expression (A.U)			
N	**Sex**	**Genotype**	**Sham**	**Den**
244	F	WT	0.094826	0.553159
272	M	WT	0.09573	0.186612
267	F	WT	0.071026	0.443589
268	F	WT	0.096372	1.055877
273	M	WT	0.337426	0.374643
270	F	WT	0.064646	0.908594
271	M	WT	0.157733	0.65705
282	F	WT	0.177432	0.576051
277	M	WT	0.319229	0.737301
283	F	WT	0.222341	1.097882
238	F	KO	0.077941	0.402148
247	M	KO	0.387866	1.015987
258	M	KO	0.115806	1.134491
255	M	KO	0.305476	0.87325
262	F	KO	0.111458	0.711077
260	F	KO	0.047808	0.628851
261	F	KO	0.091715	0.70965
257	M	KO	0.0547	0.419461
263	M	KO	0.074666	0.501835
264	M	KO	0.093766	0.663934
288	M	KO	0.33997	0.965225
290	M	KO	0.223789	1.251996
304	F	KO	0.185057	0.921613

MALE - Two Way ANOVA with Repeated Measures

Uncorrected Fisher's LSD	Predicted (LS) mean	95.00% CI of diff.	Below threshold?	Summary	Individual P Value
SHAM					
WT vs. KO	0.02802	-0.2553 to 0.3114	No	ns	0.8386
DEN					
WT vs. KO	-0.3644	-0.6477 to -0.08104	Yes	*	0.0143
WT					
SHAM vs. DEN	-0.2614	-0.5307 to 0.007989	No	ns	0.0559
KO					
SHAM vs. DEN	-0.6538	-0.8442 to -0.4633	Yes	****	<0.0001

FEMALE - Two Way ANOVA with Repeated Measures

Uncorrected Fisher's LSD	Predicted (LS) mean diff.	95.00% CI of diff.	Below threshold?	Summary	Individual P Value
SHAM					
WT vs. KO	0.01831	-0.2082 to 0.2448	No	ns	0.8670
DEN					
WT vs. KO	0.09786	-0.1286 to 0.3243	No	ns	0.3760
WT					
SHAM vs. DEN	-0.6514	-0.8585 to -0.4443	Yes	****	<0.0001
KO					
SHAM vs. DEN	-0.5719	-0.7987 to -0.3450	Yes	***	0.0003

Table 2A. LC3 II Protein Expression in sham-operated and denervated samples of WT/KO male/female mice

	LC3 II Protein Expression (A.U)			
N	**Sex**	**Genotype**	**Sham**	**Den**
244	F	WT	0.10816219	0.81802729
272	M	WT	0.03393691	0.19663564
267	F	WT	0.0530102	0.55877127
268	F	WT	0.04340908	0.53365018
273	M	WT	0.1372377	0.09939374
270	F	WT	0.08814952	0.42719371
271	M	WT	0.03949186	0.1665397
282	F	WT	0.07035928	0.24630795
283	F	WT	0.17232817	1.0993407
277	M	WT	0.33821008	0.47227792
238	F	KO	0.08069602	0.42932507
247	M	KO	0.17658436	0.3098622
258	M	KO	0.05069304	0.54745659
255	M	KO	0.06452837	0.19811756
262	F	KO	0.075922	0.21266616
260	F	KO	0.05150947	0.26894103
261	F	KO	0.01948689	0.25819068
257	M	KO	0.07500139	0.36058569
263	M	KO	0.04626749	0.087435
264	M	KO	0.06571166	0.17565678
288	M	KO	0.21834663	0.34646721
290	M	KO	0.12409075	0.98844469
304	F	KO	0.11596479	0.52650454

MALE - Two Way ANOVA with Repeated Measures

Uncorrected Fisher's LSD	Predicted (LS) mean diff.	95.00% CI of diff.	Below threshold?	Summary	Individual P Value
SHAM					
WT vs. KO	0.03457	-0.2104 to 0.2795	No	ns	0.7715
DEN					
WT vs. KO	-0.1430	-0.3880 to 0.1019	No	ns	0.2373
WT					
SHAM vs. DEN	-0.09649	-0.3613 to 0.1683	No	ns	0.4357
KO					
SHAM vs. DEN	-0.2741	-0.4613 to -0.08685	Yes	**	0.0085

FEMALE - Two Way ANOVA with Repeated Measures

Uncorrected Fisher's LSD	Predicted (LS) mean diff.	95.00% CI of diff.	Below threshold?	Summary	Individual P Value
SHAM					
WT vs. KO	0.02052	-0.2006 to 0.2416	No	ns	0.8476
DEN					
WT vs. KO	0.2748	0.05366 to 0.4959	Yes	*	0.0177
WT					
SHAM vs. DEN	-0.5246	-0.7196 to -0.3297	Yes	***	0.0002
KO					
SHAM vs. DEN	-0.2704	-0.4840 to -0.05681	Yes	*	0.0187

Table 3A. LC3 II/I Protein Expression in sham-operated and denervated samples of WT/KO male/female mice

	LC3 II/I Protein Expression (A.U)			
N	**Sex**	**Genotype**	**Sham**	**Den**
244	F	WT	1.140634	1.47883
272	M	WT	0.354506	1.053715
267	F	WT	0.746346	1.25966
268	F	WT	0.450431	0.50541
273	M	WT	0.406719	0.265302
270	F	WT	1.609038	1.421147
271	M	WT	0.250372	0.253466
282	F	WT	0.396542	0.42758
283	F	WT	0.775062	1.001328
277	M	WT	1.059459	0.64055
238	F	KO	1.035346	1.06758
247	M	KO	0.455271	0.304986
258	M	KO	1.606072	0.761431
255	M	KO	0.211239	0.226874
262	F	KO	0.681171	0.299076
260	F	KO	1.077416	0.42767
261	F	KO	0.212473	0.363828
257	M	KO	1.371138	0.85964
263	M	KO	0.619662	0.174231
264	M	KO	0.700807	0.26457
288	M	KO	0.642253	0.35895
290	M	KO	0.554499	0.789495
304	F	KO	0.626643	0.571286

MALE - Two Way ANOVA with Repeated Measures

Uncorrected Fisher's LSD	Predicted (LS) Mean diff.	95.00% CI of diff.	Below threshold?	Summary	Individual P Value
SHAM					
WT vs. KO	-0.2524	-0.7441 to 0.2394	No	ns	0.2971
DEN					
WT vs. KO	0.08574	-0.4060 to 0.5775	No	ns	0.7199
WT					
SHAM vs. DEN	-0.03549	-0.4625 to 0.3915	No	ns	0.8568
KO					
SHAM vs. DEN	0.3026	0.0006738 to 0.6045	Yes	*	0.0496

FEMALE - Two Way ANOVA with Repeated Measures

Uncorrected Fisher's LSD	Predicted (LS) Mean diff.	95.00% CI of diff.	Below threshold?	Summary	Individual P Value
SHAM					
WT vs. KO	0.1264	-0.3897 to 0.6425	No	ns	0.6131
DEN					
WT vs. KO	0.4698	-0.04635 to 0.9859	No	ns	0.0719
WT					
SHAM vs. DEN	-0.1627	-0.4277 to 0.1024	No	ns	0.1985
KO					
SHAM vs. DEN	0.1807	-0.1097 to 0.4711	No	ns	0.1928

Table 4A. Beclin1 Protein Expression in sham-operated and denervated samples of WT/KO male/female mice

	Beclin1 Protein Expression (A.U)			
N	**Sex**	**Genotype**	**Sham**	**Den**
270	F	WT	0.09966733	0.4336057
275	M	WT	0.19036233	0.28153794
198	F	WT	0.49361986	0.86523083
267	F	WT	0.43900428	0.82716079
268	F	WT	0.55599511	0.7190672
272	M	WT	0.23496012	0.44742212
277	M	WT	0.36830802	0.99810854
283	F	WT	0.43457717	1.01558054
276	M	WT	0.44013381	0.75768851
247	M	KO	0.34195907	0.79921729
223	F	KO	0.51517563	0.8604994
225	F	KO	0.59774102	0.58662024
258	M	KO	0.4331456	0.58662315
260	F	KO	0.24444751	0.39114516
262	F	KO	0.31489882	0.37207813
290	M	KO	0.57811026	1.12009063
304	F	KO	0.44340587	0.65276733
255	M	KO	0.40115603	0.7193725

MALE - Two Way ANOVA with Repeated Measures

Uncorrected Fisher's LSD	Mean Diff.	95.00% CI of diff.	Below threshold?	Summary	Individual P Value
SHAM					
WT vs. KO	-0.1302	-0.4543 to 0.1940	No	ns	0.3988
DEN					
WT vs. KO	-0.1851	-0.5093 to 0.1390	No	ns	0.2371
WT					
SHAM vs. DEN	-0.3127	-0.5607 to -0.06480	Yes	*	0.0215
KO					
SHAM vs. DEN	-0.3677	-0.6157 to -0.1198	Yes	*	0.0110

FEMALE - Two Way ANOVA with Repeated Measures

Uncorrected Fisher's LSD	Mean Diff.	95.00% CI of diff.	Below threshold?	Summary	Individual P Value
SHAM					
WT vs. KO	-0.01856	-0.2694 to 0.2323	No	ns	0.8773
DEN					
WT vs. KO	0.1995	-0.05131 to 0.4503	No	ns	0.1112
WT					
SHAM vs. DEN	-0.3676	-0.5158 to -0.2194	Yes	***	0.0004
KO					
SHAM vs. DEN	-0.1495	-0.2977 to -0.001291	Yes	*	0.0485

Table 5A. P62 Protein Expression in sham-operated and denervated samples of WT/KO male/female mice

	P62 Protein Expression (A.U)			
N	**Sex**	**Genotype**	**Sham**	**Den**
198	F	WT	0.109762	0.704541
244	F	WT	0.245951	1.324226
275	M	WT	0.211477	0.762186
267	F	WT	0.234075	0.745419
268	F	WT	0.216505	0.752943
276	M	WT	0.448697	1.176646
273	M	WT	0.436837	0.473232
271	M	WT	0.21541	0.732392
280	F	WT	0.219518	0.557588
223	F	KO	0.129181	0.311298
225	F	KO	0.31132	0.483291
238	F	KO	0.376371	0.904712
247	M	KO	0.158921	0.552395
258	M	KO	0.152226	0.616678
260	F	KO	0.098615	0.3905
261	F	KO	0.106068	0.502957
256	M	KO	0.145369	0.945275
259	F	KO	0.367713	0.529896
255	M	KO	0.285033	0.897324
262	F	KO	0.109318	0.407815
304	F	KO	0.373451	0.80498

MALE - Two Way ANOVA with Repeated Measures

Uncorrected Fisher's LSD	Mean Diff.	95.00% CI of diff.	Below threshold?	Summary	Individual P Value
SHAM					
WT vs. KO	0.1427	-0.1511 to 0.4366	No	ns	0.3108
DEN					
WT vs. KO	0.03320	-0.2606 to 0.3270	No	ns	0.8097
WT					
SHAM vs. DEN	-0.4580	-0.7575 to -0.1585	Yes	**	0.0096
KO					
SHAM vs. DEN	-0.5675	-0.8671 to -0.2680	Yes	**	0.0036

FEMALE - Two Way ANOVA with Repeated Measures

Uncorrected Fisher's LSD	Predicted (LS) Mean diff.	95.00% CI of diff.	Below threshold?	Summary	Individual P Value
SHAM					
WT vs. KO	-0.02884	-0.2519 to 0.1942	No	ns	0.7911
DEN					
WT vs. KO	0.2750	0.05194 to 0.4981	Yes	*	0.0180
WT					
SHAM vs. DEN	-0.6118	-0.8078 to -0.4158	Yes	****	<0.0001
KO					
SHAM vs. DEN	-0.3079	-0.4629 to -0.1530	Yes	**	0.0011

Table 6A. ATF4 Protein Expression in sham-operated and denervated samples of WT/KO male/female mice

	ATF4 Protein Expression (A.U)			
N	**Sex**	**Genotype**	**Sham**	**Den**
271	M	WT	0.342187	0.586326
272	M	WT	0.146468	1.222361
273	M	WT	0.48621	0.655325
267	F	WT	0.56404	1.081139
268	F	WT	0.202396	0.431162
277	M	WT	0.408399	0.959964
283	F	WT	0.38428	1.021592
275	M	WT	0.262406	1.180893
280	F	WT	0.153372	0.485476
257	M	KO	0.512395	0.881455
247	M	KO	0.199846	0.68919
258	M	KO	0.235056	0.430397
260	F	KO	0.251949	0.55413
261	F	KO	0.525222	0.847924
290	M	KO	0.127979	0.394504
304	F	KO	0.14028	0.148511
255	M	KO	0.042717	0.052813
262	F	KO	0.032841	0.046422

MALE - Two Way ANOVA with Repeated Measures

Uncorrected Fisher's LSD	Mean Diff.	95.00% CI of diff.	Below threshold?	Summary	Individual P Value
SHAM					
WT vs. KO	0.1055	-0.2184 to 0.4295	No	ns	0.4997
DEN					
WT vs. KO	0.4313	0.1073 to 0.7553	Yes	*	0.0123
WT					
SHAM vs. DEN	-0.5918	-0.9124 to -0.2712	Yes	**	0.0028
KO					
SHAM vs. DEN	-0.2661	-0.5867 to 0.05454	No	ns	0.0920

FEMALE - Two Way ANOVA with Repeated Measures

Uncorrected Fisher's LSD	Mean Diff.	95.00% CI of diff.	Below threshold?	Summary	Individual P Value
SHAM					
WT vs. KO	0.08845	-0.3579 to 0.5348	No	ns	0.6736
DEN					
WT vs. KO	0.3556	-0.09072 to 0.8019	No	ns	0.1082
WT					
SHAM vs. DEN	-0.4288	-0.6476 to -0.2101	Yes	**	0.0030
KO					
SHAM vs. DEN	-0.1617	-0.3804 to 0.05706	No	ns	0.1205

Table 7A. CHOP Protein Expression in sham-operated and denervated samples of WT/KO male/female mice

	CHOP Protein Expression (A.U)			
N	**Sex**	**Genotype**	**Sham**	**Den**
271	M	WT	0.442713	0.895678
198	F	WT	0.413601	0.971649
267	F	WT	0.478815	1.043775
268	F	WT	0.463758	0.888479
272	M	WT	0.302539	0.986798
270	F	WT	0.888082	1.359147
271	M	WT	0.442713	0.895678
275	M	WT	0.268968	1.187875
280	F	WT	0.289338	0.854767
277	M	WT	0.495591	1.266594
283	F	WT	0.526543	0.830623
223	F	KO	0.623727	1.173985
247	M	KO	0.636752	0.840192
258	M	KO	0.661014	0.732341
256	M	KO	0.374181	0.305495
225	F	KO	0.821395	0.66077
260	F	KO	0.375489	0.561887
261	F	KO	0.531511	0.625287
259	F	KO	0.654088	0.652952
257	M	KO	0.464697	0.727867
259	F	KO	0.803887	0.787123
255	M	KO	0.120952	0.241005
262	F	KO	0.213715	0.166828
290	M	KO	0.257746	0.557676
304	F	KO	0.203475	0.225375

MALE - Two Way ANOVA with Repeated Measures

Uncorrected Fisher's LSD	Predicted (LS) Mean diff.	95.00% CI of diff.	Below threshold?	Summary	Individual P Value
SHAM					
WT vs. KO	-0.02872	-0.2767 to 0.2193	No	ns	0.8105
DEN					
WT vs. KO	0.4791	0.2311 to 0.7271	Yes	***	0.0007
WT					
SHAM vs. DEN	-0.6560	-0.8275 to -0.4845	Yes	****	<0.0001
KO					
SHAM vs. DEN	-0.1482	-0.3048 to 0.008347	No	ns	0.0609

FEMALE - Two Way ANOVA with Repeated Measures

Uncorrected Fisher's LSD	Predicted (LS) Mean diff.	95.00% CI of diff.	Below threshold?	Summary	Individual P Value
SHAM					
WT vs. KO	-0.01839	-0.2983 to 0.2615	No	ns	0.8933
DEN					
WT vs. KO	0.3846	0.1048 to 0.6645	Yes	**	0.0091
WT					
SHAM vs. DEN	-0.4814	-0.6398 to -0.3230	Yes	****	<0.0001
KO					
SHAM vs. DEN	-0.07836	-0.2156 to 0.05883	No	ns	0.2371

Table 8A. Total-eIF2α Protein Expression in sham-operated and denervated samples of WT/KO male/female mice

	Total-eIF2α Protein Expression (A.U)			
N	**Sex**	**Genotype**	**Sham**	**Den**
198	F	WT	0.2966153	0.98440761
270	F	WT	0.41359022	0.7133059
267	F	WT	0.35785231	0.72793035
244	F	WT	0.16840437	0.80891429
268	F	WT	0.19764114	0.59572234
272	M	WT	0.20344123	0.79767371
273	M	WT	0.6097026	0.72132987
271	M	WT	0.51101158	0.74976043
277	M	WT	0.34038018	1.15849851
283	F	WT	0.44725193	1.00374821
223	F	KO	0.44560712	0.63040139
225	F	KO	0.46629602	0.34909596
247	M	KO	0.11556365	0.65140431
258	M	KO	0.13204251	0.34488609
238	F	KO	0.20993357	0.80006536
260	F	KO	0.23135927	0.65561578
261	F	KO	0.1346554	0.50174144
257	M	KO	0.32511931	0.53912302
263	M	KO	0.29250376	0.84630276
264	M	KO	0.15869107	0.616591
259	F	KO	0.25719909	0.45648387
290	M	KO	0.35369971	0.9647776
304	F	KO	0.25590635	0.78623099

MALE - Two Way ANOVA with Repeated Measures

Uncorrected Fisher's LSD	Predicted (LS) mean diff.	95.00% CI of diff.	Below threshold?	Summary	Individual P Value
SHAM					
WT vs. KO	0.1865	-0.06046 to 0.4335	No	ns	0.1289
DEN					
WT vs. KO	0.1963	-0.05069 to 0.4433	No	ns	0.1114
WT					
SHAM vs. DEN	-0.4407	-0.7199 to -0.1615	Yes	**	0.0066
KO					
SHAM vs. DEN	-0.4309	-0.6589 to -0.2030	Yes	**	0.0024

FEMALE - Two Way ANOVA with Repeated Measures

Uncorrected Fisher's LSD	Predicted (LS) mean diff.	95.00% CI of diff.	Below threshold?	Summary	Individual P Value
SHAM					
WT vs. KO	0.02771	-0.1387 to 0.1941	No	ns	0.7332
DEN					
WT vs. KO	0.2086	0.04215 to 0.3750	Yes	*	0.0164
WT					
SHAM vs. DEN	-0.4921	-0.6796 to -0.3046	Yes	***	0.0001
KO					
SHAM vs. DEN	-0.3112	-0.4848 to -0.1377	Yes	**	0.0023

Table 9A. Phosphorylated-eIF2α Protein Expression in sham-operated and denervated samples of WT/KO male/female mice

		Phosphorylated-eIF2α Protein Expression (A.U)		
N	**Sex**	**Genotype**	**Sham**	**Den**
267	F	WT	0.47385	0.352906
244	F	WT	0.407529	0.487968
268	F	WT	0.233064	0.228832
272	M	WT	0.423317	0.579714
273	M	WT	0.578962	0.594293
271	M	WT	0.277291	0.304365
277	M	WT	0.418838	0.37908
283	F	WT	0.406833	0.186923
223	F	KO	0.92934	0.666894
225	F	KO	0.295227	0.143616
247	M	KO	0.447119	0.341529
258	M	KO	0.896318	0.203169
257	M	KO	0.509862	0.472941
263	M	KO	0.650665	1.2575
259	F	KO	0.500458	0.416781
290	M	KO	0.941136	0.14005
304	F	KO	0.135467	0.308014
255	M	KO	0.43655	0.896933
262	F	KO	0.86485	0.179889

MALE - Two Way ANOVA with Repeated Measures

Uncorrected Fisher's LSD	Predicted (LS) Mean diff.	95.00% CI of diff.	Below threshold?	Summary	Individual P Value
SHAM					
WT vs. KO	-0.2223	-0.6152 to 0.1706	No	ns	0.2477
DEN					
WT vs. KO	-0.08766	-0.4805 to 0.3052	No	ns	0.6426
WT					
SHAM vs. DEN	-0.03976	-0.5684 to 0.4889	No	ns	0.8666
KO					
SHAM vs. DEN	0.09492	-0.3367 to 0.5265	No	ns	0.6257

FEMALE - Two Way ANOVA with Repeated Measures

Uncorrected Fisher's LSD	Predicted (LS) Mean diff.	95.00% CI of diff.	Below threshold?	Summary	Individual P Value
SHAM					
WT vs. KO	-0.1647	-0.4971 to 0.1676	No	ns	0.3057
DEN					
WT vs. KO	-0.02888	-0.3612 to 0.3035	No	ns	0.8548
WT					
SHAM vs. DEN	0.06616	-0.2322 to 0.3645	No	ns	0.6162
KO					
SHAM vs. DEN	0.2020	-0.06481 to 0.4689	No	ns	0.1165

Table 10A. Phosphorylated/Total-eIF2α Protein Expression in sham-operated and denervated samples of WT/KO male/female mice

	Phosphorylated/Total-eIF2α Protein Expression (A.U)			
N	**Sex**	**Genotype**	**Sham**	**Den**
267	F	WT	1.324151	0.48480697
244	F	WT	2.419941	0.60323777
268	F	WT	1.179231	0.38412483
272	M	WT	2.080784	0.72675596
273	M	WT	0.94958	0.82388549
271	M	WT	0.542631	0.40595024
277	M	WT	1.2305	0.32721683
283	F	WT	0.909628	0.18622455
223	F	KO	2.08556	1.05788799
225	F	KO	0.633133	0.41139428
247	M	KO	3.869027	0.52429606
258	M	KO	6.788101	0.58908943
257	M	KO	1.568231	0.87724082
263	M	KO	2.224467	1.48587468
259	F	KO	1.945799	0.91302457
290	M	KO	2.660833	0.14516309
304	F	KO	0.529362	0.3917603

MALE - Two Way ANOVA with Repeated Measures

Uncorrected Fisher's LSD	Predicted (LS) Mean diff.	95.00% CI of diff.	Below threshold?	Summary	Individual P Value
SHAM					
WT vs. KO	-2.221	-3.916 to -0.5266	Yes	*	0.0139
DEN					
WT vs. KO	-0.1534	-1.848 to 1.541	No	ns	0.8489
WT					
SHAM vs. DEN	0.6299	-1.450 to 2.710	No	ns	0.4972
KO					
SHAM vs. DEN	2.698	0.8371 to 4.559	Yes	*	0.0110

FEMALE - Two Way ANOVA with Repeated Measures

Uncorrected Fisher's LSD	Mean diff.	95.00% CI of diff.	Below threshold?	Summary	Individual P Value
SHAM					
WT vs. KO	0.1598	-0.7117 to 1.031	No	ns	0.6966
DEN					
WT vs. KO	-0.2789	-1.150 to 0.5926	No	ns	0.4989
WT					
SHAM vs. DEN	1.044	0.4257 to 1.662	Yes	**	0.0061
KO					
SHAM vs. DEN	0.6049	-0.01301 to 1.223	No	ns	0.0536

Table 11A. LONP1 Protein Expression in sham-operated and denervated samples of WT/KO male/female mice

	LONP1 Protein Expression (A.U)			
N	**Sex**	**Genotype**	**Sham**	**Den**
270	F	WT	0.763962	1.614074
244	F	WT	0.490019	1.331557
198	F	WT	0.393591	0.93483
208	M	WT	0.625314	1.544154
267	F	WT	0.587583	1.924981
268	F	WT	0.586213	0.677539
272	M	WT	0.581952	0.653374
273	M	WT	0.499251	0.616555
277	M	WT	0.975228	1.192365
283	F	WT	0.946795	0.934912
223	F	KO	0.61667	1.112292
225	F	KO	0.882497	1.02327
247	M	KO	0.989429	1.124327
238	F	KO	0.596839	0.229259
258	M	KO	0.781747	0.738732
260	F	KO	0.521182	0.486961
261	F	KO	0.541173	0.789155
257	M	KO	0.858959	1.084184
263	M	KO	0.580386	1.326903
264	M	KO	0.927304	0.522928
290	M	KO	1.138944	1.185862
304	F	KO	0.747201	0.970543

MALE - Two Way ANOVA with Repeated Measures

Uncorrected Fisher's LSD	Predicted (LS) mean diff.	95.00% CI of diff.	Below threshold?	Summary	Individual P Value
SHAM					
WT vs. KO	-0.2090	-0.6099 to 0.1919	No	ns	0.2854
DEN					
WT vs. KO	0.004456	-0.3964 to 0.4053	No	ns	0.9815
WT					
SHAM vs. DEN	-0.3312	-0.7744 to 0.1121	No	ns	0.1232
KO					
SHAM vs. DEN	-0.1177	-0.4796 to 0.2442	No	ns	0.4748

FEMALE - Two Way ANOVA with Repeated Measures

Uncorrected Fisher's LSD	Mean Diff.	95.00% CI of diff.	Below threshold?	Summary	Individual P Value
SHAM					
WT vs. KO	-0.02290	-0.4045 to 0.3587	No	ns	0.9016
DEN					
WT vs. KO	0.4677	0.08616 to 0.8493	Yes	*	0.0188
WT					
SHAM vs. DEN	-0.6083	-0.9867 to -0.2298	Yes	**	0.0050
KO					
SHAM vs. DEN	-0.1177	-0.4961 to 0.2608	No	ns	0.5043

Table 12A. mtHSP70 Protein Expression in sham-operated and denervated samples of WT/KO male/female mice

	mtHSP70 Protein Expression (A.U)			
N	**Sex**	**Genotype**	**Sham**	**Den**
270	F	WT	0.552178	1.101333
271	M	WT	0.421569	0.427089
198	F	WT	0.394508	1.384652
267	F	WT	0.36269	1.243312
268	F	WT	0.36182	0.395084
272	M	WT	0.640035	0.407367
273	M	WT	0.389607	0.528319
277	M	WT	0.147402	0.268273
283	F	WT	0.379429	0.77566
208	M	WT	0.763187	0.923242
247	M	KO	0.769246	1.086239
256	M	KO	0.591478	1.114416
259	F	KO	0.563377	0.519371
258	M	KO	0.593373	0.379952
260	M	KO	0.542533	0.63545
261	F	KO	0.427846	0.925494
223	F	KO	0.634861	1.486912
225	M	KO	0.943301	1.397947
290	M	KO	0.165871	0.555858
304	F	KO	0.504737	0.998076

MALE - Two Way ANOVA with Repeated Measures

Uncorrected Fisher's LSD	Mean diff.	95.00% CI of diff.	Below threshold?	Summary	Individual P Value
SHAM					
WT vs. KO	-0.1303	-0.5206 to 0.2599	No	ns	0.4807
DEN					
WT vs. KO	-0.3764	-0.7666 to 0.01386	No	ns	0.0574
WT					
SHAM vs. DEN	-0.008109	-0.3244 to 0.3082	No	ns	0.9520
KO					
SHAM vs. DEN	-0.2541	-0.5704 to 0.06217	No	ns	0.0969

FEMALE - Two Way ANOVA with Repeated Measures

Uncorrected Fisher's LSD	Predicted (LS) Mean diff.	95.00% CI of diff.	Below threshold?	Summary	Individual P Value
SHAM					
WT vs. KO	-0.1927	-0.5701 to 0.1848	No	ns	0.2978
DEN					
WT vs. KO	-0.01387	-0.3913 to 0.3636	No	ns	0.9393
WT					
SHAM vs. DEN	-0.5699	-0.9249 to -0.2149	Yes	**	0.0055
KO					
SHAM vs. DEN	-0.3911	-0.7152 to -0.0670	Yes	*	0.0232

Table 13A. HSP60 Protein Expression in sham-operated and denervated samples of WT/KO male/female mice

	HSP60 Protein Expression (A.U)			
N	**Sex**	**Genotype**	**Sham**	**Den**
208	M	WT	0.515418	1.286708
283	F	WT	0.636839	0.902619
198	F	WT	0.368414	1.139507
267	F	WT	0.68783	1.955366
268	F	WT	0.625721	0.551843
275	M	WT	0.383705	0.807938
280	F	WT	0.70704	0.768441
272	M	WT	0.628404	0.58036
273	M	WT	0.669285	0.851892
271	M	WT	0.588859	0.745736
247	M	KO	0.922366	0.973856
223	F	KO	0.753217	1.042112
225	F	KO	0.707623	0.876303
257	M	KO	0.814193	1.140576
258	M	KO	0.571132	0.364989
260	F	KO	0.670382	0.736438
261	F	KO	0.539626	0.948534
255	M	KO	0.48669	0.717697
262	F	KO	0.728688	0.71342
290	M	KO	0.481577	0.902619
304	F	KO	0.535218	0.722923
259	F	KO	0.669789	0.491336

MALE - Two Way ANOVA with Repeated Measures

Uncorrected Fisher's LSD	Mean Diff.	95.00% CI of diff.	Below threshold?	Summary	Individual P Value
SHAM					
WT vs. KO	-0.09806	-0.4052 to 0.2090	No	ns	0.5082
DEN					
WT vs. KO	0.03458	-0.2725 to 0.3417	No	ns	0.8144
WT					
SHAM vs. DEN	-0.2974	-0.5890 to -0.005817	Yes	*	0.0465
KO					
SHAM vs. DEN	-0.1648	-0.4563 to 0.1268	No	ns	0.2288

FEMALE - Two Way ANOVA with Repeated Measures

Uncorrected Fisher's LSD	Predicted (LS) mean diff.	95.00% CI of diff.	Below threshold?	Summary	Individual P Value
SHAM					
WT vs. KO	-0.05262	-0.3866 to 0.2813	No	ns	0.7458
DEN					
WT vs. KO	0.2734	-0.06055 to 0.6074	No	ns	0.1032
WT					
SHAM vs. DEN	-0.4584	-0.8390 to -0.07782	Yes	*	0.0229
KO					
SHAM vs. DEN	-0.1324	-0.4540 to 0.1893	No	ns	0.3808

Table 14A. ClpP Protein Expression in sham-operated and denervated samples of WT/KO male/female mice

	ClpP Protein Expression (A.U)			
N	**Sex**	**Genotype**	**Sham**	**Den**
270	F	WT	0.450098	0.687733
198	F	WT	0.4036	1.209854
208	M	WT	0.863244	2.409121
244	F	WT	0.450199	1.178327
272	M	WT	0.275227	0.449144
273	M	WT	0.540188	0.779376
275	M	WT	0.209305	0.400928
280	F	WT	0.675717	0.848738
223	F	KO	0.645087	1.4568
225	F	KO	0.712135	1.154901
238	F	KO	0.608186	0.55997
257	M	KO	0.569643	0.326551
263	M	KO	0.393888	0.355393
260	F	KO	0.34131	0.674131
261	F	KO	0.450372	0.815664
264	M	KO	0.306968	0.245724
255	M	KO	0.450676	0.775329
262	F	KO	0.488229	0.771826

MALE - Two Way ANOVA with Repeated Measures

Uncorrected Fisher's LSD	Mean Diff.	95.00% CI of diff.	Below threshold?	Summary	Individual P Value
SHAM					
WT vs. KO	0.04170	-0.7498 to 0.8332	No	ns	0.9105
DEN					
WT vs. KO	0.5839	-0.2076 to 1.375	No	ns	0.1340
WT					
SHAM vs. DEN	-0.5377	-1.155 to 0.07961	No	ns	0.0771
KO					
SHAM vs. DEN	0.004545	-0.6127 to 0.6218	No	ns	0.9862

FEMALE - Two Way ANOVA with Repeated Measures

Uncorrected Fisher's LSD	Predicted (LS) mean diff.	95.00% CI of diff.	Below threshold?	Summary	Individual P Value
SHAM					
WT vs. KO	-0.04598	-0.3706 to 0.2786	No	ns	0.7678
DEN					
WT vs. KO	0.07561	-0.2490 to 0.4002	No	ns	0.6281
WT					
SHAM vs. DEN	-0.4863	-0.8285 to -0.1440	Yes	*	0.0112
KO					
SHAM vs. DEN	-0.3647	-0.6441 to -0.08523	Yes	*	0.0168

Table 15A. CPN10 Protein Expression in sham-operated and denervated samples of WT/KO male/female mice

	CPN10 Protein Expression (A.U)			
N	**Sex**	**Genotype**	**Sham**	**Den**
272	M	WT	1.091652	0.867145
273	M	WT	0.467353	0.942803
198	F	WT	0.42606	1.009888
244	F	WT	0.788619	1.163417
268	F	WT	0.736812	0.84735
275	M	WT	0.403014	0.735533
271	M	WT	1.122645	1.388944
283	F	WT	0.377251	0.787697
223	F	KO	0.83555	1.021416
225	F	KO	0.848578	1.085862
247	M	KO	1.070413	0.730209
260	F	KO	1.225744	1.131101
258	M	KO	1.219834	0.758249
261	F	KO	0.434814	0.729858
257	M	KO	1.446754	1.303549
259	F	KO	0.994087	0.767205
290	M	KO	0.392947	0.725944
304	F	KO	0.51847	0.602681
255	M	KO	0.873398	0.900468

MALE - Two Way ANOVA with Repeated Measures

Uncorrected Fisher's LSD	Predicted (LS) mean diff.	95.00% CI of diff.	Below threshold?	Summary	Individual P Value
SHAM					
WT vs. KO	-0.2295	-0.7118 to 0.2528	No	ns	0.3248
DEN					
WT vs. KO	0.09992	-0.3824 to 0.5822	No	ns	0.6636
WT					
SHAM vs. DEN	-0.2124	-0.5782 to 0.1533	No	ns	0.2120
KO					
SHAM vs. DEN	0.1170	-0.2102 to 0.4441	No	ns	0.4257

FEMALE - Two Way ANOVA with Repeated Measures

Uncorrected Fisher's LSD	Predicted (LS) mean diff.	95.00% CI of diff.	Below threshold?	Summary	Individual P Value
SHAM					
WT vs. KO	-0.2274	-0.5502 to 0.09548	No	ns	0.1549
DEN					
WT vs. KO	0.06240	-0.2604 to 0.3852	No	ns	0.6874
WT					
SHAM vs. DEN	-0.3699	-0.6011 to -0.1387	Yes	**	0.0061
KO					
SHAM vs. DEN	-0.08015	-0.2689 to 0.1086	No	ns	0.3562

Table 16A. Nrf-2 Protein Expression in sham-operated and denervated samples of WT/KO male/female mice

	Nrf-2 Protein Expression (A.U)			
N	**Sex**	**Genotype**	**Sham**	**Den**
282	F	WT	0.330937	0.827604
283	F	WT	0.420823	0.776772
272	M	WT	0.225735	0.191437
273	M	WT	0.228529	0.237603
198	F	WT	0.254089	0.54635
277	M	WT	0.303533	0.446756
270	F	WT	0.46646	0.279776
271	M	WT	0.097678	0.581359
255	M	KO	0.361892	0.794554
288	M	KO	0.626329	0.710989
260	F	KO	0.218641	0.361044
262	F	KO	0.150098	0.421412
261	F	KO	0.266479	0.477105
263	M	KO	0.234792	0.368665
223	F	KO	0.746657	0.874192
257	M	KO	0.296033	0.595458

MALE - Two Way ANOVA with Repeated Measures

Uncorrected Fisher's LSD	Mean diff.	95.00% CI of diff.	Below threshold?	Summary	Individual P Value
SHAM					
WT vs. KO	-0.1659	-0.4149 to 0.08308	No	ns	0.1722
DEN					
WT vs. KO	-0.2531	-0.5021 to -0.004157	Yes	*	0.0468
WT					
SHAM vs. DEN	-0.1504	-0.3957 to 0.09490	No	ns	0.1842
KO					
SHAM vs. DEN	-0.2377	-0.4830 to 0.007666	No	ns	0.0555

FEMALE - Two Way ANOVA with Repeated Measures

Uncorrected Fisher's LSD	Mean diff.	95.00% CI of diff.	Below threshold?	Summary	Individual P Value
SHAM					
WT vs. KO	0.02261	-0.3213 to 0.3666	No	ns	0.8885
DEN					
WT vs. KO	0.07419	-0.2698 to 0.4181	No	ns	0.6468
WT					
SHAM vs. DEN	-0.2395	-0.5026 to 0.02347	No	ns	0.0674
KO					
SHAM vs. DEN	-0.1880	-0.4510 to 0.07505	No	ns	0.1309

Table 17A. NQO1 Protein Expression in sham-operated and denervated samples of WT/KO male/female mice

	NQO1 Protein Expression (A.U)			
N	**Sex**	**Genotype**	**Sham**	**Den**
198	F	WT	0.755869	0.59787
270	F	WT	0.722384	0.567885
271	M	WT	0.416249	0.976507
282	F	WT	0.490349	0.737636
272	M	WT	0.245714	0.835661
273	M	WT	0.895646	0.848334
283	F	WT	0.419394	0.731849
277	M	WT	0.468449	0.627952
223	F	KO	0.353043	0.509762
225	F	KO	0.498849	0.44577
257	M	KO	0.040723	0.272464
263	M	KO	0.127281	0.474841
264	M	KO	0.044884	0.116109
260	F	KO	0.111934	0.204286
261	F	KO	0.068252	0.32509
255	M	KO	0.035388	0.161373
288	M	KO	0.047492	0.128014
290	M	KO	0.017156	0.106823
304	F	KO	0.06674	0.122752

MALE - Two Way ANOVA with Repeated Measures

Uncorrected Fisher's LSD	Predicted (LS) mean diff.	95.00% CI of	Below threshold?	Summary	Individual P Value
SHAM					
WT vs. KO	0.4544	0.2376 to 0.67	Yes	***	0.0004
DEN					
WT vs. KO	0.6122	0.3954 to 0.82	Yes	****	<0.0001
WT					
SHAM vs. DEN	-0.3156	-0.5574 to -0.(	Yes	*	0.0168
KO					
SHAM vs. DEN	-0.1578	-0.3552 to 0.0	No	ns	0.1026

FEMALE - Two Way ANOVA with Repeated Measures

Uncorrected Fisher's LSD	Predicted (LS) mean diff.	95.00% CI of diff.	Below threshold?	Summary	Individual P Value
SHAM					
WT vs. KO	0.3772	0.1449 to 0.6096	Yes	**	0.0037
DEN					
WT vs. KO	0.3373	0.1049 to 0.5697	Yes	**	0.0076
WT					
SHAM vs. DEN	-0.06181	-0.2833 to 0.1596	No	ns	0.5303
KO					
SHAM vs. DEN	-0.1018	-0.2998 to 0.09629	No	ns	0.2638

Table 18A. HO-1 Protein Expression in sham-operated and denervated samples of WT/KO male/female mice

	HO1 Protein Expression (A.U)			
N	**Sex**	**Genotype**	**Sham**	**Den**
275	M	WT	0.421739	1.1677
276	M	WT	0.568855	0.608332
279	F	WT	0.345919	0.759195
280	F	WT	0.081274	0.203673
271	M	WT	0.131512	0.455957
277	M	WT	0.290119	0.931337
282	F	WT	0.609508	1.089172
283	F	WT	0.289656	0.585848
273	M	WT	0.250211	0.23426
267	F	WT	0.256366	0.706681
255	M	KO	0.176965	0.235268
304	F	KO	0.195914	0.255921
259	F	KO	0.252736	0.212634
290	M	KO	0.088767	0.346572
258	M	KO	0.225077	0.390758
262	F	KO	0.056441	0.101075
260	F	KO	0.124977	0.269749
261	F	KO	0.295243	0.491191
247	M	KO	0.330685	0.36351

MALE - Two Way ANOVA with Repeated Measures

Uncorrected Fisher's LSD	Predicted (LS) Mean diff.	95.00% CI of diff.	Below threshold?	Summary	Individual P Value
SHAM					
WT vs. KO	0.1271	-0.1974 to 0.4517	No	ns	0.4150
DEN					
WT vs. KO	0.3455	0.02095 to 0.6700	Yes	*	0.0386
WT					
SHAM vs. DEN	-0.3470	-0.6310 to -0.06307	Yes	*	0.0233
KO					
SHAM vs. DEN	-0.1287	-0.4461 to 0.1888	No	ns	0.3699

FEMALE - Two Way ANOVA with Repeated Measures

Uncorrected Fisher's LSD	Mean diff.	95.00% CI of diff.	Below threshold?	Summary	Individual P Value
SHAM					
WT vs. KO	0.1315	-0.1437 to 0.4066	No	ns	0.3261
DEN					
WT vs. KO	0.4028	0.1277 to 0.6779	Yes	**	0.0068
WT					
SHAM vs. DEN	-0.3524	-0.4783 to -0.2265	Yes	***	0.0002
KO					
SHAM vs. DEN	-0.08105	-0.2070 to 0.04486	No	ns	0.1760

Table 19A. Catalase Protein Expression in sham-operated and denervated samples of WT/KO male/female mice

	Catalase Protein Expression (A.U)			
N	**Sex**	**Genotype**	**Sham**	**Den**
282	F	WT	0.285173	0.871224
283	F	WT	0.254863	0.631152
272	M	WT	0.5323	1.068633
273	M	WT	0.74201	0.711884
275	M	WT	0.195808	0.818577
276	M	WT	0.688109	0.771362
279	F	WT	0.413957	0.86525
280	F	WT	0.191748	0.732818
255	M	KO	0.24754	0.902785
288	M	KO	0.297311	0.80932
260	F	KO	0.369199	1.044472
261	F	KO	0.331382	0.798927
255	M	KO	0.251038	0.688042
304	F	KO	0.209008	0.372007
259	F	KO	0.175935	0.611852
290	M	KO	0.147982	0.66515

MALE - Two Way ANOVA with Repeated Measures

Uncorrected Fisher's LSD	Mean Diff.	95.00% CI of diff.	Below threshold?	Summary	Individual P Value
SHAM					
WT vs. KO	0.3036	0.05845 to 0.5487	Yes	*	0.0194
DEN					
WT vs. KO	0.07629	-0.1688 to 0.3214	No	ns	0.5106
WT					
SHAM vs. DEN	-0.3031	-0.5946 to -0.01148	Yes	*	0.0439
KO					
SHAM vs. DEN	-0.5304	-0.8219 to -0.2388	Yes	**	0.0043

FEMALE - Two Way ANOVA with Repeated Measures

Uncorrected Fisher's LSD	Mean Diff.	95.00% CI of diff.	Below threshold?	Summary	Individual P Value
SHAM					
WT vs. KO	0.01505	-0.2427 to 0.2728	No	ns	0.9008
DEN					
WT vs. KO	0.06830	-0.1895 to 0.3261	No	ns	0.5744
WT					
SHAM vs. DEN	-0.4887	-0.6879 to -0.2895	Yes	***	0.0010
KO					
SHAM vs. DEN	-0.4354	-0.6346 to -0.2363	Yes	**	0.0017

Table 20A. Glutathione Reductase Protein Expression in sham-operated and denervated samples of WT/KO male/female mice

	Glutathione Reductase Expression (A.U)			
N	**Sex**	**Genotype**	**Sham**	**Den**
282	F	WT	0.502164	0.770973
283	F	WT	0.599933	0.927892
272	M	WT	0.400474	0.674744
273	M	WT	0.647084	0.640956
279	F	WT	1.147701	1.507904
280	F	WT	0.489583	0.726127
271	M	WT	0.37925	0.716923
277	M	WT	0.631201	0.874428
255	M	KO	0.488374	0.762339
288	M	KO	0.524983	1.055866
260	F	KO	0.633901	0.826481
261	F	KO	0.650724	0.809608
259	F	KO	0.856914	1.00067
290	M	KO	0.378227	0.468961
258	M	KO	0.602011	0.758336
262	F	KO	0.328226	0.423574

MALE - Two Way ANOVA with Repeated Measures

Uncorrected Fisher's LSD	Mean Diff.	95.00% CI of diff.	Below threshold?	Summary	Individual P Value
SHAM					
WT vs. KO	0.01610	-0.2245 to 0.2567	No	ns	0.8865
DEN					
WT vs. KO	-0.03461	-0.2752 to 0.2060	No	ns	0.7593
WT					
SHAM vs. DEN	-0.2123	-0.4249 to 0.0003314	No	ns	0.0503
KO					
SHAM vs. DEN	-0.2630	-0.4756 to -0.05038	Yes	*	0.0232

FEMALE - Two Way ANOVA with Repeated Measures

Uncorrected Fisher's LSD	Mean Diff.	95.00% CI of diff.	Below threshold?	Summary	Individual P Value
SHAM					
WT vs. KO	0.06740	-0.3779 to 0.5128	No	ns	0.7473
DEN					
WT vs. KO	0.2181	-0.2272 to 0.6635	No	ns	0.3069
WT					
SHAM vs. DEN	-0.2984	-0.3581 to -0.2387	Yes	****	<0.0001
KO					
SHAM vs. DEN	-0.1476	-0.2074 to -0.08793	Yes	***	0.0009

Table 21A. Cathepsin B (Immature) Protein Expression in sham-operated and denervated samples of WT/KO male/female mice

	Cathepsin B (Immature) Expression (A.U)			
N	**Sex**	**Genotype**	**Sham**	**Den**
282	F	WT	0.468847	0.910872
283	F	WT	0.166532	0.7909
272	M	WT	0.105146	0.585814
273	M	WT	0.508269	0.826768
198	F	WT	0.036774	0.510024
277	M	WT	0.063487	0.30787
270	F	WT	0.448093	0.873193
271	M	WT	0.132606	0.6378
283	F	WT	0.044739	0.36815
290	M	KO	0.122024	0.351233
304	F	KO	0.044658	0.527305
260	F	KO	0.088412	0.405245
262	F	KO	0.0669	0.392948
261	F	KO	0.029893	0.091578
263	M	KO	0.0831	0.113921
223	F	KO	0.203391	0.660744
257	M	KO	0.105567	0.3086
255	M	KO	0.032954	0.160816
288	M	KO	0.049097	0.199147

MALE - Two Way ANOVA with Repeated Measures

Uncorrected Fisher's LSD	Predicted (LS) Mean diff.	95.00% CI of diff.	Below threshold?	Summary	Individual P Value
SHAM					
WT vs. KO	0.1238	-0.09053 to 0.3382	No	ns	0.2357
DEN					
WT vs. KO	0.3628	0.1485 to 0.5772	Yes	**	0.0027
WT					
SHAM vs. DEN	-0.3872	-0.5067 to -0.2677	Yes	***	0.0001
KO					
SHAM vs. DEN	-0.1482	-0.2551 to -0.04129	Yes	*	0.0135

FEMALE - Two Way ANOVA with Repeated Measures

Uncorrected Fisher's LSD	Mean diff.	95.00% CI of diff.	Below threshold?	Summary	Individual P Value
SHAM					
WT vs. KO	0.1463	-0.1146 to 0.4073	No	ns	0.2518
DEN					
WT vs. KO	0.2751	0.01415 to 0.5360	Yes	*	0.0400
WT					
SHAM vs. DEN	-0.4576	-0.6030 to -0.3122	Yes	****	<0.0001
KO					
SHAM vs. DEN	-0.3289	-0.4743 to -0.1835	Yes	***	0.0008

Table 22A. Cathepsin B (mature) Protein Expression in sham-operated and denervated samples of WT/KO male/female mice

	Cathepsin B (Mature) Expression (A.U)			
N	**Sex**	**Genotype**	**Sham**	**Den**
282	F	WT	0.468847	0.910872
283	F	WT	0.529682	0.578595
272	M	WT	0.402212	0.941783
273	M	WT	0.767259	0.815831
198	F	WT	0.068852	0.482971
277	M	WT	0.12587	0.434644
270	F	WT	0.057611	0.283314
271	M	WT	0.281066	0.609841
283	F	WT	0.044739	0.36815
304	F	KO	0.252257	0.690566
260	F	KO	0.326447	1.115049
262	F	KO	0.361699	1.01438
261	F	KO	0.025223	0.236941
263	M	KO	0.067271	0.147759
223	F	KO	0.422597	0.949481
257	M	KO	0.178222	0.719209
255	M	KO	0.178222	0.719209
288	M	KO	0.049097	0.199147

MALE - Two Way ANOVA with Repeated Measures

Uncorrected Fisher's LSD	Predicted (LS) Mean diff.	95.00% CI of	Below threshold?	Summary	Individual P Value
SHAM					
WT vs. KO	0.2413	-0.1574 to 0.6	No	ns	0.2152
DEN					
WT vs. KO	0.1454	-0.2532 to 0.5	No	ns	0.4470
WT					
SHAM vs. DEN	-0.3064	-0.6281 to 0.0	No	ns	0.0590
KO					
SHAM vs. DEN	-0.4023	-0.6900 to -0.1	Yes	*	0.0130

FEMALE - Two Way ANOVA with Repeated Measures

Uncorrected Fisher's LSD	Mean diff.	95.00% CI of diff.	Below threshold?	Summary	Individual P Value
SHAM					
WT vs. KO	-0.04370	-0.3896 to 0.3022	No	ns	0.7922
DEN					
WT vs. KO	-0.2765	-0.6224 to 0.06936	No	ns	0.1095
WT					
SHAM vs. DEN	-0.2908	-0.4883 to -0.09336	Yes	**	0.0094
KO					
SHAM vs. DEN	-0.5236	-0.7211 to -0.3262	Yes	***	0.0003

Table 23A. Cathepsin B (Mature/Immature) Protein Expression in sham-operated and denervated samples of WT/KO male/female mice

	Cathepsin B (Mature/Immature) Expression (A.U)			
N	**Sex**	**Genotype**	**Sham**	**Den**
282	F	WT	0.430763	0.70053195
283	F	WT	3.180657	0.73156446
272	M	WT	3.825282	1.60764912
273	M	WT	1.509554	0.9867713
198	F	WT	1.872314	0.94695638
277	M	WT	1.982621	1.41177974
270	F	WT	0.12857	0.32445756
271	M	WT	2.119563	0.95616426
290	M	KO	2.304037	3.25032114
304	F	KO	5.648631	1.30961261
260	F	KO	3.692344	2.75154172
262	F	KO	5.406576	2.58145839
261	F	KO	0.843747	2.58732502
263	M	KO	0.809516	1.2970322
223	F	KO	2.077757	1.436986
257	M	KO	1.688233	2.33055355
255	M	KO	5.719599	3.5311017
288	M	KO	4.383569	2.74117147

MALE - Two Way ANOVA with Repeated Measures

Uncorrected Fisher's LSD	Predicted (LS) mean diff.	95.00% CI of diff.	Below threshold?	Summary	Individual P Value
SHAM					
WT vs. KO	-0.6217	-2.457 to 1.213	No	ns	0.4793
DEN					
WT vs. KO	-1.389	-3.224 to 0.4453	No	ns	0.1266
WT					
SHAM vs. DEN	1.119	-0.3142 to 2.552	No	ns	0.1074
KO					
SHAM vs. DEN	0.3510	-0.9307 to 1.633	No	ns	0.5379

FEMALE - Two Way ANOVA with Repeated Measures

Uncorrected Fisher's LSD	Predicted (LS) Mean diff.	95.00% CI of diff.	Below threshold?	Summary	Individual P Value
SHAM					
WT vs. KO	-2.131	-4.071 to -0.1903	Yes	*	0.0336
DEN					
WT vs. KO	-1.458	-3.398 to 0.4829	No	ns	0.1295
WT					
SHAM vs. DEN	0.7272	-1.560 to 3.014	No	ns	0.4766
KO					
SHAM vs. DEN	1.400	-0.6450 to 3.446	No	ns	0.1495

Table 24A. LAMP1 Protein Expression in sham-operated and denervated samples of WT/KO male/female mice

	LAMP1 Expression (A.U)			
N	Sex	Genotype	Sham	Den
276	M	WT	0.798463	0.739862
272	M	WT	0.597016	0.672266
279	F	WT	0.98908	1.315378
280	F	WT	0.694975	0.306851
273	M	WT	0.638875	0.642759
271	M	WT	0.753689	0.963073
277	M	WT	0.935509	1.104448
282	F	WT	0.403077	0.684131
283	F	WT	0.090105	0.219849
273	M	WT	0.377826	0.570115
267f	F	WT	0.624811	0.621521
300	M	KO	0.596963	0.831052
259	F	KO	0.197354	0.323249
290	M	KO	0.316331	0.289667
258	M	KO	1.184214	1.331934
262	F	KO	0.963371	0.929965
260	F	KO	0.427029	0.982953
261	F	KO	0.290123	0.33617
247	M	KO	0.233588	0.476247

MALE - Two Way ANOVA with Repeated Measures

Uncorrected Fisher's LSD	Predicted (LS) Mean diff.	95.00% CI of diff.	Below threshold?	Summary	Individual P Value
SHAM					
WT vs. KO	0.1008	-0.3299 to 0.5315	No	ns	0.6266
DEN					
WT vs. KO	0.04986	-0.3808 to 0.4806	No	ns	0.8093
WT					
SHAM vs. DEN	-0.09852	-0.2074 to 0.01040	No	ns	0.0705
KO					
SHAM vs. DEN	-0.1495	-0.2829 to -0.01605	Yes	*	0.0324

FEMALE - Two Way ANOVA with Repeated Measures

Uncorrected Fisher's LSD	Predicted (LS) Mean diff.	95.00% CI of diff.	Below threshold?	Summary	Individual P Value
SHAM					
WT vs. KO	0.09094	-0.4451 to 0.6270	No	ns	0.7214
DEN					
WT vs. KO	-0.01354	-0.5496 to 0.5225	No	ns	0.9576
WT					
SHAM vs. DEN	-0.06914	-0.3619 to 0.2237	No	ns	0.5940
KO					
SHAM vs. DEN	-0.1736	-0.5010 to 0.1537	No	ns	0.2501

Table 25A. Cytochrome c Oxidase enzyme activity in sham-operated and denervated samples of WT/KO male/female mice

	COX Enzyme Activity			
N	**Sex**	**Genotype**	**Sham**	**Den**
244f	F	WT	21.04	15.27
198f	F	WT	26.31	19.43
208m	M	WT	15.43	7.46
273m	M	WT	15.2	11.78
270f	F	WT	19.78	10.23
272m	M	WT	22.21	16.88
268f	F	WT	16.76	19.81
271m	M	WT	20.08	12.84
277m	M	WT	15.36	13.67
267f	F	WT	24.5	9.48
283f	F	WT	16.32	14.39
275m	M	WT	21.63	12.24
280f	F	WT	28.85	24.77
223f	F	KO	28.87	19.91
247m	M	KO	20.48	14.72
225f	F	KO	22.66	14.47
238f	F	KO	17.34	28.74
260f	F	KO	14.59	16.63
261f	F	KO	22.57	15.93
256m	M	KO	18.33	12.24
258m	M	KO	25.77	23.91
259f	F	KO	20.19	21.43
264m	M	KO	15.35	23.85
262f	F	KO	20.29	20.8
263m	M	KO	24.25	13.49
255m	M	KO	12.22	14.91
257m	M	KO	20.24	17.72
290m	M	KO	24.74	24.9
304f	F	KO	22.47	16.94

MALE - Two Way ANOVA with Repeated Measures

Uncorrected Fisher's LSD	Predicted (LS) mean diff.	95.00% CI of diff.	Below threshold?	Summary	Individual P Value
SHAM					
WT vs. KO	-1.854	-6.690 to 2.982	No	ns	0.4365
DEN					
WT vs. KO	-5.739	-10.58 to -0.9031	Yes	*	0.0220
WT					
SHAM vs. DEN	5.840	1.488 to 10.19	Yes	*	0.0127
KO					
SHAM vs. DEN	1.955	-1.814 to 5.724	No	ns	0.2805

FEMALE - Two Way ANOVA with Repeated Measures

Uncorrected Fisher's LSD	Predicted (LS) mean diff.	95.00% CI of diff.	Below threshold?	Summary	Individual P Value
SHAM					
WT vs. KO	0.8146	-4.243 to 5.872	No	ns	0.7432
DEN					
WT vs. KO	-3.159	-8.217 to 1.898	No	ns	0.2105
WT					
SHAM vs. DEN	5.740	0.5290 to 10.95	Yes	*	0.0333
KO					
SHAM vs. DEN	1.766	-3.108 to 6.641	No	ns	0.4478

Table 26A. Respiration levels in sham-operated and denervated samples of WT/KO male/female mice

	Complex I (pmol/s/mg tissue)			
N	**Sex**	**Genotype**	**Sham**	**Den**
316	M	WT	25.12309	20.659253
313	M	WT	41.21692	16.747519
314	M	WT	21.06905	17.289011
318	M	WT	62.38829	25.334182
364	M	KO	51.44406	60.294321
342	M	KO	36.4536	26.67983
343	M	KO	10.23838	27.211716
344	M	KO	58.91	70.729

MALE - Two Way ANOVA with Repeated Measures

Uncorrected Fisher's LSD	Mean Diff.	95.00% CI of diff.	Below threshold?	Summary	Individual P Value
SHAM					
WT vs. KO	-1.812	-30.05 to 26.42	No	ns	0.8911
DEN					
WT vs. KO	-26.22	-54.45 to 2.012	No	ns	0.0659
WT					
SHAM vs. DEN	17.44	0.1643 to 34.72	Yes	*	0.0484
KO					
SHAM vs. DEN	-6.967	-24.24 to 10.31	No	ns	0.3619

	Complex I Active (pmol/s/mg tissue)			
N	**Sex**	**Genotype**	**Sham**	**Den**
316	M	WT	118.0173	113.358822
313	M	WT	119.3804	87.5015413
314	M	WT	77.75484	72.6031307
318	M	WT	110.3149	67.5702418
364	M	KO	115.0312	123.232774
342	M	KO	74.80609	109.191014
343	M	KO	131.6504	180.621376
344	M	KO	117.15	147.93

MALE - Two Way ANOVA with Repeated Measures

Uncorrected Fisher's LSD	Mean Diff.	95.00% CI of diff.	Below threshold?	Summary	Individual P Value
SHAM					
WT vs. KO	-3.293	-40.86 to 34.27	No	ns	0.8517
DEN					
WT vs. KO	-54.99	-92.55 to -17.42	Yes	**	0.0078
WT					
SHAM vs. DEN	21.11	-1.020 to 43.24	No	ns	0.0583
KO					
SHAM vs. DEN	-30.58	-52.71 to -8.455	Yes	*	0.0148

	Complex I+II Active (pmol/s/mg tissue)			
N	**Sex**	**Genotype**	**Sham**	**Den**
316	M	WT	144.5711	153.578716
313	M	WT	150.4547	125.784712
314	M	WT	81.41616	96.9444127
318	M	WT	261.1813	154.733412
364	M	KO	160.2167	182.192199
342	M	KO	101.9011	172.693605
343	M	KO	162.755	298.748306
344	M	KO	206.54	349.2

MALE - Two Way ANOVA with Repeated Measures

Uncorrected Fisher's LSD	Mean Diff.	95.00% CI of diff.	Below threshold?	Summary	Individual P Value
SHAM					
WT vs. KO	1.553	-95.18 to 98.29	No	ns	0.9727
DEN					
WT vs. KO	-117.9	-214.7 to -21.21	Yes	*	0.0209
WT					
SHAM vs. DEN	26.65	-42.70 to 95.99	No	ns	0.3834
KO					
SHAM vs. DEN	-92.86	-162.2 to -23.51	Yes	*	0.0169

Table 27A. Reactive oxygen species production in sham-operated and denervated samples of WT/KO male/female mice

	Complex I (pmol H2O2/pmol O2 consumed)			
N	**Sex**	**Genotype**	**Sham**	**Den**
316	M	WT	0.149758	2.7002151
313	M	WT	0.109539	0.2861764
314	M	WT	0.721174	4.8550009
318	M	WT	0.002075	3.7646203
364	M	KO	0.560141	1.1474592
342	M	KO	0.039623	9.1951102
343	M	KO	0.132291	2.4717021
344	M	KO	0.001	4.88

MALE - Two Way ANOVA with Repeated Measures

Uncorrected Fisher's LSD	Mean Diff.	95.00% CI of diff.	Below threshold?	Summary	Individual P Value
SHAM					
WT vs. KO	0.06237	-3.066 to 3.191	No	ns	0.9661
DEN					
WT vs. KO	-1.522	-4.650 to 1.606	No	ns	0.3100
WT					
SHAM vs. DEN	-2.656	-6.226 to 0.9143	No	ns	0.1186
KO					
SHAM vs. DEN	-4.240	-7.810 to -0.6702	Yes	*	0.0271

	Complex I Active (pmol H2O2/pmol O2 consumed)			
N	**Sex**	**Genotype**	**Sham**	**Den**
316	M	WT	0.009457	0.37843416
313	M	WT	0.010722	0.03250377
314	M	WT	0.063639	0.93113488
318	M	WT	0.000513	1.27355632
364	M	KO	0.136758	0.41944345
342	M	KO	0.006017	1.85934245
343	M	KO	0.009042	0.29109681
344	M	KO	0.0005	2.3

MALE - Two Way ANOVA with Repeated Measures

Uncorrected Fisher's LSD	Mean Diff.	95.00% CI of diff.	Below threshold?	Summary	Individual P Value
SHAM					
WT vs. KO	-0.01700	-0.9084 to 0.8744	No	ns	0.9675
DEN					
WT vs. KO	-0.5636	-1.455 to 0.3278	No	ns	0.1935
WT					
SHAM vs. DEN	-0.6328	-1.660 to 0.3940	No	ns	0.1823
KO					
SHAM vs. DEN	-1.179	-2.206 to -0.1526	Yes	*	0.0307

	Complex I+II Active (pmol H2O2/pmol O2 consumed)			
N	**Sex**	**Genotype**	**Sham**	**Den**
316	M	WT	0.008661	0.27481638
313	M	WT	0.009986	0.01513339
314	M	WT	0.069424	0.75741427
318	M	WT	0.000294	0.61514121
364	M	KO	0.098914	0.2658692
342	M	KO	0.054086	1.47626931
343	M	KO	0.007418	0.1721231
344	M	KO	0.00019	1.046

MALE - Two Way ANOVA with Repeated Measures

Uncorrected Fisher's LSD	Mean Diff.	95.00% CI of diff.	Below threshold?	Summary	Individual P Value
SHAM					
WT vs. KO	-0.01806	-0.5680 to 0.5319	No	ns	0.9441
DEN					
WT vs. KO	-0.3244	-0.8744 to 0.2255	No	ns	0.2229
WT					
SHAM vs. DEN	-0.3935	-1.008 to 0.2212	No	ns	0.1683
KO					
SHAM vs. DEN	-0.6999	-1.315 to -0.08522	Yes	*	0.0317

Table 28A. Gastrocnemius muscle weight normalized to bodyweight in sham-operated and denervated samples of WT/KO male/female mice

	GAS Weight/BW (mg/g)			
N	**Sex**	**Genotype**	**Sham**	**Den**
244	F	WT	4.824427	3.698473
208	M	WT	3.266667	3.012698
198	F	WT	4.232558	4.07309
271	M	WT	4.311111	3.483951
253	F	WT	4.994898	4.423469
267	F	WT	4.723022	4.280576
273	M	WT	4.170029	3.579251
268	F	WT	4.662222	4.475556
270	F	WT	4.51136	3.974035
272	M	WT	4.371661	3.793264
278	M	WT	4.333333	3.514583
277	M	WT	4.164114	3.527352
283	F	WT	3.125514	2.687243
282	F	WT	4.011299	3.254237
280	F	WT	4.803922	4.088235
279	F	WT	4.386905	3.85119
276	M	WT	3.799172	3.335197
275	M	WT	3.869658	3.551282
247	M	KO	4.319703	3.94052
225	F	KO	5.700935	5.149533
223	F	KO	5.856502	4.892377
238	F	KO	5.619048	4.679654
258	M	KO	5.415441	4.889706
260	F	KO	5.369863	4.228311
262	F	KO	4.904545	3.840909
257	M	KO	5.200155	4.772639
255	M	KO	3.907216	4.209622
261	F	KO	5.229186	4.901777
264	M	KO	3.807692	5
263	M	KO	4.404432	3.872576
256	M	KO	4.487543	3.740145
259	F	KO	6.182462	5.186005
298	F	KO	4.594104	3.773243
297	F	KO	5.329973	5.582035
288	M	KO	4.762658	4.339399
289	M	KO	5.580779	4.945138
290	M	KO	5.413779	3.933958
300	M	KO	4.426647	3.902439
301	M	KO	4.296188	3.131965
304	F	KO	4.6875	4.168269
299	M	KO	4.812057	3.588652
305	F	KO	5.295938	4.468085

MALE - Two Way ANOVA with Repeated Measures

Uncorrected Fisher's LSD	Predicted (LS) mean diff.	95.00% CI of diff.	Below thresh	Summary	Individual P Value
SHAM					
WT vs. KO	-0.8074	-1.144 to -0.4708	Yes	****	<0.0001
DEN					
WT vs. KO	-0.7409	-1.078 to -0.4043	Yes	****	<0.0001
WT					
SHAM vs. DEN	0.5363	0.3396 to 0.7330	Yes	****	<0.0001
KO					
SHAM vs. DEN	0.6028	0.4188 to 0.7868	Yes	****	<0.0001

FEMALE - Two Way ANOVA with Repeated Measures

Uncorrected Fisher's LSD	Predicted (LS) mean diff.	95.00% CI of diff.	Below threshold?	Summary	Individual P Value
SHAM					
WT vs. KO	-0.9151	-1.395 to -0.4352	Yes	***	0.0004
DEN					
WT vs. KO	-0.7440	-1.224 to -0.2641	Yes	**	0.0033
WT					
SHAM vs. DEN	0.5470	0.3127 to 0.7813	Yes	***	0.0001
KO					
SHAM vs. DEN	0.7182	0.4948 to 0.9416	Yes	****	<0.0001

	SOL Weight/BW (mg/g)			
N	**Sex**	**Genotype**	**Sham**	**Den**
244	F	WT	0.21374	0.263359
208	M	WT	0.326984	0.24127
198	F	WT	0.232558	0.209302
271	M	WT	0.274074	0.232099
253	F	WT	0.428571	0.255102
267	F	WT	0.341727	0.28777
273	M	WT	0.244957	0.247839
268	F	WT	0.351111	0.195556
270	F	WT	0.288496	0.212766
272	M	WT	0.248548	0.243902
278	M	WT	0.258333	0.214583
277	M	WT	0.199125	0.19256
283	F	WT	0.187243	0.164609
282	F	WT	0.254237	0.223164
280	F	WT	0.284314	0.25817
279	F	WT	0.255952	0.25
276	M	WT	0.223602	0.20911
275	M	WT	0.241453	0.228632
247	M	KO	0.242152	0.210762
225	F	KO	0.28972	0.224299
223	F	KO	0.219331	0.193309
238	F	KO	0.329004	0.251082
258	M	KO	0.294118	0.216912
260	F	KO	0.26484	0.210046
262	F	KO	0.313636	0.259091
257	M	KO	0.268169	0.229304
255	M	KO	0.195876	0.199313
261	F	KO	0.224509	0.177736
264	M	KO	0.272727	0.22028
263	M	KO	0.252078	0.121884
256	M	KO	0.239672	0.179754
259	F	KO	0.323295	0.265722
298	F	KO	0.231293	0.208617
297	F	KO	0.307058	0.247479
288	M	KO	0.265032	0.25712
289	M	KO	0.382142	0.242149
290	M	KO	0.228292	0.220139
300	M	KO	0.22206	0.196578
301	M	KO	0.208211	0.196481
304	F	KO	0.259615	0.192308
299	M	KO	0.248227	0.187943
305	F	KO	0.266925	0.235977

Table 29A. Soleus muscle weight normalized to bodyweight in sham-operated and denervated samples of WT/KO male/female mice

MALE - Two Way ANOVA with Repeated Measures

Uncorrected Fisher's LSD	Predicted (LS) mean diff.	95.00% CI of diff.	Below threshold?	Summary	Individual P Value
SHAM					
WT vs. KO	0.002160	-0.02265 to 0.02697	No	ns	0.8630
DEN					
WT vs. KO	0.01301	-0.01180 to 0.03783	No	ns	0.3000
WT					
SHAM vs. DEN	0.03930	0.02052 to 0.05808	Yes	***	0.0001
KO					
SHAM vs. DEN	0.05015	0.03259 to 0.06772	Yes	****	<0.0001

FEMALE - Two Way ANOVA with Repeated Measures

Uncorrected Fisher's LSD	Predicted (LS) mean diff.	95.00% CI of diff.	Below threshold?	Summary	Individual P Value
SHAM					
WT vs. KO	0.008411	-0.03335 to 0.05017	No	ns	0.6858
DEN					
WT vs. KO	0.007828	-0.03393 to 0.04959	No	ns	0.7064
WT					
SHAM vs. DEN	0.05182	0.01979 to 0.08384	Yes	**	0.0031
KO					
SHAM vs. DEN	0.05123	0.02070 to 0.08176	Yes	**	0.0023

	Total Bodyweight (g)		
N	Sex	Genotype	Bodyweight (g)
270	F	WT	27
244	F	WT	26.2
198	F	WT	30.1
271	M	WT	40.5
253	F	WT	19.6
267	F	WT	27.8
273	M	WT	34.7
268	F	WT	22.5
272	M	WT	43.05
278	M	WT	48
277	M	WT	45.7
282	F	WT	35.4
279	F	WT	33.6
276	M	WT	48.3
275	M	WT	46.8
280	F	WT	30.6
223	F	KO	22.3
225	F	KO	21.4
247	M	KO	26.9
238	F	KO	23.1
258	M	KO	27.2
262	F	KO	22
260	F	KO	21.9
257	M	KO	25.73
261	F	KO	21.38
255	M	KO	29.1
264	M	KO	28.6
263	M	KO	36.1
256	M	KO	31.71
259	F	KO	22.58
298	F	KO	22.05
297	F	KO	21.82
288	M	KO	25.28
289	M	KO	26.43
290	M	KO	24.53
300	M	KO	27.47
301	M	KO	34.1
304	F	KO	20.8
299	M	KO	28.2
305	F	KO	25.84

Table 30A. Total bodyweight of WT/KO male/female mice

Two Way ANOVA with Repeated Measures

Uncorrected Fisher's LSD	Predicted (LS) mean diff.	95.00% CI of diff.	Below threshold?	Summary	Individual P Value
Male					
WT vs. KO	15.30	11.73 to 18.87	Yes	****	<0.0001
Female					
WT vs. KO	5.801	2.377 to 9.225	Yes	**	0.0015
WT					
Male vs. Female	15.78	11.94 to 19.61	Yes	****	<0.0001
KO					
Male vs. Female	6.277	3.156 to 9.398	Yes	***	0.0002

Table 31A. Male epididymal fat normalized to bodyweight in WT/KO mice

	Male Epididymal Fat (Fat/Bodyweight (g))		
N	**Sex**	**Genotype**	**Epididymal Fat**
276	M	WT	0.02839959
275	M	WT	0.03261325
256	M	KO	0.02581835
288	M	KO	0.00959256
300	M	KO	0.02373134
290	M	KO	0.02154912
289	M	KO	0.02989784
299	M	KO	0.01755319
316	M	WT	0.0479661
313	M	WT	0.03710472
319	M	WT	0.04985714
364	M	KO	0.00890052
341	M	KO	0.0232591
318	M	WT	0.04072558
319	M	WT	0.04837624
314	M	WT	0.03321285
316	M	WT	0.0479661
344	M	KO	0.02196959

Unpaired t test	
P value	<0.0001
P value summary	****
Significantly different (P < 0.05)?	Yes

APPENDIX B: ADDITIONAL DATA (STATISTIC TABLES NOT SHOWN

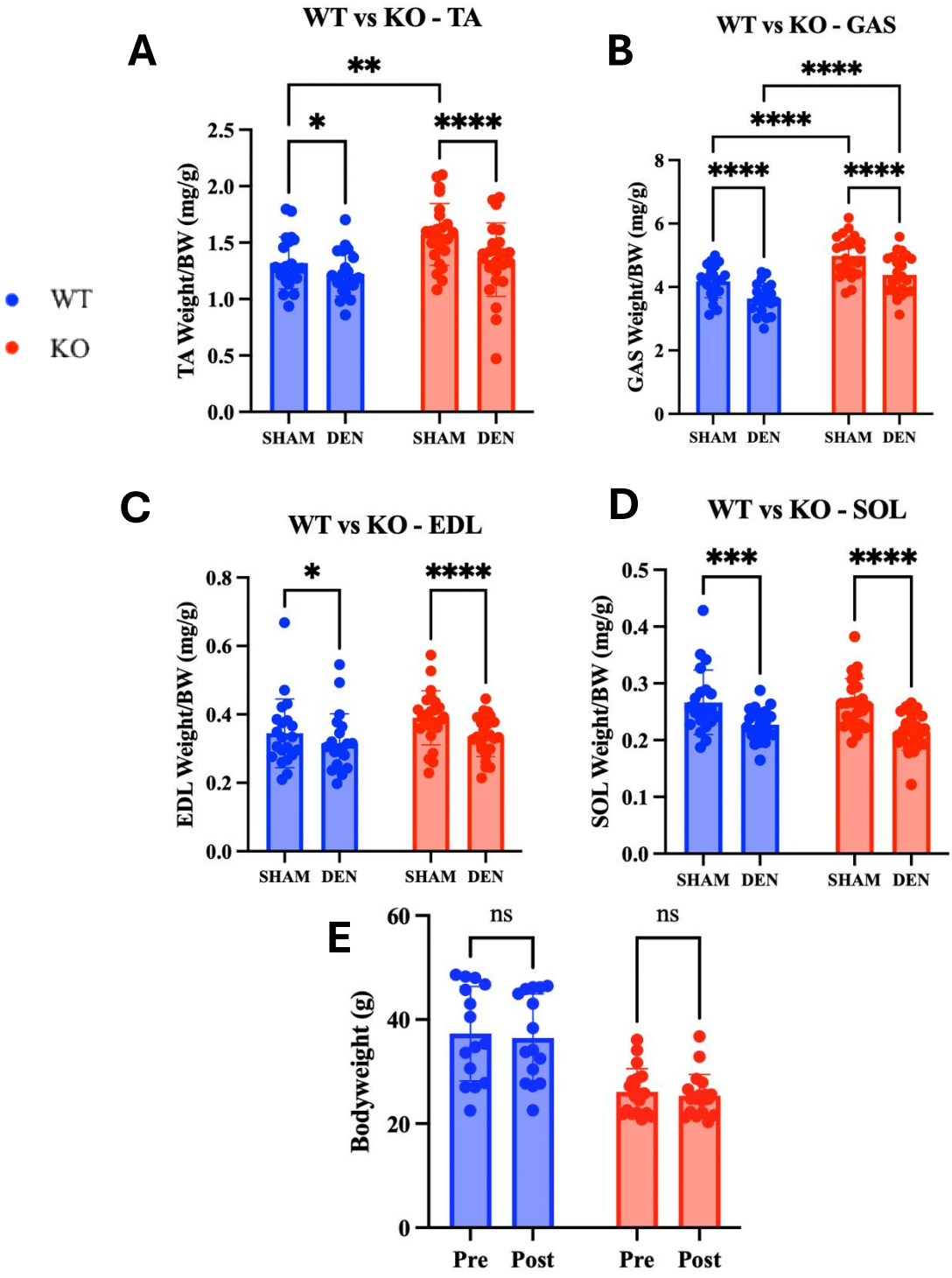

Supplemental Figure 1: Additional hindlimb muscle weight and bodyweight measurements of WT and ATF5 KO mice post denervation: Comparisons between sham-operated and denervated muscle weights of the TA, GAS, EDL and SOL in WT and ATF5 KO male/female mice (A-D). Bodyweight (g) measurements comparing pre and post denervation in WT and ATF5 KO male/female mice (E). (WT: n = 18, KO n = 24, WT (males) n = 8-9, WT (females) n = 10-11, KO (males) = 13, KO (females) = 11)) *P < 0.05, **P < 0.01, ***P < 0.001, ****P < 0.0001. Comparisons between CON vs DEN and total bodyweight from WT and ATF5 KO animals are evaluated using two-way ANOVA with repeated measures.

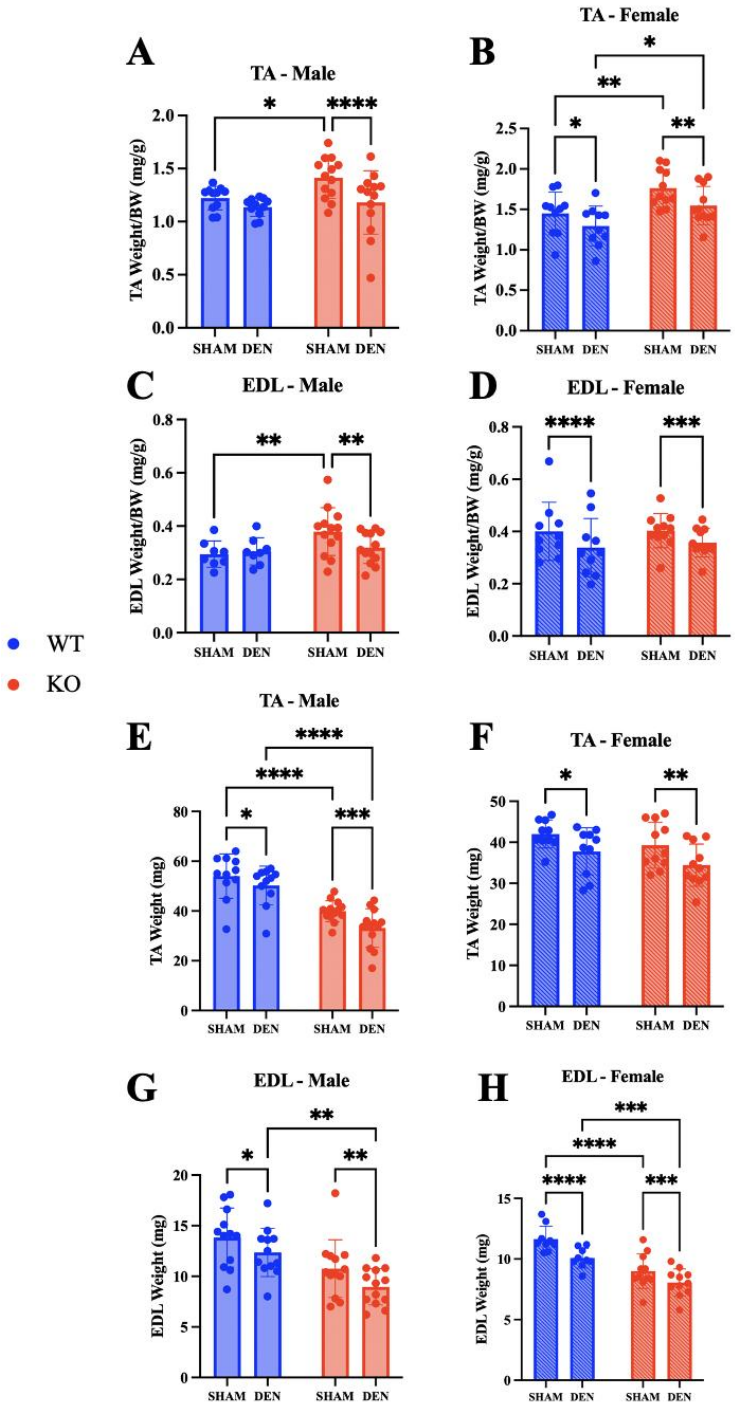

Supplemental Figure 2: Raw hindlimb muscle weight measurements of male and female WT and ATF5 KO mice. Raw hindlimb muscle weight measurements of TA and EDL in WT and ATF5 KO male/female mice (A-H). (WT: n = 18, KO n = 24, WT (males) n = 8-9, WT (females) n = 10-11, KO (males) = 13, KO (females) = 11)) *P < 0.05, **P < 0.01, ***P < 0.001, ****P < 0.0001. Comparisons between CON vs DEN from WT and ATF5 KO animals are evaluated using two-way ANOVA with repeated measures.

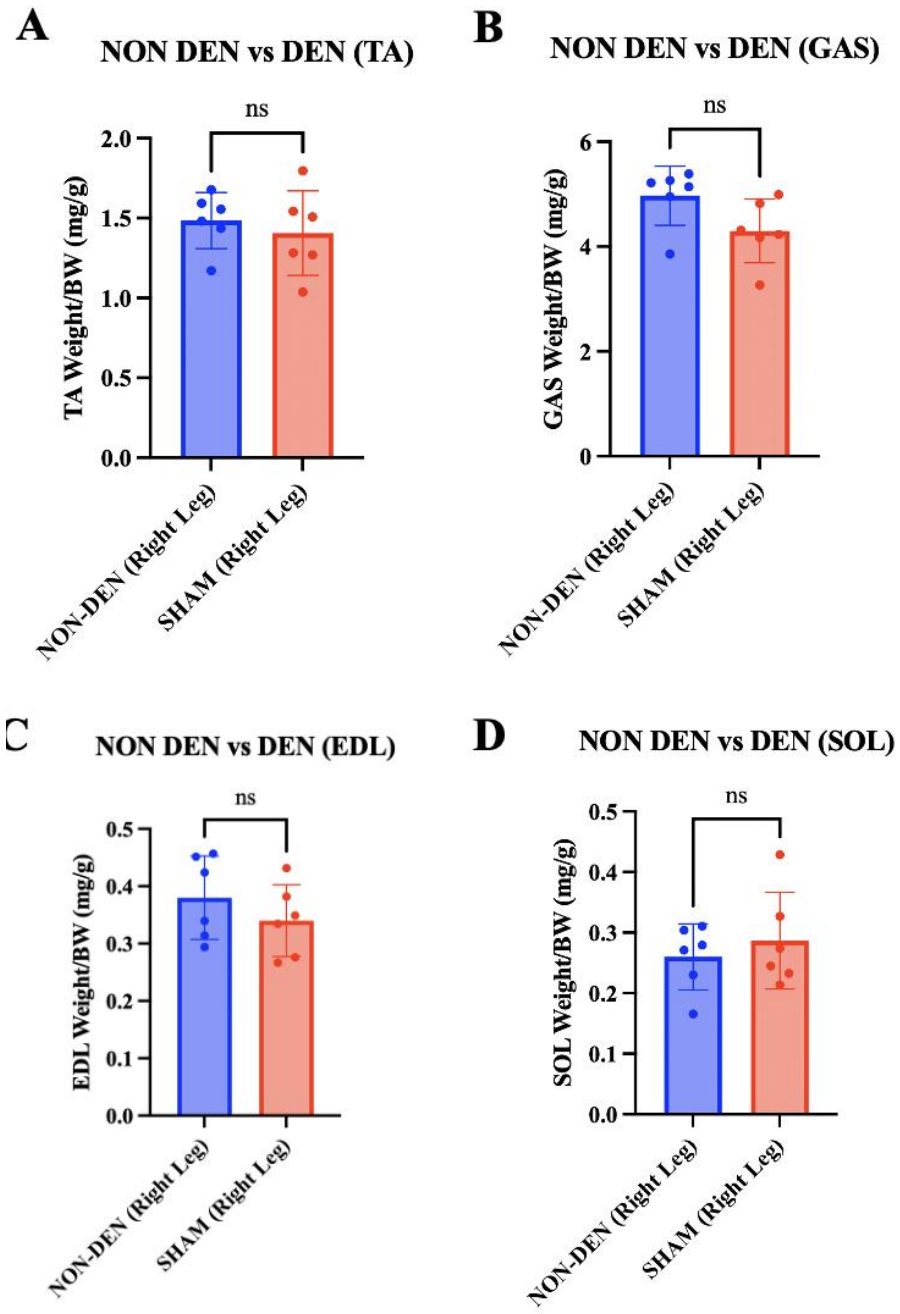

Supplemental Figure 3: Comparisons between right and left hindlimb muscle groups in non-denervated WT mice. Normalized hindlimb muscle weights of TA, GAS, EDL and SOL in non-denervated WT mice (A-B).

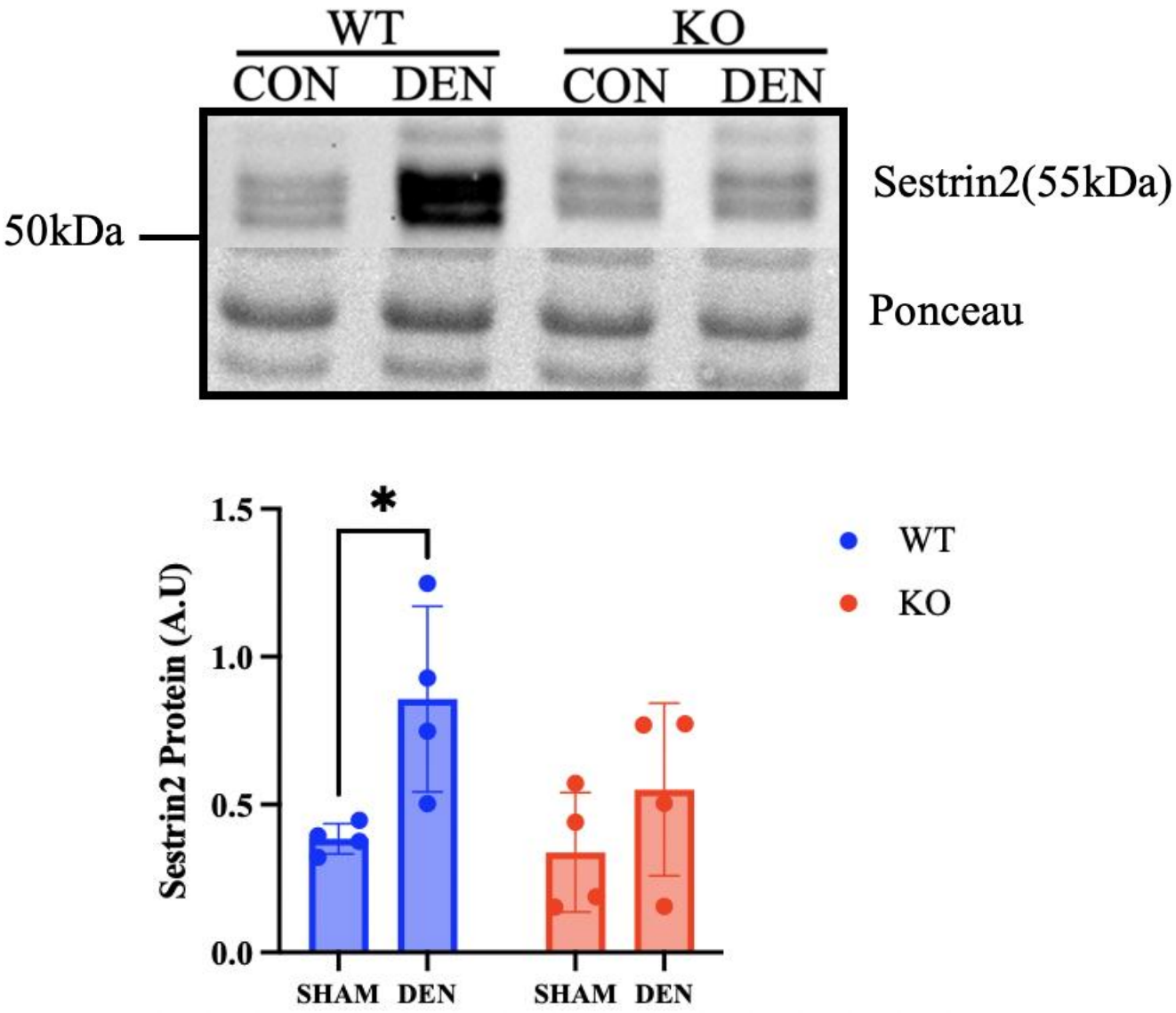

Supplemental Figure 4: Total protein content of sestrin2 in WT and ATF5 KO mice. Comparison of total sestrin2 protein content between WT and ATF5 KO male/female mice post denervation (WT: n = 4, KO n = 4, WT (males) n = 2, WT (females) n = 2, KO (males) = 2, KO (females) = 2)) *P < 0.05)

APPENDIX C: LABORATORY METHODS AND PROTOCOLS

SCIATIC NERVE TRANSECTION

Sterilize surgical instruments through autoclaving prior to surgery

1. Collect all surgical instruments and sterilize with 70% ethanol. All surgical tools should be kept in 70% ethanol when not in use.

2. After the mouse is anesthetized and weighed, place tear gel on the eyes to avoid dryness throughout the duration of the surgery. 113

3. Landmark incision site by locating the femur, and the incision will be parallel with the femur, approximately half-way between the hip and knee joint. Shave the incision area with an electric razor.

4. After shaving, wipe the site with by 70% ethanol, followed iodine to prep the skin for surgery.

5. Using small scissors, make a small incision in the skin, below the femur bone, and locate the sciatic nerve through the muscle. It should appear as a thick white band below the surface of the muscle.

6. Following this, make another incision into the muscle, perpendicular to the first cut to reveal the nerve.

7. Using blunt scissors, remove a 3-5mm section of the sciatic nerve to denervate the hindlimb muscles.

8. Suture the incision in the muscle closed by tying two knots, ensuring that they are tied in opposite directions.

9. To close the incision in the skin, use 2-3 surgical staples, ensuring to fully squeeze the staples closed.

10. Sham-operate the opposite leg, as an internal control, by performing steps 3-9, without transecting the nerve. If the tear gel has dissipated, reapply as needed throughout the procedure.

11. Following the surgery, use a 29g syringe to inject Metacam (2µg/g of body weight), subcutaneously. Create the working stock of Metacam by adding 1mL to 9mL of 0.9% saline solution. In brief, pinch the skin along the spine to create a “tent’ shape and inject it into the center of the skin.

12. Put the mouse in a new, fresh cage and keep a heat lamp on the animal to help normalize body temperature. The heat lamp should be left on even after the animal regains consciousness, until any abnormal behaviour subsides. If abnormal behaviour persists for over 20 minutes, crush up a piece of chow with tap water in a small petri dish and place in cage.

13. To help avoid the risk of infection, Baytril is incorporated into the water for the remainder of the denervation period. In brief, 1mL of Baytril is added to 200mL of water. The following day:

14. Give a second Metacam injection (1µg/g of body weight) approximately 24 hours after the surgery.

15. Continue to carefully monitor the animal throughout the duration of the denervation period.

ISOLATING WHOLE MUSCLE PROTEIN EXTRACTS

Reagents:
1. Muscle Extraction Buffer (Sakamoto et al., JBC 277:11910, 2002)
a. 20mM Hepes (ph 7.4) 2.383g/500ml
b. 2mM EGTA 0.3804g/500ml
c. 1% Trition-X100 5ml/500ml
d. 50% Glycerol 10ml/500ml
e. 50mM b-Glycerophosphate 5.4g/500ml
Volume up to 500ml with double distilled water (ddH2O) pH to 7.4

2. Make extraction buffer with protease and phosphatase inhibitors:
In a 15ml tube, mix the following at the appropriate ratio as outlined below and keep on ice:
a. 1 ml Sakamoto Muscle Extraction Buffer
b. 10 ul Protease Inhibitor Stock (1 tablet in 500uL ddH2O)
c. 10 ul Cocktail 2 Phosphatase Inhibitor
d. 10 ul Cocktail 3 Phosphatase Inhibitor

Procedure:
1. Add 100µl of Sakamoto Muscle Extraction Buffer to a set of Eppendorf tubes.
2. Weigh out 15-20mg of tissue into the first set of Eppendorf tubes and record the exact weight of each sample in a table.
3. Add the appropriate volume of buffer solution to each Eppendorf to produce 10x volume.
4. Insert a metal bead into each Eppendorf.
5. Place Eppendorfs in balanced manner in metal brackets (kept in freezer)
6. Insert brackets into TissueLyser and homogenize (shake) at 30 Hz for 1 min at a time.
7. Remove blocks, check for homogeneity and repeat if necessary (flip orientation of blocks for each cycle)
8. Remove beads with magnet and centrifuge at 14,000g for 10 minutes at 4°C.
9. Completely withdraw the supernatant and pipette the solution into the new pre-labeled Eppendorf tubes.
10. Store at -80°C

WESTERN BLOTTING PROTOCOL

GEL ELECTROPHORESIS-SDS PAGE (PROTEIN BIORAD SYSTEM)

Reagents:
1. Acrylamide/Bis-Acrylamide, 30% Solution 37.5:1 (BioShop 10.502)
a. Store at 4°C

2. Under Tris Buffer
a. 1M Tris, pH 8.8 (60.5g/500ml)
b. Store at 4°C

3. Over Tris Buffer
a. 1M Tris, pH 6.8 (12.1g/100ml)
b. Bromophenol Blue (for colour)
c. Store at 4°C

4. Ammonium Persulfate (APS)
a. 10% (w/v) APS in ddH20 (1g/10ml)
b. Stored at 4°C

5. Sodium Dodecyl Sulfate (SDS)
a. 10% (w/v) in ddH20 (1g/10ml)
b. Store at room temperature

6. TEMED (Sigma T-9281)

7. Electrophoresis Buffer, pH 8.3 (10L)
a. 25mM Tris 30.34g, 192mM Glycine 144g, 0.1% SDS 10g
b. Volume to 10L with ddH20
c. Store at room temperature

8. 6X SDS
a. Warm 100% glycerol in water bath at 65°C for 30 minutes
b. Combine 1.2g SDS, 0.06g Bromophenol Blue, 3mls of 1M Tris, pH 6.8 and 1ml of ddH20 and stir at 4°C for 5 minutes
c. Add 3mls of 100% glycerol, stir and aliquot mixture.
d. Store at -20°C e. Add 5% (v/v) ß-mercaptoethanol (Sigma M6250) to 6X SDS just prior to use

9. tetra-Amyl alcohol ReagentPlus, 99% (Sigma 152463)

Procedure:
1. Prepare gel electrophoresis rack:
a. Clean glass plates thoroughly with soap followed by 95% ethanol then ddH20.
b. Dry carefully with a kimwipe.
c. Assemble glass plates as shown below:
d. Check the seal by adding a small volume of ddH20 then pour off and let dry.

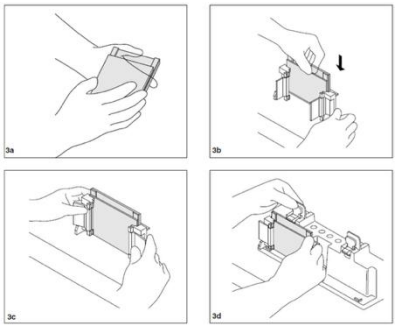

2. Prepare separating gels: 117
a. Mini Protean 3 Bio-Rad System volumes:

	8%	**10%**	**12%**	**15%**	**18%**
Acrylamide	2.7 ml	3.3 ml	4.0 ml	5.0 ml	6.0 ml
ddH_20	4.1 ml	3.5 ml	2.8 ml	1.8 ml	0.8 ml
Under Tris	3.0 ml	3.0 ml	3.0 ml	3.0 ml	3.0 ml
SDS	100µl	100µl	100µl	100µl	100µl
APS	100µl	100µl	100µl	100µl	100µl
TEMED	10µl	10µl	10µl	10µl	10µl

b. Mix the contents of the separating gel without adding APS or TEMED. Stir.
c. Add APS and TEMED. Stir.
d. Slowly pour the entire volume of the solution into the space between the two plates while keeping plates tilted to prevent bubble formation.
e. Add tert-Amyl alcohol to coat top surface of gel solution.
f. Allow 30 minutes for gel polymerization.
g. Remove tert-Amyl alcohol by pouring it off and remove any remainder with a kimwipe. Rinse with ddH20.

3. Prepare stacking gel:
a. For a single mini gel use the following volumes à
b. Mix the contents of the stacking gel without adding APS or TEMED. Stir.
c. Add APS and TEMED. Stir.
d. Using a Pasteur pipette slowly add the entire volume from the beaker in between the plates.
e. Add comb for desired number of wells.
f. Allow 30 minutes for gel polymerization.

Acrylamide	500 µl
Over Tris	625 µl
ddH_20	3.75 ml
SDS	50 µl
APS	50 µl
TEMED	7.5 µl

4. Prepare samples:
a. Turn on the block heater to 95ºC.
b. Pipette required volume of sample into new eppendorf with same amount of lysis buffer and 5 µl of sample dye. Keep samples on ice until all samples are prepared (use pipette plan).
c. Briefly spin each sample to bring volume to the bottom of the eppendorf.
d. Incubate each sample at 95 ºC for 5 minutes in the heating block to denature the proteins.
e. Briefly spin again to return volume to the bottom of the eppendorf.

5. Assemble Mini-PROTEAN gel caster system:
a. If you are only running one gel a rectangular plastic pseudo plate must be clamped on the other side of the caster.
b. Fill with electrophoresis buffer between the plates and outside of the plates in the chamber.
c. Slowly remove the comb using both hands (one on each side) by pulling the comb straight upwards.
d. Fix any wells that are deformed using a small spatula.
e. Clean out the wells using a syringe filled with electrophoresis buffer.
f. Withdraw the entire volume of the sample using a Hamilton syringe. Inject volume slowly into the bottom of the well.

6. Gel electrophoresis:
a. Immediately after all samples are loaded place the lid on the gel chamber.
b. Place positive and negative plugs into the power supply and turn on power supply.
c. Set power supply to 120V. Gel will run for ~2 hours depending on percent gel made.
d. When the bromophenol blue has run off the bottom of the gel (or when gel has separated the desire amount) turn off the power supply. Remove plugs from power supply and remove lid.
e. Prepare for electrotransfer of proteins from the gel to nitrocellulose membrane.

WESTERN BLOTTING – TRANSFER AND IMMUNODETECTION

Reagents:

1. Transfer Buffer
a. 0.025M Tris-HCl pH 8.3; 12.14g
b. 0.15M Glycine ; 45.05g
c. 20% Methanol; 800ml
d. make up to 4L with ddH20
e. store at 4°C

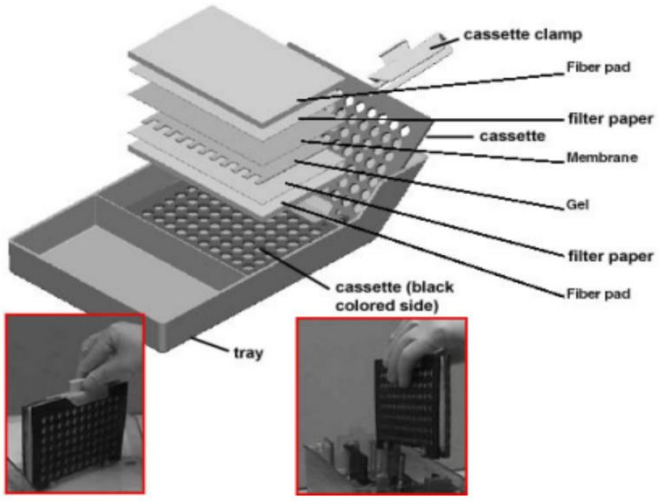

2. Ponceau S stain
a. 0.1% (w/v) Ponceau S 119
b. 0.5% (v/v) Acetic Acid
c. Store at room temperature

3. Wash Buffer
a. Tris-HCl pH 7.5; 12g
b. NaCl; 58.5g
c. 0.1% Tween; 10ml
d. Store at room temperature

4. Blocking Solution
a. 5% (w/v) skim milk power in wash buffer OR
b. 5% (w/v) BSA in wash buffer

5. Enhanced Chemiluminescence Fluid (ECL; Santa Cruz sc-2048)

Procedure:

1. Transfer Procedure:
a. Remove electrophoresis plates from chamber and separate the plates.

b. Cut away unnecessary parts of the gel using a spatula and measure remaining gel size.

c. Using a paper cutter cut 6 pieces of Whatman paper per gel to the same size as the gel. Wearing gloves cut nitrocellulose membrane (GE Healthcare RPN303D) to the dimensions of the gel.

d. Assemble Whatman paper, nitrocellulose membrane and gel as shown above:

e. Close the cassette and place in the transfer chamber with the black side of the cassette facing the back side of the chamber.

f. Place ice pack in the chamber.

g. Place lid on the chamber and connect the leads to the power supply.

h. Turn on the power supply and run at 120V for 2 hours. This can vary depending on the size of the protein of interest.
2. Removal of transfer membrane:

a. Turn off the power supply and disconnect leads from the power supply then remove the lid from the chamber.

b. Remove the cassette from the chamber.

c. With gloves on, remove the Whatman paper and gel and place the nitrocellulose membrane in a plastic dish.

d. Add Ponceau S stain on the membrane and gently swirl.

e. Drain off the remaining Ponceau S and save for reuse. 120

f. Rinse the membrane with ddH20 to reduce the red background. Wrap membrane in saran wrap and scan image.

g. Cut the membrane while protein bands are still visible at the desired molecular weight.

h. Rotate membrane at room temperature in wash buffer until remaining Ponceau S has been removed.

i. Incubate membrane for 1 hour with rotation in blocking solution.

j. Incubate membrane with desired antibody diluted in blocking solution overnight at 4ºC. Membrane is placed face up into the solution on a glass plate covered in parafilm. To maintain a moist environment overnight, wet a small kimwipe and form it into a ball and place in each corner of the dish. Cover the dish with saran wrap.

3. Immunodetection:
a. Wash the blots in wash buffer with gentle rotation for 5 minutes 3X.

b. Incubate the blots for 1 hour in room temperature with the appropriate secondary antibody diluted in blocking solution.

c. Membrane is placed face up in solution on a glass plate covered with parafilm. Place moist kimwipes in each corner of the dish and cover the dish with saran wrap.

d. Following the incubation, wash the membrane 3X for 5 minutes with wash buffer.

4. Enhanced Chemiluminescence Detection:
a. Mix ECL fluids “A” and “B” in a 1:1 ratio in a disposable Rohr tube.

b. Place blots on saran wrap face up and apply ECL solution for 4 minutes.

c. Dab off excess ECL on a kimwipe and place blot in imager for appropriate amount of time for optimal band exposure.

COX ENZYME ACTIVITY ASSAY

Reagents:
1. 100 mM K-Phosphate Buffer:
a. make up 0.1 M KH_2PO_4; MW = 136.09 = 13.6g/1000ml pH ~ 5.0, Room Temperature
b. make up 0.1 M $K_2HPO_4.3H_2O$ MW = 174.18 = 17.4g/1000ml pH ~ 8.0, Room Temperature
c. Mix in equal proportions, pH to 7.0

2. 10 Mm K-Phosphate Buffer:
b. dilute 0.1 M KPO_4 Buffer prepared above 1:10 with dH_2O (e.g. 10 ml Buffer and 90 ml H_2O)

3. Extraction Buffer (100 mM Na-K Phosphate, 2 mM EDTA; pH 7.2)
a. 500ml 0.1 M Na_2HPO_4. $2H_20$ Combine 8.9g Sodium Phosphate with 0.372g EDTA up to 500ml
b. 200ml 0.1M KH_2PO_4 Combine 2.7g Potassium Phosphate with 0.149g EDTA up to 200ml
c. Mix both solutions, pH to 7.2

4. Test Solution (reduced cytochrome c, 1mg/ml), for 10ml:
a. Weight out 10mg of horse heart cytochrome c (Sigma, C-2506) in a scintillation vial
b. Add 1ml of 10 mM KPO_4 buffer and dissolve the cytochrome c
c. Make up a small volume of 15mg/ml sodium dithionite-10 mM KPO_4 stock solution
d. Add 40µl of sodium dithionite stock solution to the vial with the test solution and observe red-orange colour change
e. Add 8ml of ddH_20
f. Add 1ml of 100mM KPO_4 Buffer
g. Wrap it up in foil and put in oven at 30°C

Procedure:
1. Add 200µl of Extraction Buffer to a 2.0ml eppendorf on the scale

2. Add the liquid nitrogen flash frozen muscle tissue to the Eppendorf and add the volume of Extraction Buffer required to obtain a 40-fold dilution

3. Homogenize samples using a TissueLyser and metal beads.

4. Remove beads and sonicate each tube 3 x 3 seconds, cleaning the probe between samples

5. Add 200µl of sample to eppendorfs containing 200µl Extraction Buffer

6. In a 96-well plate, pipette 50 µl of sample into wells

7. Open COX Activity plate reader program on plate reader (Cytation 5, BioTek) and start
a. Set temperature at 30°C
b. Dispense 240ul of test solution
c. Absorbance at 550nm
d. 3s intervals, 21 reads

HIGH-RESOLUTION RESPIROMETRY AND ROS EMISSION IN PERMEABILIZED FIBERS

Reagents:
1. Buffer Z, for 500ml:
a. 105mM K-MES; 12.26g
b. 30mM KCl; 1.12g
c. 10mM KH2PO4; 0.7g
d. 5mM MgCl2 •6H2O; 0.51g
e. 1mM EGTA; 0.19g
f. 5mg/ml BSA; 2.5 pH 7.4; Store at -20°C

2. BIOPS Buffer, for 1L:
a. 2.77mM CaK2EGTA; 27.7ml
b. 7.23mM K2EGTA; 72.3ml
c. 5.77mM Na2ATP; 3.14g
d. 6.56mM MgCl2 •6H2O; 1.335g
e. 20mM Taurine; 2.51g
f. 15mM Na2Phosphocreatine; 3.825g
g. 20mM Imidazole; 1.36g
h. 0.5mM Dithiothreitol (DTT); 0.077g
i. 50mM MES Hydrate; 9.76g pH 7.1; Store at -20°C

3. Permeabilization Buffer
a. BIOPS Buffer; 1.5ml
b. Saponin (10mg/ml); 6µl
c. 10.5mM CDNB; 5µl

4. Amplex Ultra Red Buffer
a. Buffer Z; 1.5mL
b. 5mM AUR; 650µL i. 666.6µL DMSO ii. 1mg AUR
c. 5000IU/ml SOD1; 1625µl i. pH 7.0 125
d. 10mM BLEB; 32.5µl
e. 0.5M EGTA i. pH 7.5-8.0
f. Store in black 5ml tubes at -20°C.

5. Horseradish peroxidase; 0.5U/mL (HRP)
a. Store at -20ºC.

6. 0.1µM H2O2

7. Pyruvate (P2256, Sigma)
a. 27.5mg/125µl
b. Make fresh each day

8. Malate (M1000, Sigma), for 10ml stock:
a. 1.073g
b. pH 7.1
c. Store at -20°C

9. ADP (A2754, Sigma), for 10ml stock:
a. 2.13g

b. pH 7.1
c. Store at -20°C

10. Succinate (S2378, Sigma), for 10ml stock:
a. 2.7014g
b. pH 7.1
c. Store at -20°C

Procedure:
1. Collect medial portion of the TA and store in ice cold BIOPS Buffer

2. Gently tease apart muscle fibers with fine-tip forceps in BIOPS Buffer over ice

3. Place bundles in Permeabilization Buffer and permeabilize on orbital for 30 mins at 4°C

4. Transfer bundles to Eppendorf with Buffer Z and wash for 7.5mins

5. Transfer bundles to another Eppendorf with Buffer Z and was for 7.5 mins

6. Measure wet weight muscle bundle (~2-5mg)

7. Set up experiment using O2K
a. Set up chamber by rinsing with 3x ddH2O then 1x 70% EtOH. Repeat 3 times ending with ddH2O. Remove all liquid with suction 126
b. Add 3x710ul AUR Buffer into the chamber and close part-way
c. Wait for oxygen reading to level out and adjust for background detection
d. Add 1ul BLEB to chamber with p10
e. Stop stir bar and add muscle bundle
f. Close chamber part-way and start stir bar
g. Add 50ml O2 and close chamber fully for an O2 reading of ~380
h. Once O2 stabilizes, turn on fluorescence
i. Add 4ul HRP
j. Calibrate ROS signal

8. Run experiment
a. Add 5ul pyruvate and 5ul malate to the chamber and wait until O2 levels stabilize
b. Add 20ul ADP to the chamber and wait until O2 levels stabilize
c. Add 20ul succinate to the chamber and wait until O2 levels stabilize

CRYOSECTIONING AND SDH STAINING

SDH Buffer
a. 150 mL 100 mM PO4 Buffer
b. 2.025 g Succinic Acid
c. 183.9 mg NBT
d. 9.75 mg NaN3
e. 10.09 mg mPMS

PO4 Buffer (1L stock pH = 7.6)

a. 1.56 g KH_2PO_4
b. 23.34 g Na_2HPO_4

Procedure:

Tissue preparation
1. Prepare a cryomold with the appropriate amount of cryomatrix for desired muscle
3. Upon removing tissue from animal, quickly place muscle in a the cryomold and completely cover the muscle in cryomatrix
4. Make sure the tissue is positioned correctly inside the cryomold to ensure a proper cut of the cross-sectional area
5. Place the cryomold with tissue in isopentane at the temperature of liquid nitrogen (do not allow the tissue to come in direct contact with liquid nitrogen)
6. Wait for muscle to turn white and wrap the tissue/cryomold in tinfoil
7. Store in -80ºC

Tissue Sectioning and Staining
1. Cut 10µm cross sections of tissue at -20°C
2. Dry slides 5-10 min at room temperature
3. Incubate slides in SDH Stain Buffer for 30 min at 37°C in dark (i.e. oven)
4. Rinse with ddH20 2 x 10 min on shaker at room temperature
5. Mount with cover slips using DPX mountant

APPENDIX D: OTHER CONTRIBUTIONS TO THE LITERATURE

PUBLISHED ABSTRACTS

1. Kuthe, J., & Hood, D. A. (2025). ATF5 is Required For The Normal Stress Response in Skeletal Muscle During Denervation. *Physiology*, *40*(S1), 1103. https://doi.org/10.1152/physiol.2025.40.S1.1103

2. Kuthe, J., & Hood, D. A. (2025). ATF5 KO Mice Exhibit Dysregulated Stress Response in Skeletal Muscle in the Presence of Denervation. Proceedings of Muscle health Awareness Day, 16th edition. Toronto, ON, Canada. May 9th, 2025